THE UNIVERSITY OF MANITOBA

TORSIONAL DYNAMICS IN FLYWHEEL MOTOR GENERATOR SETS

BY

MARK ANTHONY WEEKES

A THESIS

SUBMITTED TO THE FACULTY OF GRADUATE STUDIES

IN PARTIAL FULFILLMENT OF THE REQUIREMENTS

FOR THE DEGREE OF MASTER OF SCIENCE

DEPARTMENT OF ELECTRICAL ENGINEERING

WINNIPEG, MANITOBA, CANADA

ISBN 0-315-33541-6

TORSIONAL DYNAMICS IN FLYWHEEL MOTOR GENERATOR SETS.

by

Mark Anthony Weekes

A thesis submitted to the Faculty of Graduate Studies of the University of Manitoba in partial fulfillment of the requirements of the degree of

MASTER OF SCIENCE

ABSTRACT

Motor-generator sets are used to supply first grade power to the HVdc valve groups of Manitoba Hydro's Nelson River Bipole 1. The shaft between the motor and generator has received damage to the keys and keyways. This thesis is an investigation of the cause and solution to the problem. The system is studied with the aid of the digital modelling program MH-EMTDC.

Previous researchers have conducted studies into the torsional dynamics of shaft systems and this thesis is an extension which includes nonlinear coupling torques as well as the complete dynamic modelling of the machines and power supply system. This model was used to determine the effects of various switching operations in the system and the effect of different coupling parameters.

The results have shown that of the switching operations investigated, only the isolation of the motor-generator sets onto the HVdc converter filter banks could lead to damage consistent with that observed. Changes in coupling parameters would be of minor consequences. It is suggested that a change in operating procedures will prevent future damage.

ACKNOWLEDGEMENTS

I would like to express my deep appreciation for the help and guidance given to me by my thesis advisor, Dr. R.W. Menzies at the University of Manitoba. I would also like to thank Dr. J. Chand and Mr. R. Haywood at Manitoba Hydro for their time, assistance, and advice during the course of the work. Thanks are also due to Mr. Frank Kadlec at Manitoba Hydro for providing and assisting me with information relevant to the topic.

TABLE OF CONTENTS

LIST OF FIGURES

LIST OF FIGURES (continued)

LIST OF SYMBOLS

α	Damping coefficient (Ω /H.)
β_1, β_2, θ_1 and θ_2	All represent angles of rotation (radians)
C	Total capacitance (Farads)
EFD and U_f	The exciter field voltage (p.u.)
i	Instantaneous current (Amperes)
I_{base}	Base current (Amperes)
L	Total inductance (Henries)
L_m	Motor inductance (Henries)
L_T	Transformer inductance (Henries)
p.u.	per unit
R	Equivalent resistance (Ω)
s	Units of seconds
T mech Flywheel	The flywheel mechancial torque (N.m)
T mech generator	The generator mechanical torque (N.m)
T mech mot	The motor mechancial torque (N.m)
W and $\dot{\theta}$	The angular speed $\frac{d\theta}{dt}$ (rad/s)
$\dot{W}$ and $\ddot{\theta}$	The angular acceleration $\frac{d^2\theta}{dt^2}$ (rad/s^2)
W_c	Energy stored in the capacitor (Kilo-Joules)
W_o	Resonant frequency (rad/s)
X_a	Armature leakage reactance (p.u.)
X_c	Equivalent capacitance (Ω)
X_d''	Direct-axis subtransient reactance (p.u.)
X_f	Field leakage reactance (p.u.)
X_{kf}	Direct-axis leakage reactance (p.u.)
X_L	Equivalent inductance (Ω)
X_{md}	Direct-axis magnetizing reactance (p.u.)
Z_b	Base impendence (Ω)

CHAPTER 1 INTRODUCTION

1.1 Problem and Possible Causes

Manitoba Hydro has a problem with their flywheel motor-generator sets located at Radisson and Dorsey converter stations. These MG sets are of significant importance because they are used to supply first grade power to the valve groups. The problem was first encountered on March 26, 1981 at Radisson converter station during the annual maintenance on MG set #1. It was found that the key and keyway on the motor shaft and the motor end on the flywheel shaft had a great deal of play and were badly damaged. At this time, the motor keyway was widened and cut deeper to repair the shaft and a larger key was used. The couplings on the motor side were bored, sleeved and re-keyed to have a shrink fit of .003" - .004". It was also noted that MG set #2 and #3 were damaged but to a lesser degree. On February 4, 1983 annual maintenance again showed the keys on the motor end of the flywheel shaft and motor were partly sheared in the opposite direction of rotation. In order to prevent further damage, the flywheel was cut down approximately 3" in diameter, reducing its inertia and the original round blocks in the couplings were replaced with wedge blocks.

Similar damage was noted at the Dorsey Station but to a much lesser degree. With the present solution, no further damage has been noticed but the cause of the problem and whether the present solution has in fact eliminated the problem is not known. This thesis is an investigation of the problem.

1.2 Literature Survey

It is evident that the failures were caused by negative torque but the effect of positive torque was also shown. This suggested an oscillation or resonance problem. Mechanical resonance arises when the natural frequency of the shaft system matches the frequency of the disturbance to the system.

A paper by R. Daugherty [1] showed the effect of disturbances in the electrical supply system on an induction motor and driven equipment rotors and shafts. The paper examined the case where an induction motor is being used in an area where continuous operation is important. In these cases control systems have been used to keep the motor connected to the line for a few cycles (6 -9 cycles) while a nearby fault is cleared. The re-supplying of motor voltage within a short time after the initial disturbance can create large electrical torques. It was pointed out that the torsional response of the shaft system to power supply reclosure is not predictable based on the magnitude of the resultant vectorial volts per hertz. It is also possible that the shaft torque will be larger than the peak electrical torque. Some other important points to be stated were that the transient electrical torque generated when an induction motor is reconnected onto a power system is dependent upon the speed at which the motor shaft is rotating and is influenced by any electrical flux which may have been trapped in the motor after disconnection of the motor. Because of the trapped flux, the electrical torque resulting from reconnecting the motor is not directly comparable to that resulting from starting the motor from rest. It was stated that the shaft torque would increase if the frequency of the motor electrical torque is equal to the natural frequency of the system, assuming a linear shaft system. This shows the importance of keeping the design of the shaft system from having natural frequencies around 60 Hz, since this frequency is always in electrical transients on 60 Hz power systems. However, the

specific study for Manitoba Hydro, which will be presented later, deals with a nonlinear shaft system and natural frequencies cannot be easily found, but the importance of a suitable shaft system which would not be excited by common disturbances is still significant. The torsional oscillation in the shaft torque would eventually decay and be dependent on the amount of mechanical damping in the shaft system. The paper showed that the electrical torques produced on reconnection of power supply depended on the duration of the interruption. The magnitude of the change in average electrical torque was found to be a function of the phasor difference between the motor and power system voltages, the speed of the motor and the level of trapped flux remaining in the motor. Both initial positive and negative torques could be observed depending on the length of the power interruption period.

Another paper by F.P. Flynn, W.S. Wood and P.D. Slater [2] dealt with negative torques in induction motors due to rapid reconnections of the supply. They did an extensive study of the largest peak negative torques on induction motors (strictly electrical torques) for a selected delay and for various machines under various selected initial load conditions and for various values of external inertia. The analytical methods used involved numerical step by step solutions for the case of variable speed solutions and algebraic solutions where the speed is assumed to be constant. The algebraic solutions were only used to indicate likely accuracy of the numerical step by step solutions. The study showed that the largest torques occur when the measured phase difference between the decaying motor voltage and the supply voltage is in the region of 200°. That is when the two voltages are directly adding, **a predicted maxima would occur at an angle of 180°.** The study also indicated that a larger motor inertia actually decreased the negative torque peaks of the electrical torque but this must not be confused with mechanical shaft torque peaks for larger inertias which were not studied. It was found that generally an increase in motor horsepower increased negative

torques but there is no clear variation with size. Other factors to consider are the open circuit time constant of the motor, the number of poles on the motor (which generally decreased torques with more poles) and the type of load (generally larger torques with larger loads).

All of these factors make it quite difficult to obtain an accurate value of peak negative torques without doing a study on that specific motor with all of its defined parameters.

The paper on the transient performance of induction motors by F.J. Maginiss and N.R. Schultz [3] emphasized the dependence of negative torque on length of time before power supply reclosure. It stated the importance of not using steady-state speed-torque curves for calculation of transients. Sudden changes in applied voltage were shown, in general, to have more severe electrical torque oscillations than those due to a sudden change in mechanical loads.

The issues raised in these papers contributed to the direction used in trying to find potential causes of the problem.

1.3 Scope

A digital model of the system was suggested because of the many nonlinear aspects introduced by the couplings. A computer simulation would be the only way to incorporate these nonlinearities accurately. To this end, a subroutine for the electromagnetics transients program (EMTDC) was developed to represent the mechanical shaft, coupling and flywheel system.

Various possible operating modes were simulated using the program to determine the cause of the problem. The results and conclusions presented give firm guidelines as to what direction

should be taken to strengthen the MG system mechanically or to relieve the electrical phenomena which are causing the problem.

1.4 Damage

The couplings are located between the motor and flywheel shafts and again between the flywheel and generator shafts as in Fig 1. The role of the couplings is to reduce large transient torques transmitted to the shaft. The size and type of coupling chosen depends on the specific application. It is at the couplings (specifically the coupling between the motor and flywheel) that the damage is occurring. The round block type coupling and 97.08 $kg\text{-}m^2$ flywheel were originally used when damage was first noticed (Fig. 2).

The damage (Fig. 2) can be seen as the result of a torque in the direction opposite to that of rotation. Note, the flywheel shaft is shown in the center and the motor is turning the outer hub.

The type of torque needed to do this damage was estimated on the basis of the type of material being deformed and an estimate of the friction coefficient between the coupling hub and shaft with the given shrink-fit (Appendix A):

Torque needed to break shrink-fit = 11 to 27 p.u.
Torque needed to deform keys = 8.5 p.u.

From the first estimate, a lower bound can be set on the magnitude of torques which is of minimal value to create damage. Once the shrink-fit has been broken, the coefficient of friction between the coupling hub and the shaft will be reduced. The extent of the reduction is not known but in the worst case we can neglect shrink-fit friction after the initial 'breaking' and subsequent torques would now be limited by the minimum torque estimate (2nd estimate) needed to deform the keys.

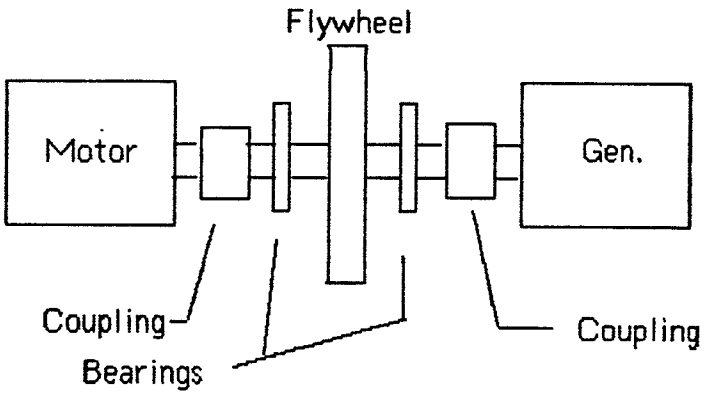

Fig. 1. MG Set (One of 4 Units per Station)

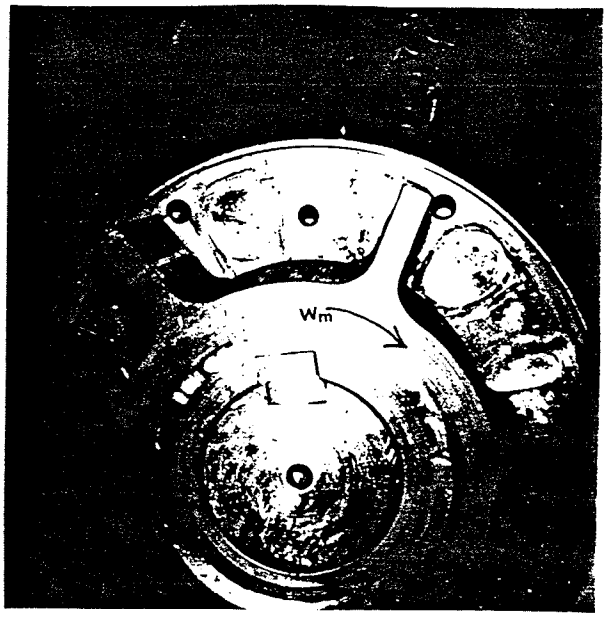

Fig. 2. Location of Key and Damage

Throughout the simulations to be presented, torque values exceeding 11 p.u. will be considered potentially responsible for the damage.

The torsional behaviour of the couplings corresponds to the type of rubber block used between the teeth of the coupling. The resilience of the rubber accounts for the amount of deflection to a given applied torque. The manufacturer has provided curves (Appendix B) which describe the resilience of the type of block used on site. The torsional stiffness of the rubber is calculated by taking the slope of the graph and thus getting a torque/angle characteristic.

1.5 Damping

The couplings are fitted with rubber blocks between the teeth and it is the rubber that introduces damping into the mechanical system. The damping of the rubber blocks was investigated as to how it could be accurately modelled within the system. Prof. Popplewell, a mechanical engineer involved with vibration studies at the University of Manitoba, pointed out that the damping behaviour of the rubber blocks would be very difficult to model accurately. Some studies had been done on the damping of rubber but only in steady state analysis (a constant stiffness and a constant input vibration). Even in these cases, the damping could only be represented to a level of 50% accuracy.

In our specific case, the rubber block had a nonlinear stiffness and the input to the system was a vibration that changed in amplitude and in frequency. The damping could not be modelled. The manufacturer, however, supplied a formula for estimating the damping in the case where the stiffness was a constant and the vibration input was steady. Prof. Popplewell stated that although one could not expect the damping to be the same in the transient case, one could use the formula simply to see the effect of

damping on the system. The given formula is:

$$D = \frac{K}{12\ W}$$

- Where K is the torsional stiffness of the rubber assumed to be constant (N•m/rad).

- W is the vibration frequency specific to the corresponding stiffness and inertias of the masses (rad/s).

- D is the specific damping coefficient which when multiplied by the difference in speed of the two masses will give the damping torque (N•m/rad/s).

- The coefficient 12 is a constant given by the manufacturer for 50° durometer rubber used.

The damping would be different for round and wedge block cases since the value of the torsional stiffness would be different for these two blocks.

The vibration frequency W is a function of the inertia of the masses and the torsional stiffness of the rubber. It can be calculated from the equation:

$$W^4 - W^2 \left[K_1 \left(\frac{1}{J_1} + \frac{1}{J_2}\right) + K_2 \left(\frac{1}{J_2} + \frac{1}{J_3}\right)\right] + K_1 K_2 \frac{J_1 + J_2 + J_3}{J_1 . J_2 . J_3} = 0$$

There are 4 W values for which this equation is true. Two of the values have negative frequencies with no physical representation. According to Prof. Popplewell, the smaller of the remaining two frequencies is more applicable to the type of input disturbance to the system (i.e. one whose amplitude and frequency decays with time). This frequency was calculated as 69 rad/s giving:

For the round blocks:

$$D = \frac{0.1245 \times 10^6}{12\ (69)} = 151\ \text{N.m/rad/s}$$

for $K = 0.1245 \times 10^6$ N.m/rad at rated torque.

This value estimates the damping within the rubber block for a constant input vibration to the system and a constant stiffness K, of the rubber.

Prof. Popplewell suggested that under transient conditions, larger damping forces could occur. Another estimate that increased the magnitude of the damping coefficient by about six times was used to represent the transient case (947 N.m/rad/sec).

For the wedge block, the same points hold except that the stiffness is now $K = 0.212 \times 10^6$ N.m/rad [9].

The manufacturer's estimate for steady state damping of the wedge block is:

$$D = \frac{K}{12W} = \frac{0.212 \times 10^6}{12\ (89.8)} = 196\ \text{N.m/rad/s}$$

And the larger estimate for transient conditions of the wedge block is now 1 235.0 N.m/rad/s.

From these two estimates, a logical if not accurate, representation of the coupling behavior was achieved. The system was first analyzed without any damping to find potential problem areas and damping estimates were only used to compare results and suggest what is really happening on the site.

CHAPTER 2 MODELLING OF THE SYSTEM

2.1 The System

The system to be studied is made up of an electrical subsystem and a mechanical subsystem, with a single-line diagram of the electrical subsystem shown in Fig. 3.

The electrical network is modelled with the assumption that the 138 kV bus is an infinite bus. The second feed via transformer T2 has been added to the network to illustrate what happens on typical bus transfers.

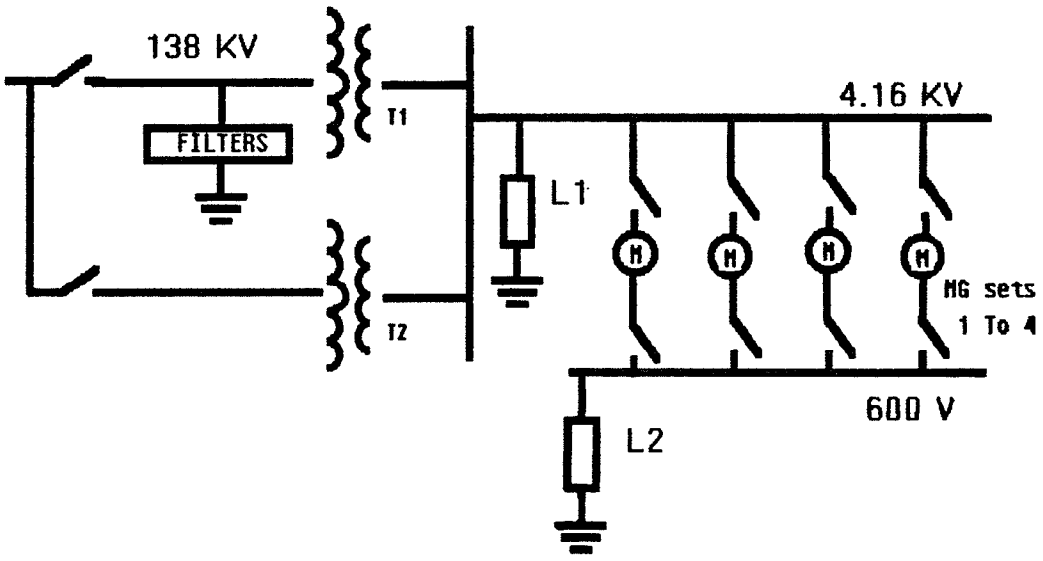

Fig. 3 The System

The actual network is more complicated and consists of 3 transformers from the 138 kV collector bus to 4.16 kV. The breakers are modelled to open on a current zero crossing and close instantaneously. The filters are modelled with complete RLC elements in each phase. Each of the motor generator sets consists of a 554 KVA squirrel cage induction motor, couplings, a flywheel supported on its own bearings, and a 421 KVA salient pole generator.

The local load L1 in parallel to the MG sets is estimated later from the oscillogram results obtained from an on site test.

The load L2 on the 600 V bus supplied by the generator of the MG sets is not known. Typical values of 0.5 p.u. resistance have been used throughout and some simulations presented show load changes between 0.05 p.u. and 1.0 p.u.

2.2 EMTDC

The electrical subsystems were completely modelled using Manitoba Hydro's electromagnetic transients program (EMTDC). The EMTDC program was chosen because it can represent three phase models of electrical networks, provides easy interfacing with user developed Fortran models and derives an electromagnetic transients solution as opposed to a solution under only steady-state conditions [4].

One concern found in using EMTDC was the emphasis on having a proper time step. Switching within the electrical system would sometimes lead to numerical instability. If the time step was sufficiently reduced and an additional smoothing factor (within the program) was used, the problem of numerical instability is solved. The choice of time step was not critical as long as the oscillations of the highest frequency are still to be represented by an adequate number of points.

Previously developed programs for the machine models are interfaced with EMTDC [5]. The programs take in voltages and provide currents to the electrical network. The torque and speed can be selected as input or output parameters. A separate program for the mechanical system model (flywheel subroutine) was written and interfaced with EMTDC.

2.3 Mechanical Subsystem

The mechanical subsystem consists of the motor, flywheel, couplings and generator as shown in Fig. 4.

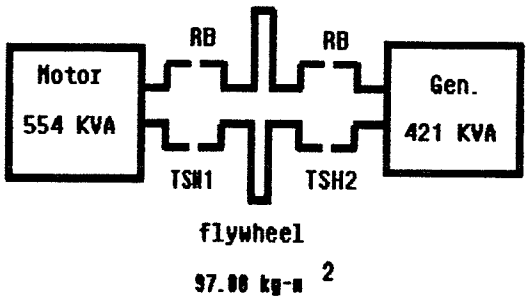

Fig. 4 The Mechanical Subsystem

This can be looked upon as a three mass system with one angle being used as a reference (i.e. $\beta_1 = \theta_1 - \theta_2$, $\beta_2 = \theta_2 - \theta_3$)

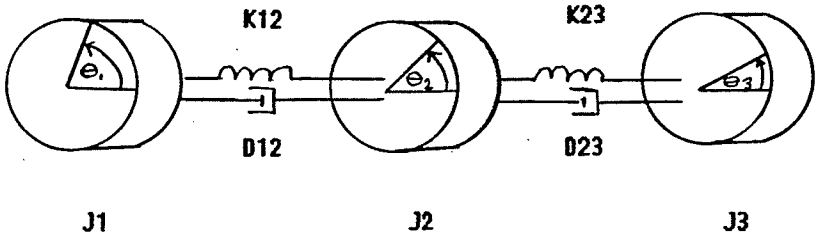

Fig. 5 The Three Mass System

In Fig. 5, each major rotating element is modelled as a lumped mass and each coupling shaft segment is modelled as a massless rotational spring with its stiffness given by a nonlinear spring constant. Viscous damping of each shaft segment is also represented in the spring.

The equations of motion are:

$$J_1 \ddot{\theta}_1 + D_{12} (\dot{\theta}_1 - \dot{\theta}_2) + K_{12} (\theta_1 - \theta_2) = T \text{ elec. motor}$$

$$J_2 \ddot{\theta}_2 + D_{12} (\dot{\theta}_2 - \dot{\theta}_1) + D_{23} (\dot{\theta}_2 - \dot{\theta}_3) + K_{12} (\theta_2 - \theta_1) + K_{23} (\theta_2 - \theta_3) = 0.$$

$$J_3 \ddot{\theta}_3 + D_{23} (\dot{\theta}_3 - \dot{\theta}_2) + K_{23} (\theta_3 - \theta_2) = -T \text{ elec. generator}$$

Where J = inertia, D = mechanical damping, K = torsional stiffness

Electrical damping of the motor and generator is included in the electrical subsystem (damper windings). Further damping of the flywheel, due to windage and friction, has not been included in the above equations and can be considered negligible.

2.4 Flywheel Subroutine

The Flywheel Subroutine was written to represent the mechanical subsystem. The program has been developed specifically for the MG sets. The torques calculated within the program are based on a 6-pole motor and generator of synchronous speed 1 200 rpm.

The inputs to the program (Fig. 6) are the motor electrical torque and the generator electrical torque. The motor shaft torque and the flywheel shaft torque are never actually calculated, but instead, the difference between these two torques is calculated. It is this difference between the torques which gives a resultant torque, TSH1, that has damaged the keys and keyways on the shaft.

$$\begin{aligned} TSH1 &= T_{mech\ mot} - T_{mech\ Flywheel} \\ &= K_{12} (\theta_1 - \theta_2) \\ &= K\beta_1 \end{aligned}$$

Similarly, TSH2 arises from the difference between the flywheel torque and the generator torque.

$$\begin{aligned} TSH2 &= T_{\text{mech flywheel}} - T_{\text{mech generator}} \\ &= K(\theta_2 - \theta_3) \\ &= K\beta_2 \end{aligned}$$

Again, the generator shaft torque was never actually calculated.

Along with the two resultant shaft torques, (TSH1 and TSH2) the speeds and the mechanical angles of the motor, the generator, and the flywheel are all calculated after each time step. This allows the transient torques and speeds to be accurately represented.

The theory is based on the differential equation:

$$J\ddot{\theta} + D\dot{\theta} + K\theta = T$$

This equation may be written as a first order system

$$\dot{\underline{w}} = (T - D\underline{w} - K\underline{\theta}) / J$$

$$\dot{\underline{\theta}} = \underline{w}$$

Using the trapezoid rule of integration and the modified Euler method, the iterative solution to the system is solved.

Derivatives at t:
$$\dot{\underline{w}}(t) = [T - D\underline{w}(t) - K\underline{\theta}(t)] / J$$
$$\dot{\underline{\theta}}(t) = \underline{w}(t)$$

Predicted Values:
$$\underline{w}p(t + \Delta t) = \underline{w}(t) + \Delta t * \dot{\underline{w}}(t)$$
$$\underline{\theta}p(t+ \Delta t) = \underline{\theta}(t) + \Delta t * \dot{\underline{\theta}}(t)$$

Derivatives at t+ Δt:
$$\dot{\underline{w}}(t+ \Delta t) = [T - D\underline{w}p(t+\Delta t) - K\underline{\theta}p(t+\Delta t)] / J$$
$$\dot{\underline{\theta}}(t+ \Delta t) = \underline{w}p(t+ \Delta t)$$

Corrected Values: $\underline{w}\ (t+\Delta t) = \underline{w}\ (t) + \frac{\Delta t}{2}\ [\dot{\underline{w}}\ (t) + \dot{\underline{w}}\ (t+\Delta t)]$

$\underline{\theta}\ (t+\Delta t) = \underline{\theta}\ (t) + \frac{\Delta t}{2}\ [\dot{\underline{\theta}}\ (t) + \dot{\underline{\theta}}\ (t+\Delta t)]$

With the Inertia Matrix J,

$$J = \begin{bmatrix} J_1 & 0 & 0 \\ 0 & J_2 & 0 \\ 0 & 0 & J_3 \end{bmatrix}$$

Damping Matrix,

$$D(\theta) = \begin{bmatrix} D_{12} & -D_{12} & 0 \\ -D_{12} & D_{12} + D_{23} & -D_{23} \\ 0 & -D_{23} & D_{23} \end{bmatrix}$$

Torsional Stiffness Matrix,

$$K(\theta) = \begin{bmatrix} K_{12} & -K_{12} & 0 \\ -K_{12} & K_{12} + K_{23} & -K_{23} \\ 0 & -K_{23} & K_{23} \end{bmatrix}$$

Torque Vector,

$$\underline{T} = \begin{bmatrix} \text{Telec motor} \\ 0 \\ -\text{Telec generator} \end{bmatrix}$$

and State Variable θ Vector

$$\underline{\theta} = \begin{bmatrix} \theta_1 \\ \theta_2 \\ \theta_3 \end{bmatrix}$$

The Feedback System would be:

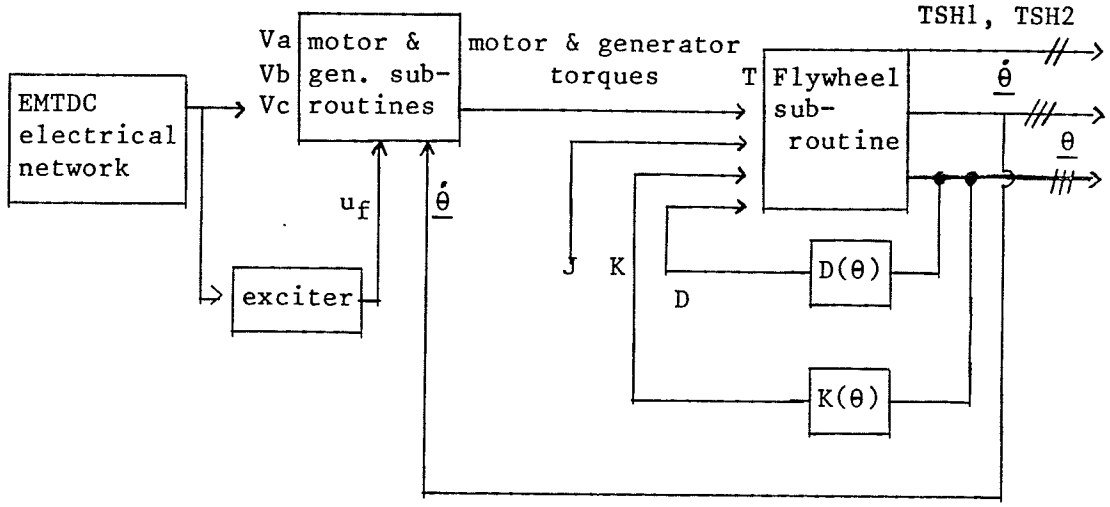

Fig. 6 Program Flow Diagram

Both the damping and torsional stiffness coefficients may be nonlinear functions of the angle θ, depending on the properties of the rubber blocks within the couplings. The suitable damping and torsional stiffness coefficients are put into the program as a curve of K or D vs. the angular deflection of the specific rubber block. The program then uses linear interpolation between the data to find the correct coefficients for any angle of deflection.

EMTDC allows the two machine programs and the flywheel program to be interfaced directly by being called as subroutines from the Main program. As shown in Fig. 6, the Main program calculates the voltages which are then used in the machine subroutines to calculate the electrical torques. The electrical torques are then used to calculate the resultant torques TSH1 and TSH2 along the shaft as well as the new mechanical angle and speeds of the machines.

Previously written machine subroutines are based on 2-pole machines while the flywheel subroutines are based on the actual 6-pole machines on site.

$$T = \frac{\#\text{ of poles}}{2}\,\frac{P}{Ws}$$

P = real power

Ws = electrical speed

= 377 rad/sec. for 60 Hz system

$$T = (\#\text{ of poles}) \times K$$

For an increase in poles, there is a proportional increase in torque (with constant power).

The electrical torques were adjusted before entering the flywheel program.

Similarly, $T = \frac{P_{mech}}{Wm}$

Wm = Machine mechanical speed (rad/sec.)

For an increase in torque, there is a proportional decrease in speed (mechanical speed of machine).

These two points were taken into account when interfacing the 2-pole machine programs with the 6-pole flywheel program. All machine electrical torques were corrected before entering the flywheel programs and the flywheel program produced the correct speed for a 6-pole machine. Before returning to the machine programs, the speeds (angles) were changed back to the appropriate speeds (angles) for a 2-pole machine (Fig. 6).

2.5 Verification of the Model

A laboratory motor at the University of Manitoba was run and checked with the results of the model of the same machine. The three values being checked as the motor started from standstill were:

i) the mechanical speed of the motor
ii) the stator current waveforms
iii) the electrical torque produced by the motor

This model was to verify that reasonable results were being obtained.

When osilloscope readings were compared with the simulated results, they were similar.

For further verification, a model of the actual motor on site was derived. This model represented the motor and the lump sum inertia of the motor, flywheel and generator together.

Two tests were conducted at Radisson Station MG Set #2. The system configuration is as below:

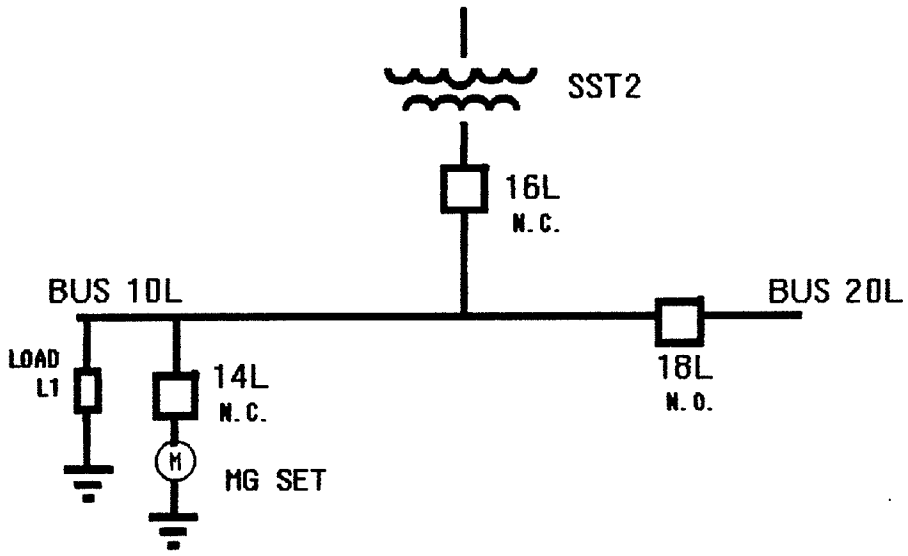

Fig. 7 Bus Configuration for Station Tests

i) The first test consisted of opening breaker 16L and approximately 4 cycles later, closing breaker 18L. The oscillograms obtained monitored the voltage of bus 10L (which the MG set is connected to) and bus 20L, which later supplied the MG set. The current entering the MG set was also monitored.

ii) The second test began with breaker 14L open. The breaker 14L then closed and starting currents and voltages were monitored as before.

From the first test, the oscillogram readings showed that the pre-opening stator current of the motor (I_a, Ib and Ic) was 48 A rms. This suggested that the motor was under light load conditions as its rated current is 76.95 A rms. Another observation from the oscillogram readings was that the stator current of the motor lagged the stator voltage by an angle of 78° at the end of the 4 cycle interval after breaker 16L had opened. This together with the magnitude of the current and voltage at the end of the 4 cycle interval gave an idea of the type of local load (parallel to the motor) that was on bus 10L at the time of testing. During the 4 cycle interval the motor is isolated onto the local load. The local load L1 is calculated below from the motor voltage and current before reclosure.

$$\text{Load L1} = \frac{1875 \angle 0°}{27.0 \angle -78°} = 69 \angle 78° = R + jX$$

The stator voltage lagged the source voltage by approximately 50° after 80 msec. and had a decayed value of 1 875 A rms.

The stator current dropped to 27 A rms. at the end of the 4 cycle interval. Upon closing breaker 18L, the stator current jumped to a symmetric 552.5A peak to peak on one phase and one sided peaks of 416.5A on another phase, while 697.0A in the opposite direction on still another phase.

Single and double cage models were used to represent the motor. These models did not include leakage inductance saturation or magnetizing inductance saturation and represented the total lumped sum inertia (H=1.38 seconds) of the motor, flywheel and generator within the motor.

The simulation results shown in Table 1 show the double cage model being closer to the actual voltage on site before the reclosure of breaker 18L. This means that the double cage model of the machine has an open circuit time constant that is closer to the actual machine on site.

	TMECH = 0.460			TMECH = 0.552	
	Single	Double	Actual	Single	Double
Reclosing Current (A rms)	137	129	195		
Final Voltage (V rms)	1760	1789	1875		
Out of phase lag	18°	18°	55°	21.6°	21.6°

TABLE 1

It can also be stated that there is an increase in phase angle with increasing mechanical load on the motor. Since the actual load on the motor is not known (estimated from preopening stator current of 48 A rms) some flexibility can be allowed. Overall, the behavior of the single and double cage models are similar in the operating torque range.

The second test on the site was starting the MG set from standstill. It was run and the results were compared with on-site test results. It was found that the on-site starting currents were 350 A rms. The double cage model gave similar starting currents of 350 A rms. The on-site starting voltages stayed at a constant 4.16 kVrms (line to line) and the simulation of the double and single cage models were similar but with a slight voltage dip on first two cycles (200 V rms L-L) of start up. This dip, seen only on the simulation, represents a more logical description of start up transients and is not seen on the actual site oscillograms because of the error introduced by the thick lined readings.

Starting waveforms were very similar to the oscillogram tests but the torque produced as the motor approached slip speed was not observed (the oscillogram tests were only of a few cycles of starting). Other simulations, however, showed that the single cage model did not accurately represent the actual motor prior to slip speed and was subject to stalling (due to a steep torque slip curve) when the motor had been open circuited and then later resupplied. It was for this reason that the double cage model was used. The actual motor on site was a deep bar motor with a torque slip curve (general to deep bar machines) that more closely resembled the double cage motor. The double cage model removed the problem of stalling when power interruption simulations were run.

The final verification was to model the 3 mass system consisting of the motor, the flywheel and the generator. The full model of the MG set included the 4 KV system, complete modelling of the motor and generator, the couplings, lump sum inertias for each mass, and the 600 V generator load bus. This model simulated the same 4 cycle power interruption previously described. The results were similar to the double cage lump sum inertia model but with higher reclosing currents more closely resembling those on site were noted. Starting currents and voltages were the same as for the lump sum inertia models.

2.5 Summary

The following conclusions can now be made:

1. The double cage model of the motor along with the flywheel and generator models have been verified as adequately modelling the system for this study.

2. Nonlinearities brought into the system by the rubber blocks in the couplings are accurately represented by supplied curves from the manufacturer.

CHAPTER 3 SYSTEM STUDIES

3.1 Torque Production

The development of transient electrical torque can be accomplished by the following procedures:

i) Starting the motor
ii) Step changes in the load
iii) Synchronization of MG sets onto the 600 V bus.
iv) Power interruption over several cycles and then resupplying the power
v) Power interruption as in iii) but with filter banks connected to system

The electrical torque can also be magnified throughout the mechanical system depending on the type of couplings used, the vibration frequency of the shaft system, the damping in the shaft system and the inertia involved.

Initially the cases were all represented with the older 97.08 $kg\text{-}m^2$ flywheel and the older round blocks originally used on site when damage was first noticed. These cases will be presented first and later the other possible configurations will be examined.

3.2 Start Up Transients

One of the areas investigated was the type of torques created during the start-up of the motor-generator sets.

This simulation was of the original system used when damage first occurred (Fig. 8). The MG set was started from standstill under no load conditions. The damping within the rubber blocks was neglected.

Starting torques were noted only in the positive direction (same as rotation) and were small in magnitude (less than 1.0 p.u.). The speed, not shown, could be seen as oscillating and the frequency of the shaft vibration was approximately 7 Hz (Fig. 9).

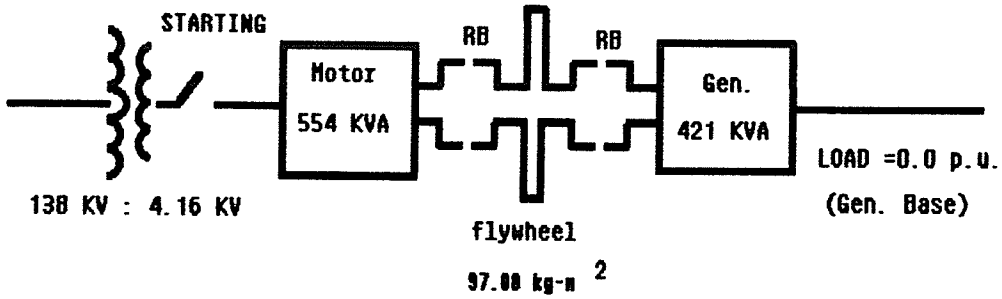

Fig. 8 System Configuration for Starting the MG Sets

Starting from standstill was not the apparent reason for the damaged keys and keyways that were found. Torques encountered in this simulation were too small for this to be the case.

Another simulation was run which started the motor up from half speed under no load conditions. This simulation represented the situation where the power to the MG set had been disconnected for some time and the motor had slowly run down to half speed. The re-starting from this half speed was examined for possible large torques. The same configuration as in Fig. 8 was modelled.

The torques encountered are larger (reaching 6.5 p.u. in Fig. 10) but still not large enough to do damage. Note the initial restarting of the motor from half speed at time zero creates very small torques but as the motor approaches slip speed the larger torques are created which again die out once slip speed has been

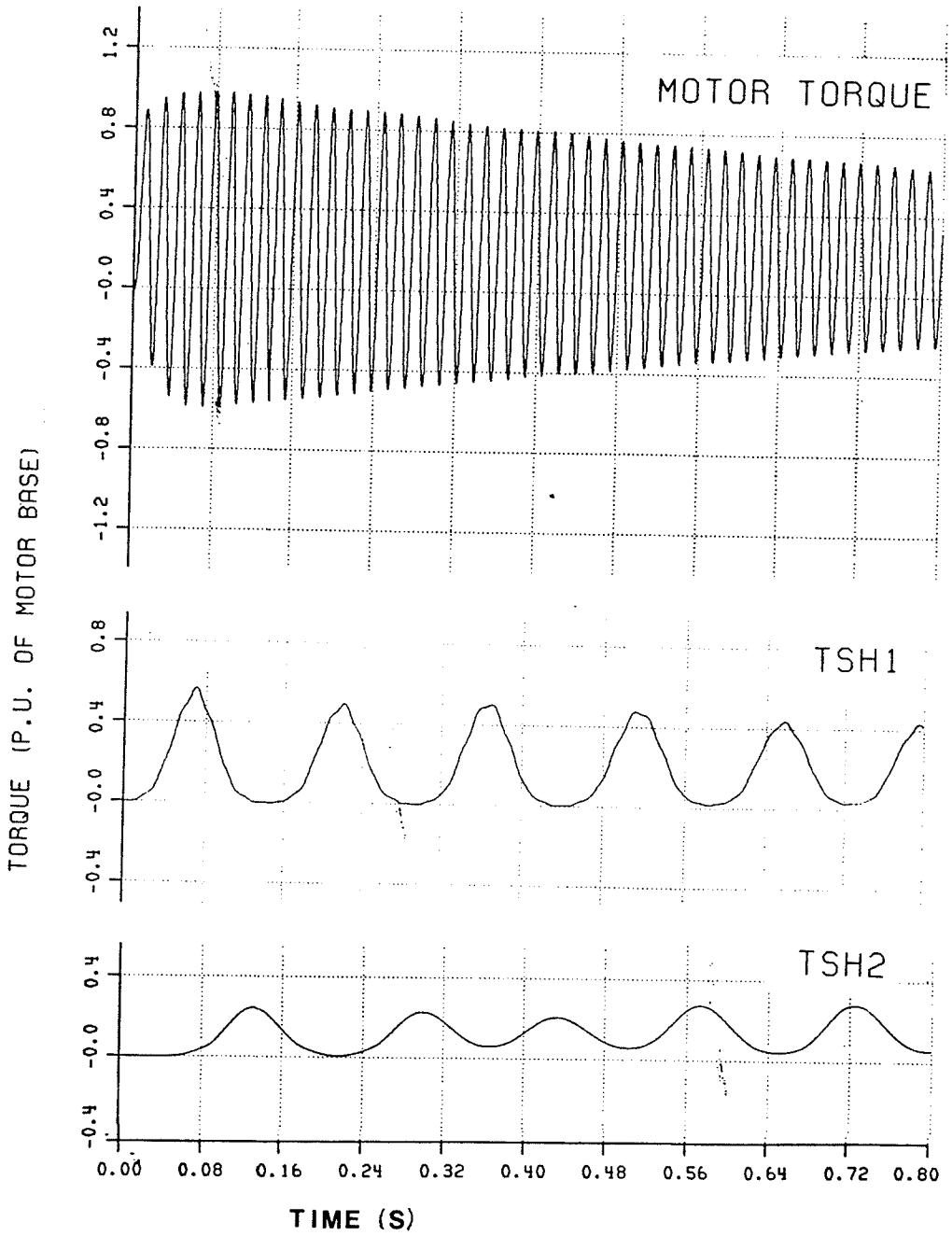

Fig. 9. Torque Waveforms of Starting From Standstill

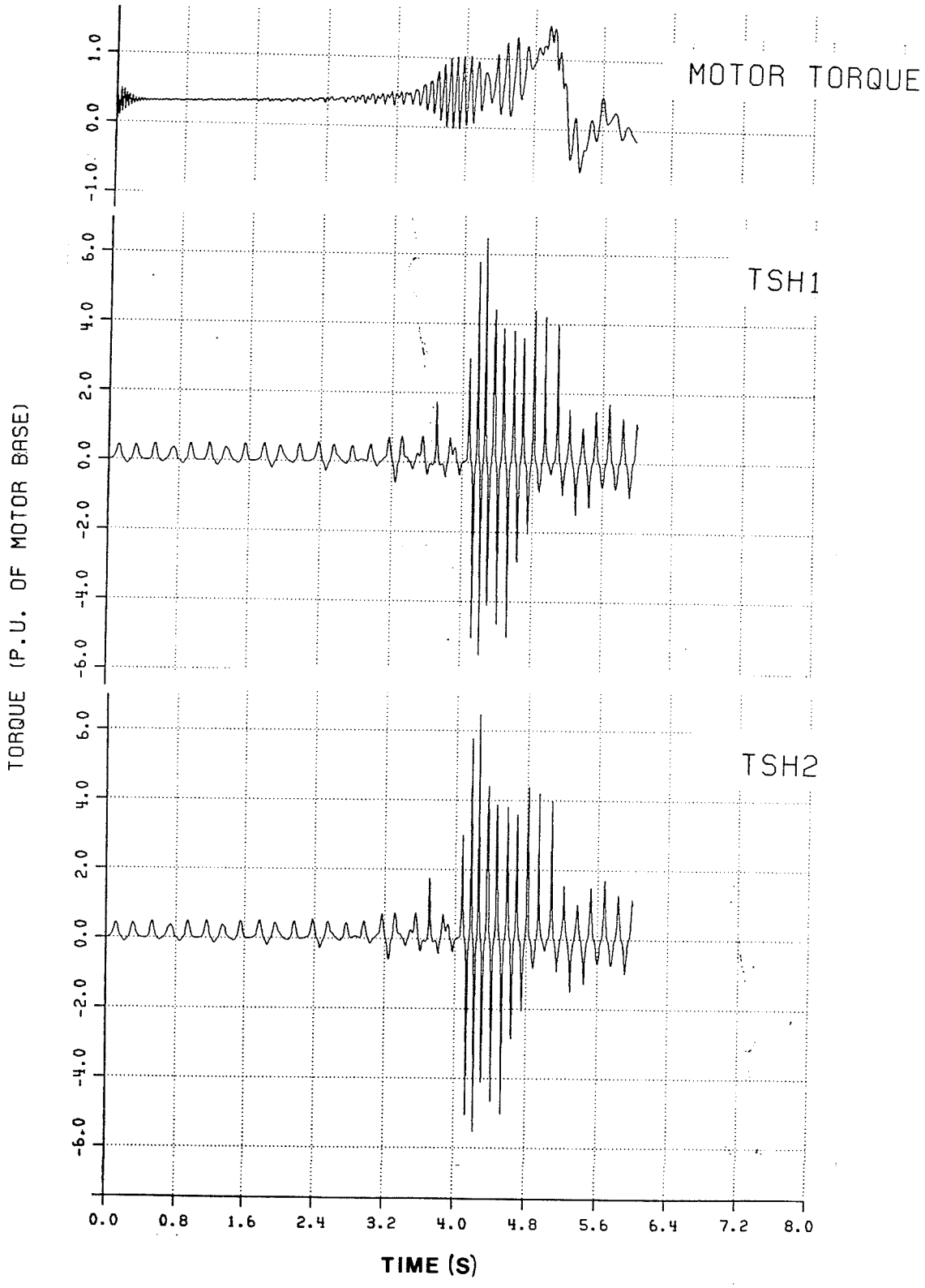

Fig. 10. Torque Waveforms of Starting From Half-Speed

reached. The larger torques are a result of the torque slip curve for the induction motor with the maximum motoring torque being reached before nominal speed.

3.3 Generator Loading Studies

Another area investigated was the type of torques created throughout the shaft system during sudden load changes on the generator. A simple exciter model was developed for the generator (shown in Fig. 11).

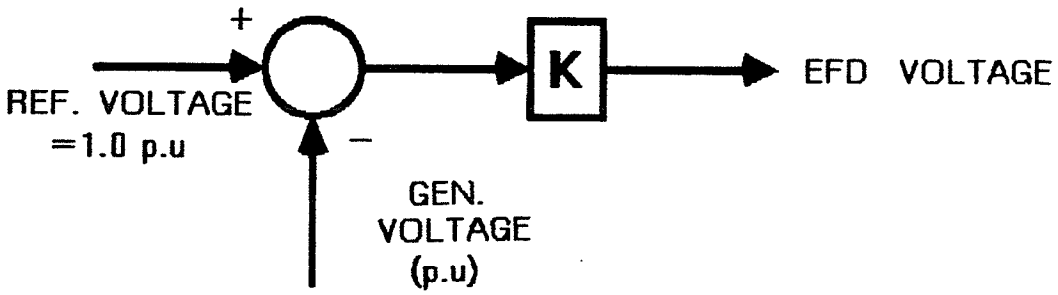

Fig. 11 The Generator Exciter Model

The motor-generator set was run up to steady-state speed and torque. A sudden step increase in the load was applied as the generator load went from 0.05 p.u. to 1.0 p.u. (Fig. 12). Shaft torques bounced between 0.0 and 5.0 p.u. as shown in Fig. 13.

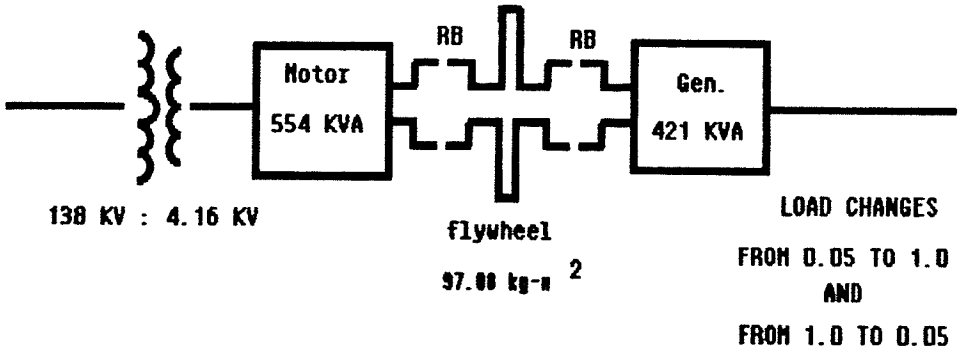

Fig. 12. System Configuration for Sudden Load Changes

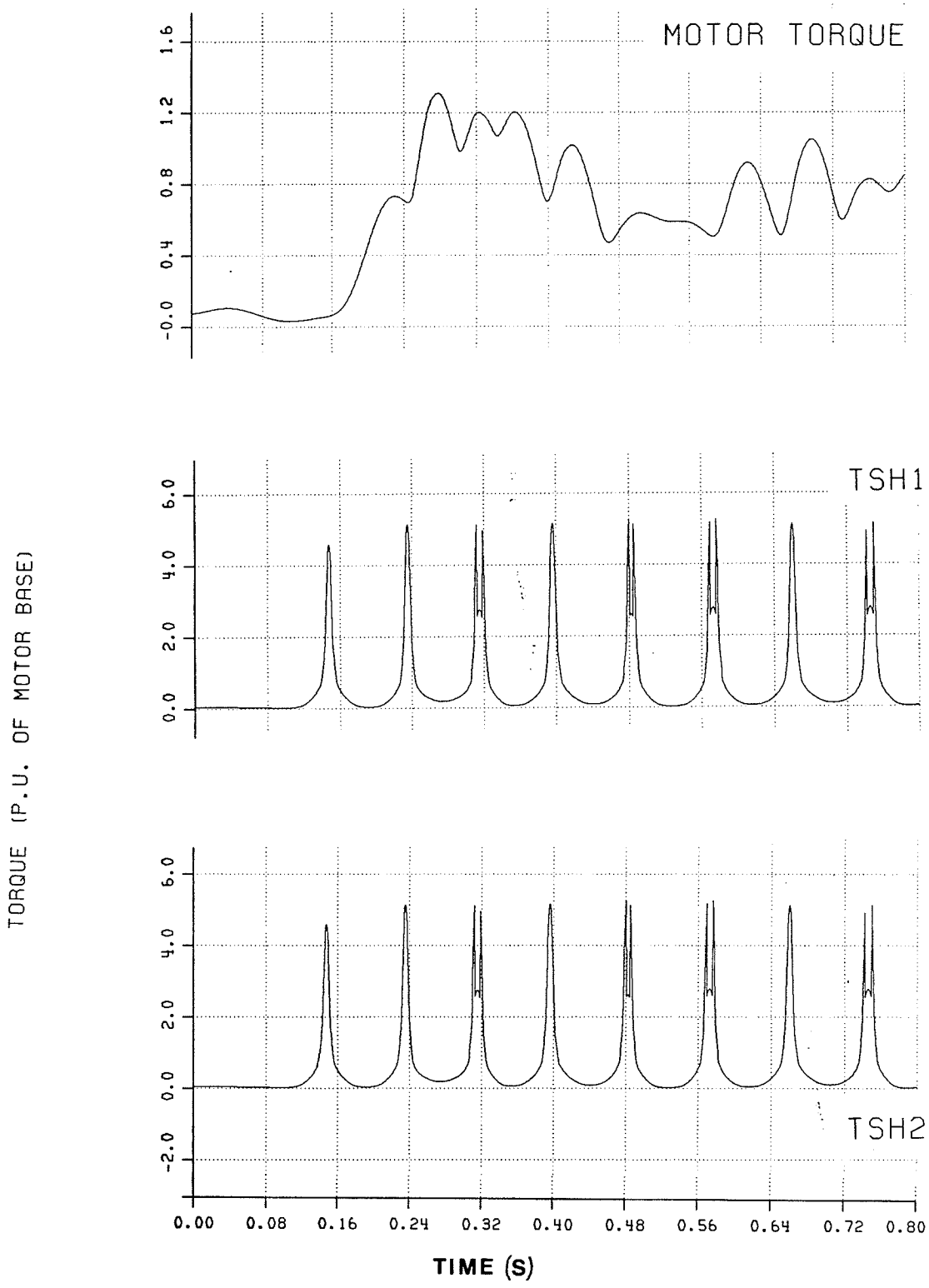

Fig. 13. Sudden Step Increase in the Load on the Generator

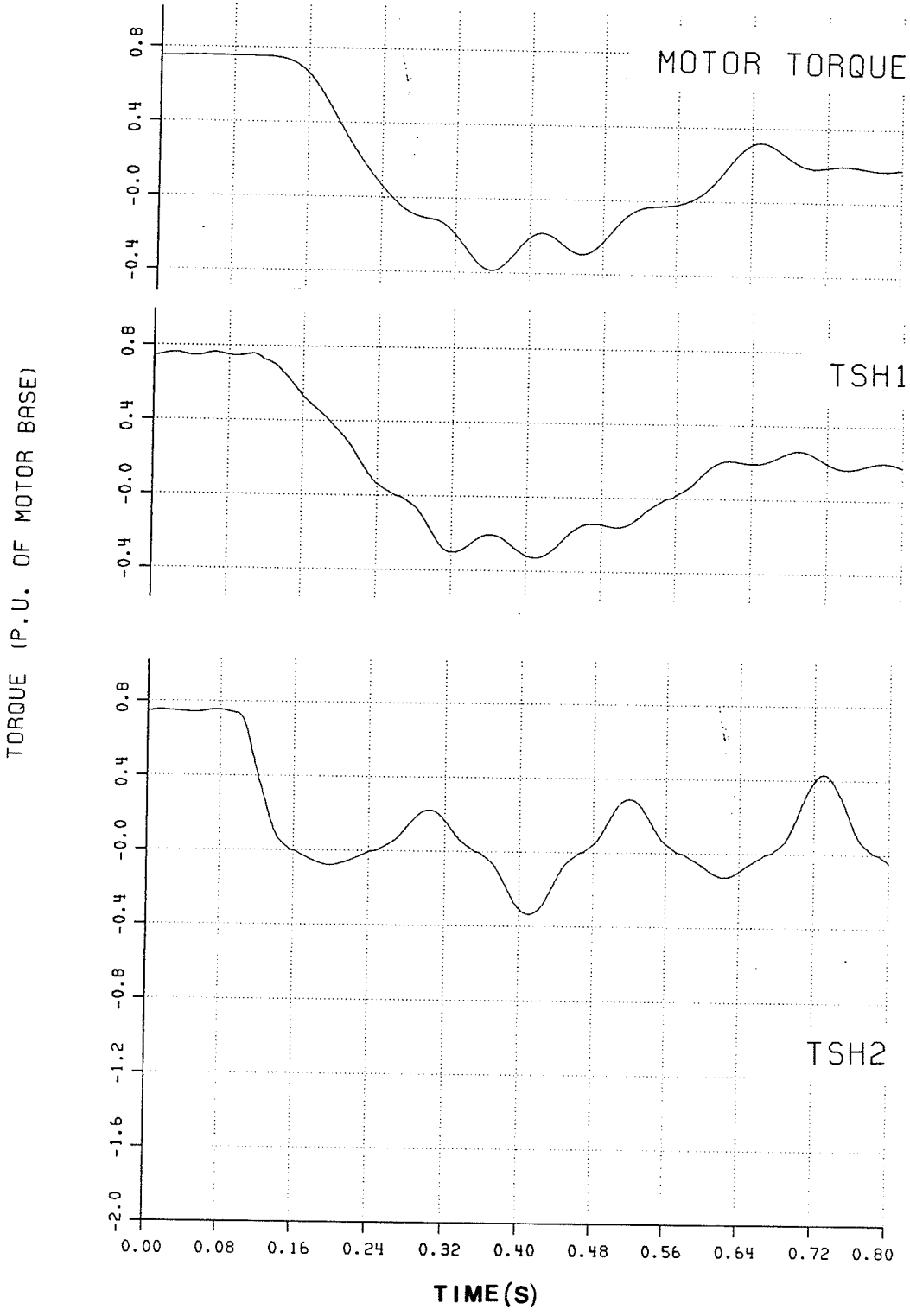

Fig. 14. Sudden Step Decrease in Load on the Generator

It is important to notice that the torques are small and only in the positive direction with this type of disturbance.

Similarly, a sudden step decrease in the load was applied as the generator load went from 1.0 p.u. to 0.05 p.u. Shaft torques dipped only slightly to -0.4 p.u. and settled to 0.25 (Fig. 14). The initial steady-state torque in the plots is 0.76 and not 1.0 p.u. because the motor electrical torque and the shaft torque have all been referred to the motor base (p.u. bases in Appendix E).

The loads on the generator at the site are primarily heaters, fans, and induction motors. Throughout operation it is quite possible to expect such changes as was shown in these two simulation runs. Both cases, in general, have shown that even with extreme load changes on the generator, shaft torques are small and that this is not the cause of shearing of the keys.

Another type of disturbance is created from the generator side when an idle MG set is brought into service and synchronized onto the same 600 V bus. This operation takes place frequently when maintenance is to be performed. The MG set brought into service is started up under no load conditions and then synchronized onto the 600 V bus. During synchronization, because of load sharing, the previously running MG set will experience a load decrease and the newly running MG set will experience a load increase. This, together with the fact that when the new MG set is synchronized it may not be in phase with the bus voltage, will create transient electrical torques on the generators. To fully examine this situation, the synchronization was performed at various phase differences between the bus voltage and the generator voltage of the machine brought into service (Fig. 15). The largest torques were created when the phase difference was around 180° (Fig. 16). This can be explained by the collapsing of voltages on the 600 V bus with a corresponding increase in generator currents. The

exciter and machine time constants then determine how long the transient high electrical torques are produced. In modelling this situation, the exciter was left equal to a constant value (steady-state value) because it was found that without this stipulation, the field voltage stepped up to a very high value and excessively high field currents followed in the few cycles before the exciter field voltage had adjusted. In practice, the exciter would have limits so that the initial slope of the field current could not be arbitrarily large.

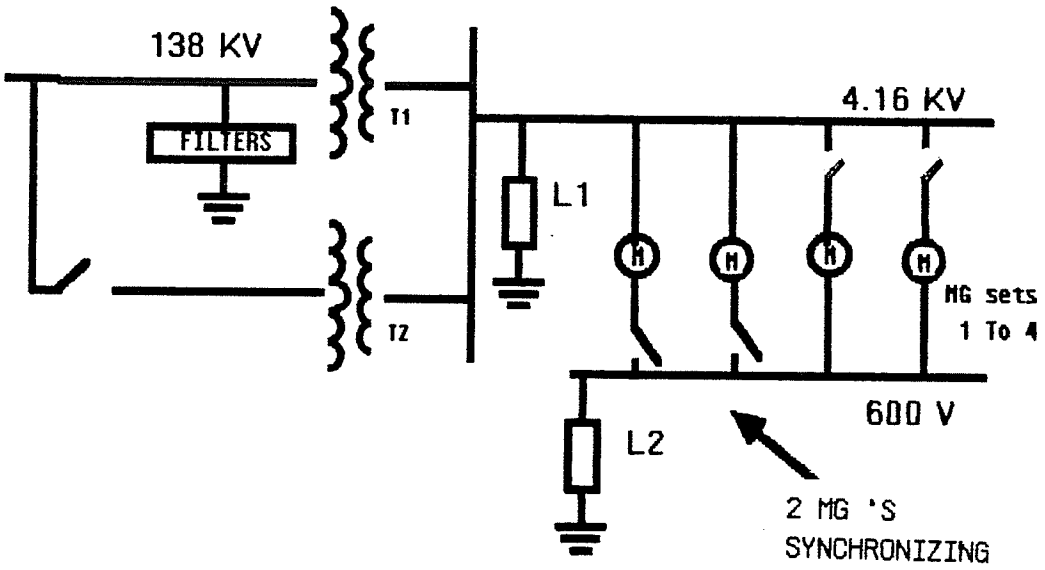

Fig. 15. System Configuration for Synchronization

The simulation (Fig. 16), shows the disturbance lasting for about 6 cycles (elec. torque GEN1 and GEN2). After this time the electrical torque on the running MG set (GEN1) returns to a lower value and the torque on the incoming MG set (GEN2) increases to share the load. The electrical torque created at the generator of the first MG set (previously running loaded) reaches a positive maximum of approximately 2.5 p.u. and then oscillates across zero torque before settling to a positive steady-state torque. This

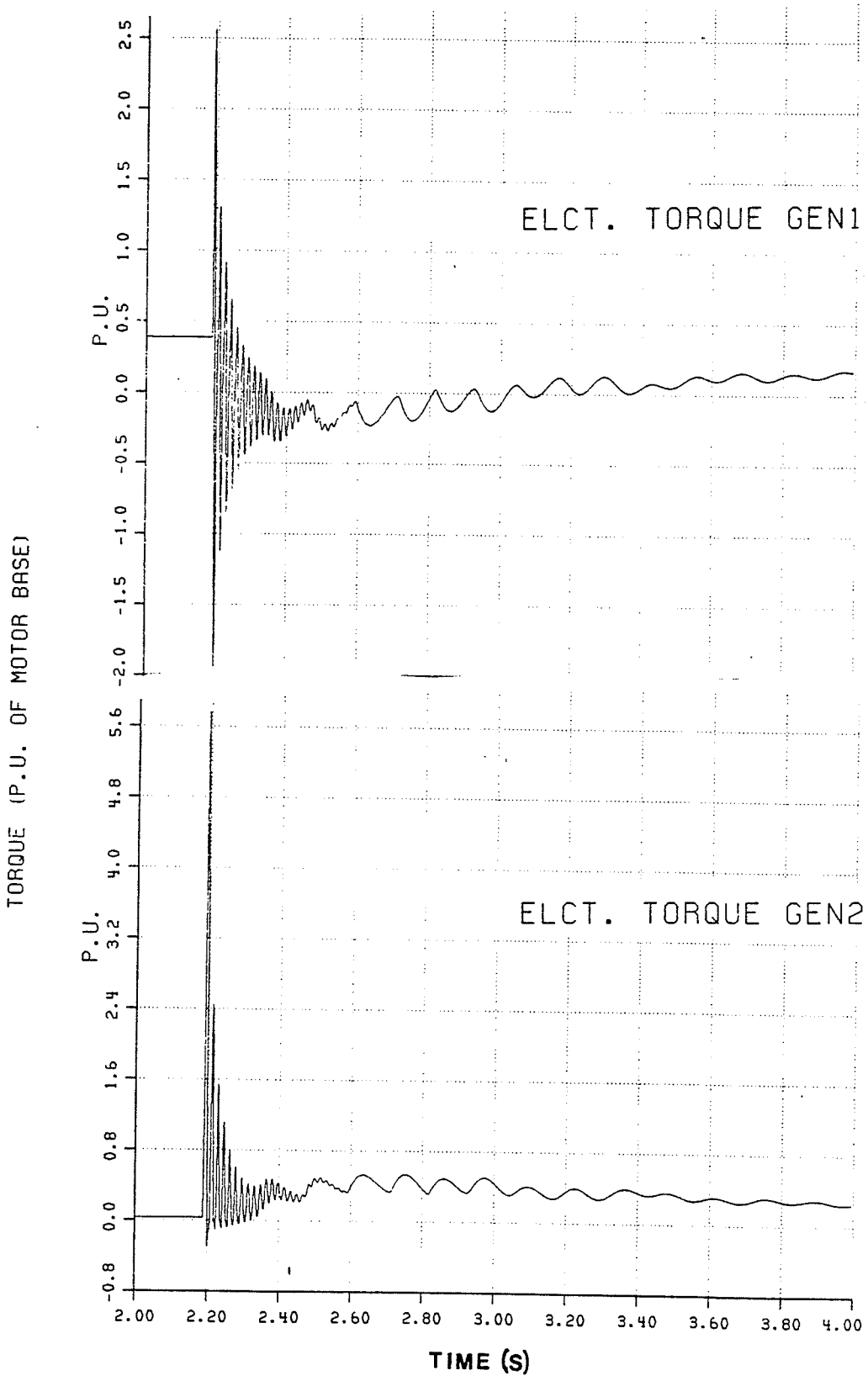

Fig. 16. Generator Torques During 180° Out of Phase Synchronizing.

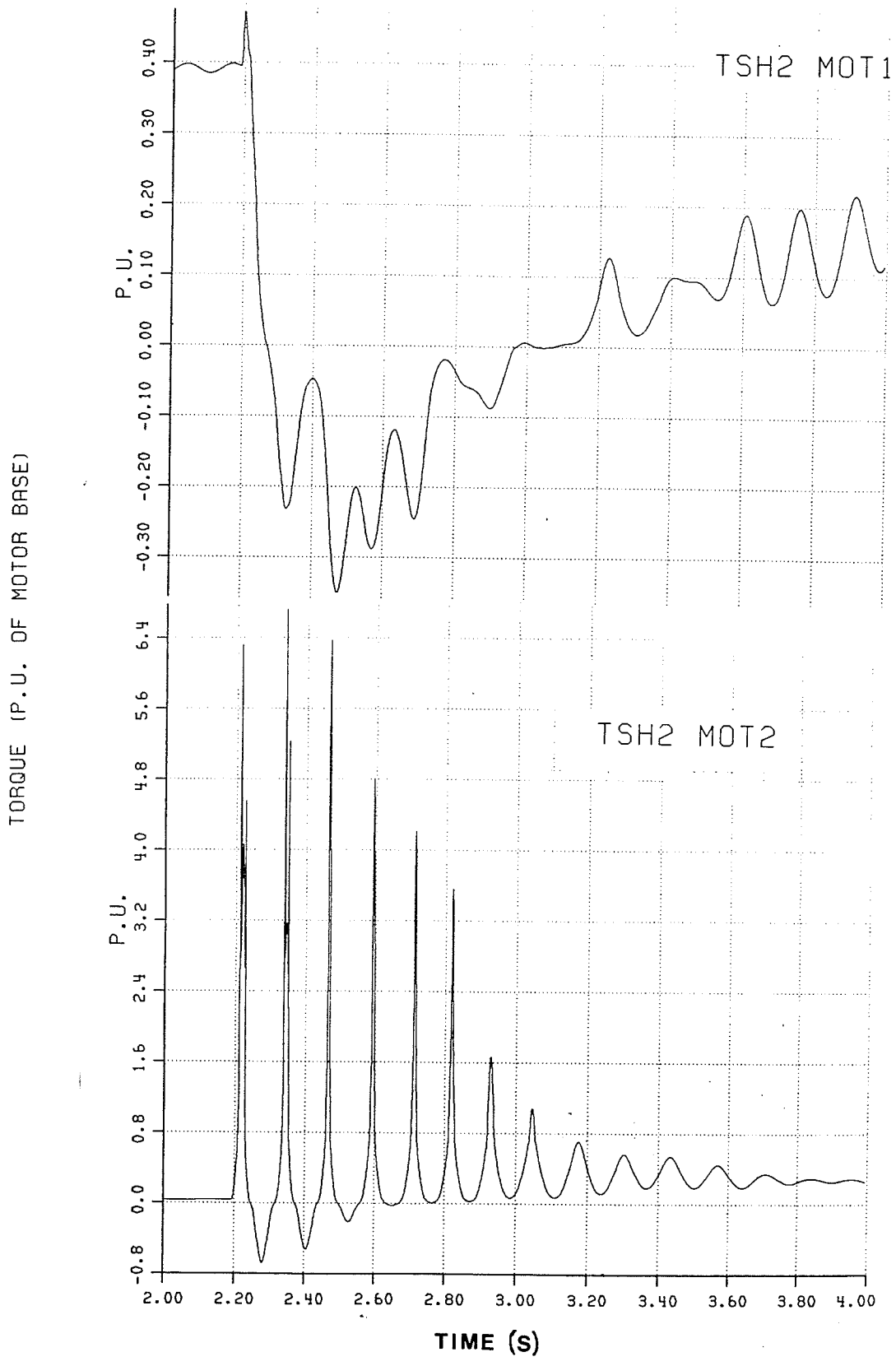

Fig. 17 Shaft Torque at Coupling Between the Flywheel and Generator During 180° Synchronization

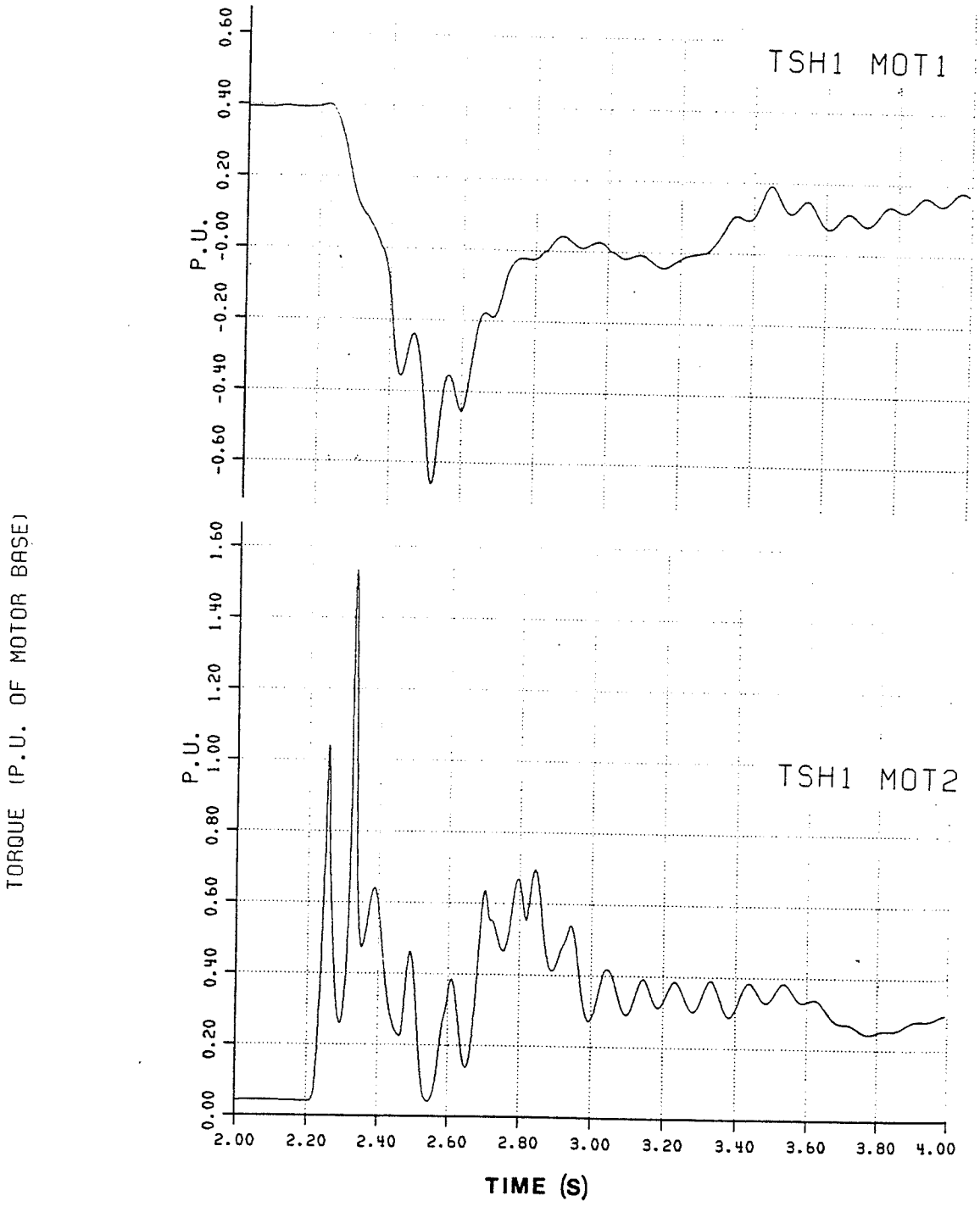

Fig. 18. Shaft Torque at Coupling Between the Motor and Flywheel During 180° Synchronization.

input torque is .35 p.u. torque at the generator side coupling (TSH2MOT1 in Fig. 17), and a slightly magnified .65 p.u. torque at the motor side coupling (TSH1MOT1 in Fig. 18). The electrical torque created at the generator of the incoming MG set (started from no load) reaches a positive maximum of 5.8 p.u. (Fig. 16), and oscillates above zero torque until settling to the same positive steady-state torque as MG set #1. The torques to the generator side coupling (TSH2MOT2) reach values of 7.0 p.u. in the positive direction while motor side coupling torques reach only 1.5 p.u. in the positive direction. This simulation shows that even with the worst case synchronization (180° out of phase) the torques created on the shaft are not large enough to cause damage. Another observation is that synchronization creates torques in the negative direction on the already running MG set which are small and creates torques in the positive direction on the MG set being synchronized onto the bus which are larger (7.0 p.u.).

3.4 Reclosing of the Motor Supply

Simulations were run which represented the case of open-circuiting the power supply to the motor for a few cycles and then later reconnecting the supply. Various delay times between open circuiting and reclosing were used. As before, the original system which consists of the old flywheel and round block couplings was first represented (Fig. 19). This situation arises under normal operating conditions during typical bus transfers.

Large negative torques (10 p.u.) are created when the delay time is around 25 cycles (Fig. 20). This 25 cycles delay time between open-circuit and reclosure is excessively long for typical automatic breaker operation. The 25 cycle delay time (approximately 0.4 sec.) is also too quick for the possibility of manual reclosing after the open-circuit of the breaker is detected. This means that although large negative torques can be

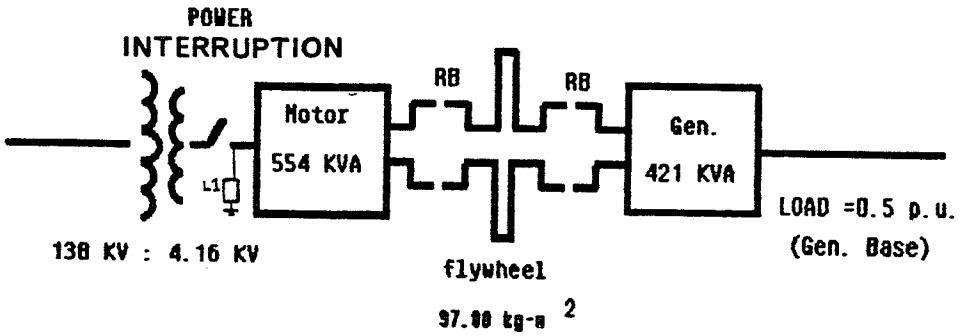

Fig. 19. System Configuration for Power Supply Interruption

created by simple power interruption to the motor, in practice they would never occur. For simulations with the typical delay time of 4-9 cycles for automatic breaker operation, the torques developed are positive and small in nature (Fig. 21).

It should be noted that the system (Fig. 19) does not include the damping within the rubber blocks. As can be seen the input motor electrical torque is negative as is the first torque on the coupling between the motor and flywheel (TSH1), but subsequent torques are positive and also quite large. This is because without damping the couplings are behaving like undamped springs and torque is seen in both direcitons. Later, damping will also be estimated for this configuration, but for now since the 25 cycle delay time is not practical, it is sufficient to show possible problems associated without damping.

It can also be noted that the torques appearing at the second coupling TSH2 (between the flywheel and the generator) are significantly smaller (less than 6 p.u. This is a product of the type of electrical motor torque created in this case, the fact that the disturbance is created at the motor side (motor electrical torque is the input disturbance), the system configuration modelled, and the delay time.

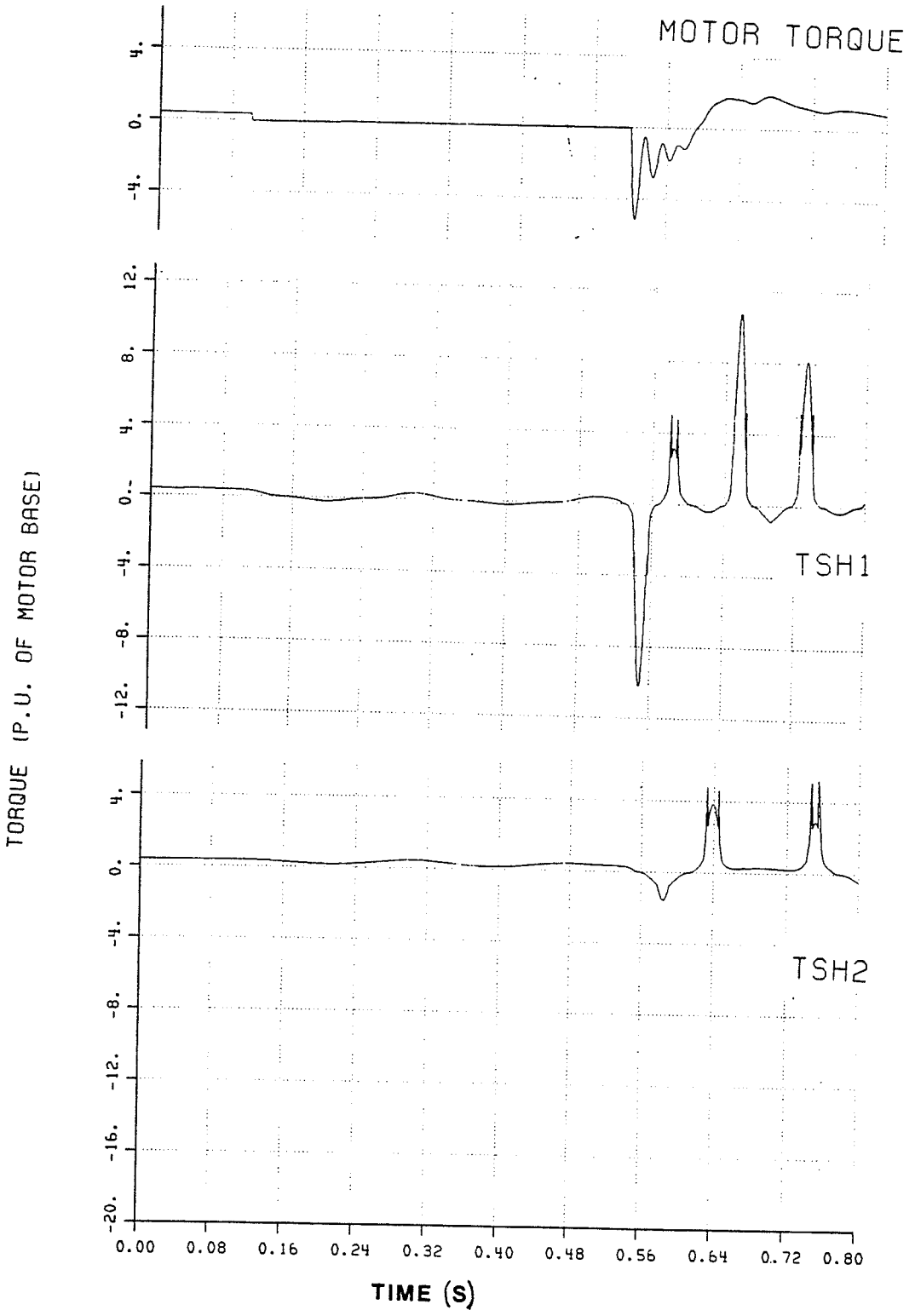

Fig. 20. Power Interruption of 25 Cycles

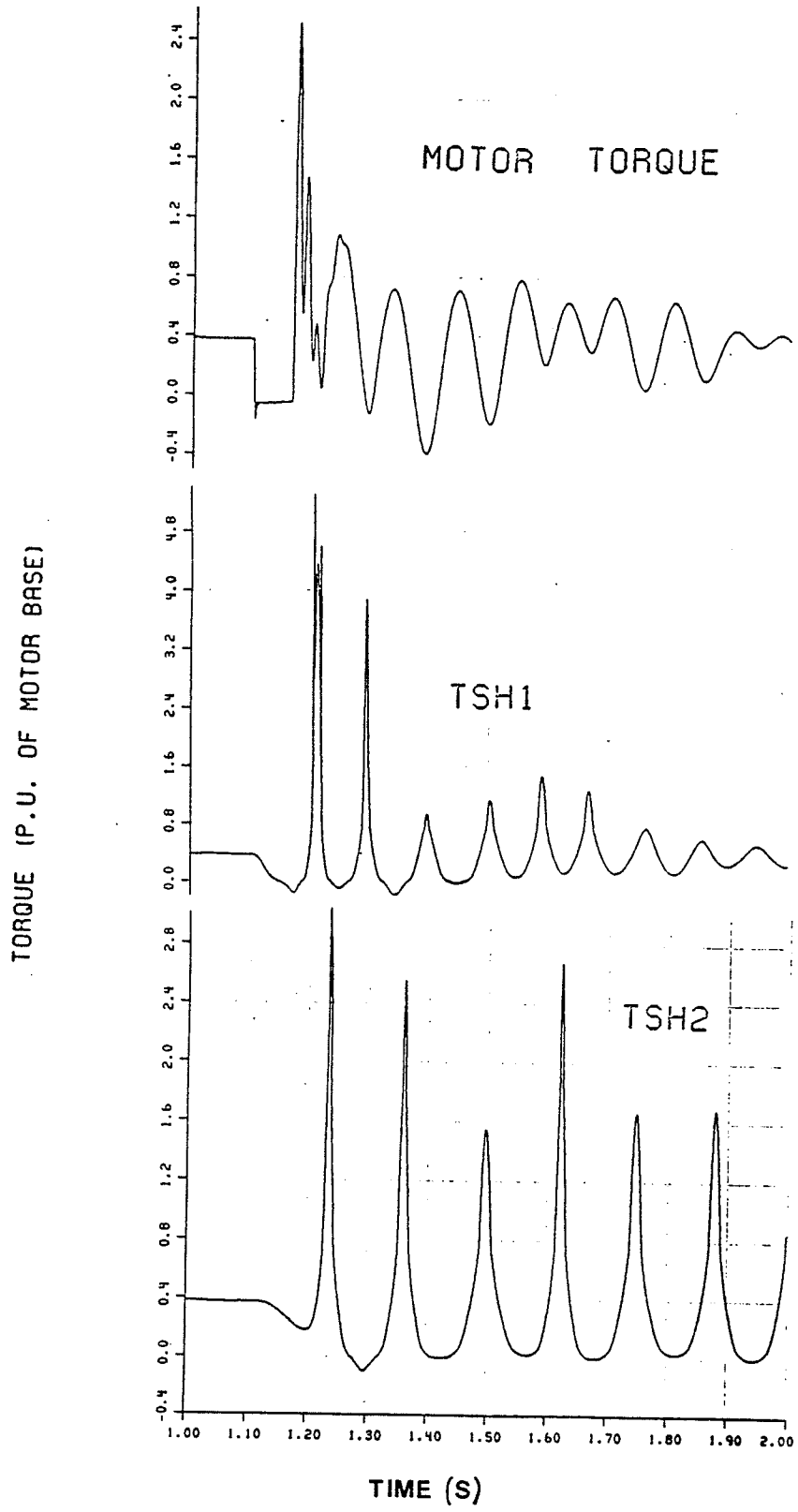

Fig. 21. Power Interruption of 4 Cycles

Other system configurations were also examined. The new system configurations depicted the coupling behavior to the same motor torque input but with different parameters for the flywheel inertia and the rubber block stiffness. To begin with the present system of the new flywheel (46.60 Kg-m^2) and wedge blocks were represented (Fig. 22). The maximum negative torque with the new system now occurs with a 20 1/4 cycle delay time between open-circuit and reclosure of the power supply to the motor. Again, without damping, the torques can be seen in both directions and reach a negative maximum of -11.0 p.u. This suggests that the new system is similar to the old system for torque due to some cancellation of the effects due to the type of blocks and the flywheel used.

The torques created at both couplings TSH1 and TSH2 appear similar in this case and we have a translation of the torque between the motor and flywheel coupling to the flywheel and generator coupling with this configuration.

To further investigate why the new system creates larger torques, configurations of the round block with the new flywheel and the wedge block with old flywheel were also run. The round block and new flywheel create a maximum negative torque of only 8 p.u. occurring at a 22 3/4 cycles delay time while the wedge block and old flywheel create a maximum negative torque of 13.7 p.u. at a 25 3/4 cycle delay. The lighter flywheel reduced torques created at the coupling between the motor and flywheel, while increasing the torque at the coupling between the flywheel and the generator. That is, there is a more even distribution of torques with the lighter flywheel. The wedge blocks basically increased torques created at both couplings. Hence, the best system suggested is the round block and new flywheel whereas the worst configuration would be the wedge block and old flywheel. These simulations suggest the round block couplings reduce the shaft torques rather than the stiffer wedge blocks. A closer

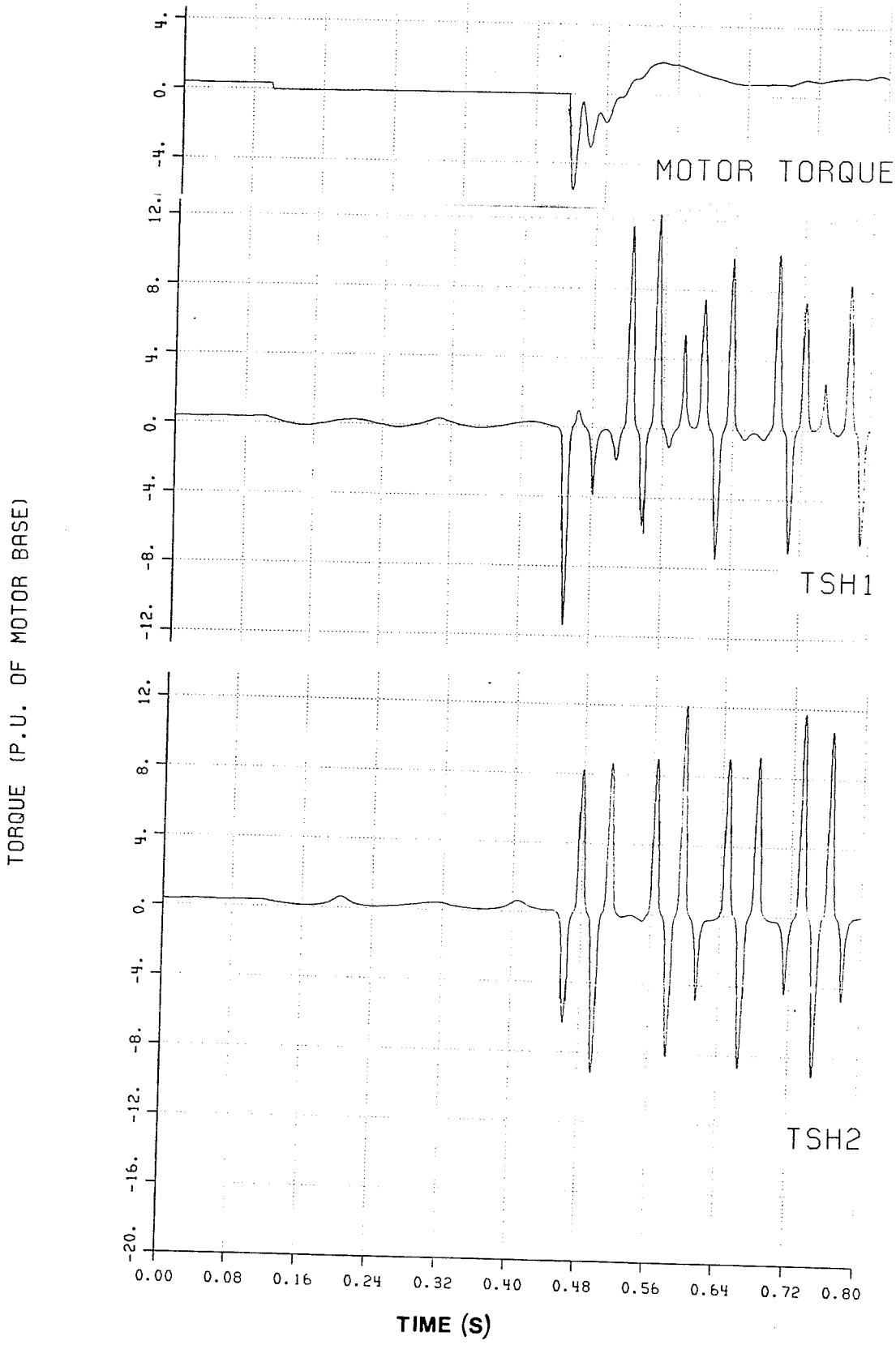

Fig. 22 Power Interruption With New Flywheel and Wedge Blocks

examination of the round and wedge block behaviour is shown in Appendix B.

It can be seen that there is no deadband area in the round blocks. That is there is no area where the angle deflection does not produce a torque and associated K stiffness. The round block couplings for our size coupling are sufficiently stiff in low deflection regions to not have to use the stiffer wedge blocks.

Finally, the damping behaviour of the rubber blocks should be included in the simulation. The original system of old flywheel and round block couplings was modelled. The first damping estimate of D = 151 N•m/rad/sec will be used within the rubber. Simulating the worst case where a delay time of 25 cycles is used, the negative torque created is about 8 p.u. with subsequent positive torques reaching only 5 p.u. (Fig. 23). As stated earlier, this damping estimate is from the manufacturer and is estimated for steady state analysis only. With the second damping estimate of D=947 N•m/rad/sec for transient conditions, the negative torque reaches 6.0 p.u. (Fig. 24). These simulations depict a more logical representation of the coupling behaviour and show that torques in the region of 8.5 p.u. (responsible for damage) are not evident in the original system even with non-practical delay times while damping of the round blocks is included.

Next, the new system consisting of the lighter new flywheel and wedge blocks was simulated with damping included in the wedge blocks (Fig. 25 and 26). Again, the worst case where a delay time of 20 1/4 cycles was run. The addition of damping significantly reduced torques at both the next coupling (TSH2) and subsequent oscillations. With the larger damping estimate (Fig. 26) torques are even smaller at both couplings.

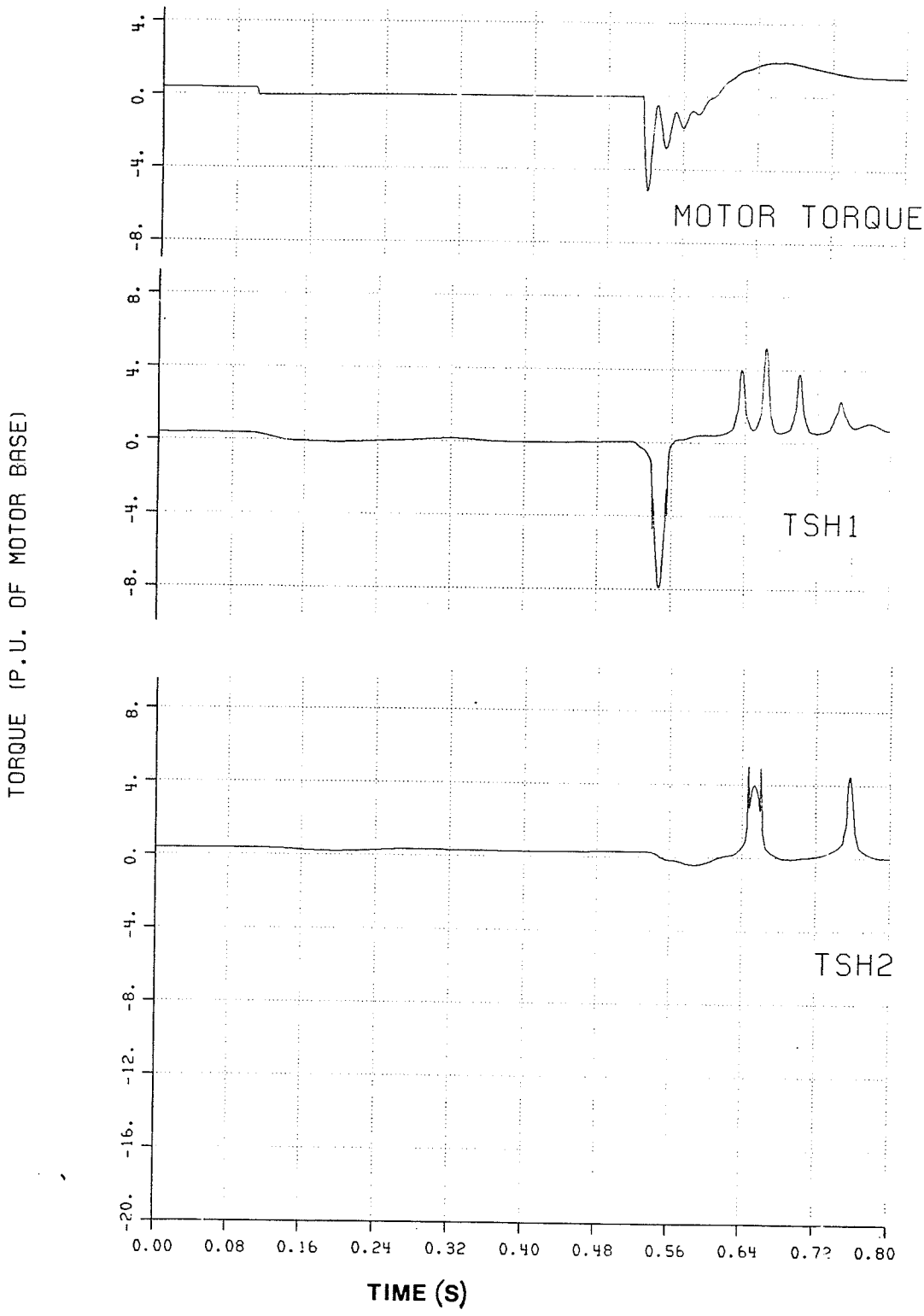

Fig. 23. Power Interruption With the Manufacturer's Estimate of Damping within the Round Blocks

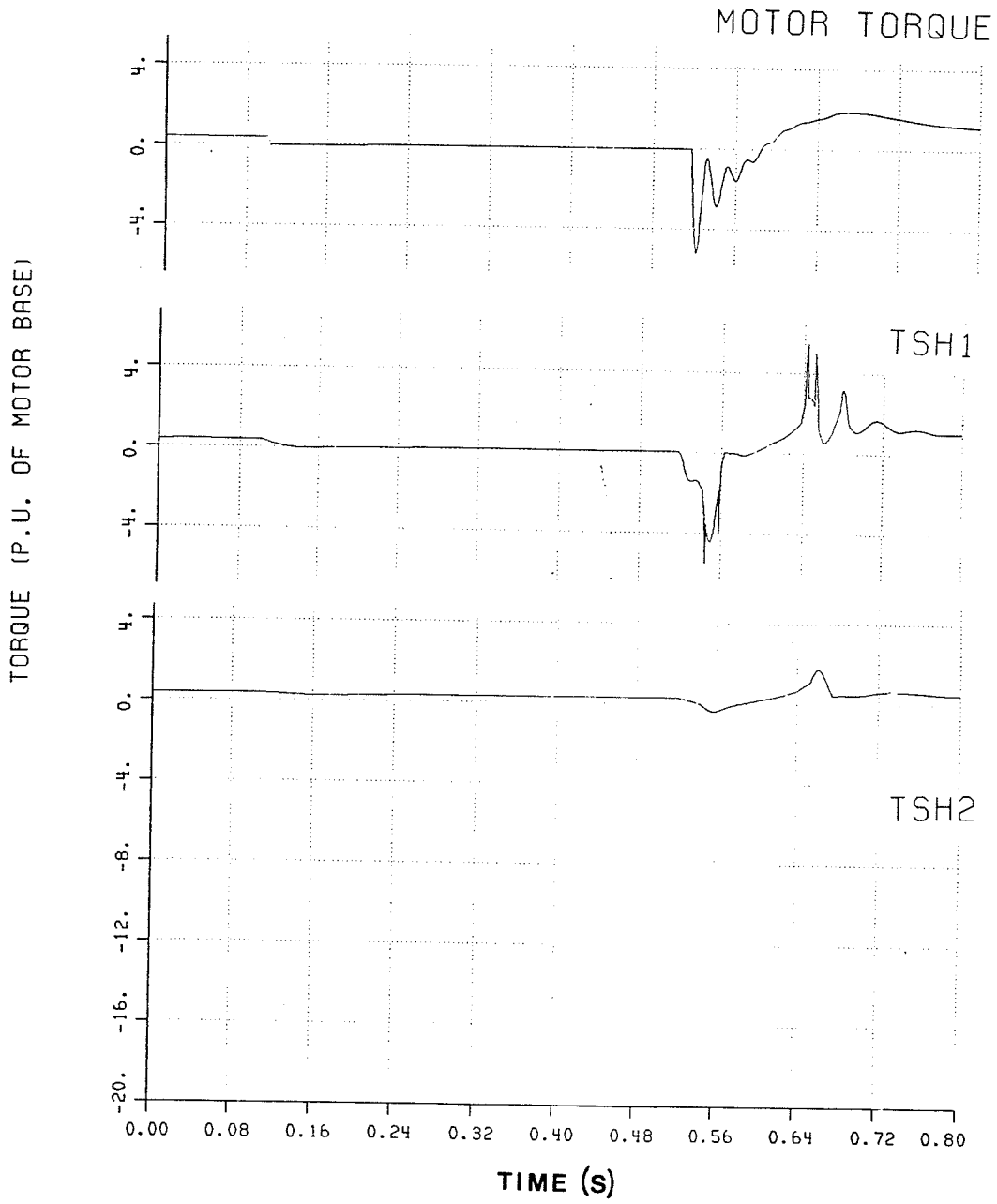

Fig. 24. Power Interruption With the Larger Estimate of Damping Within the Round Blocks

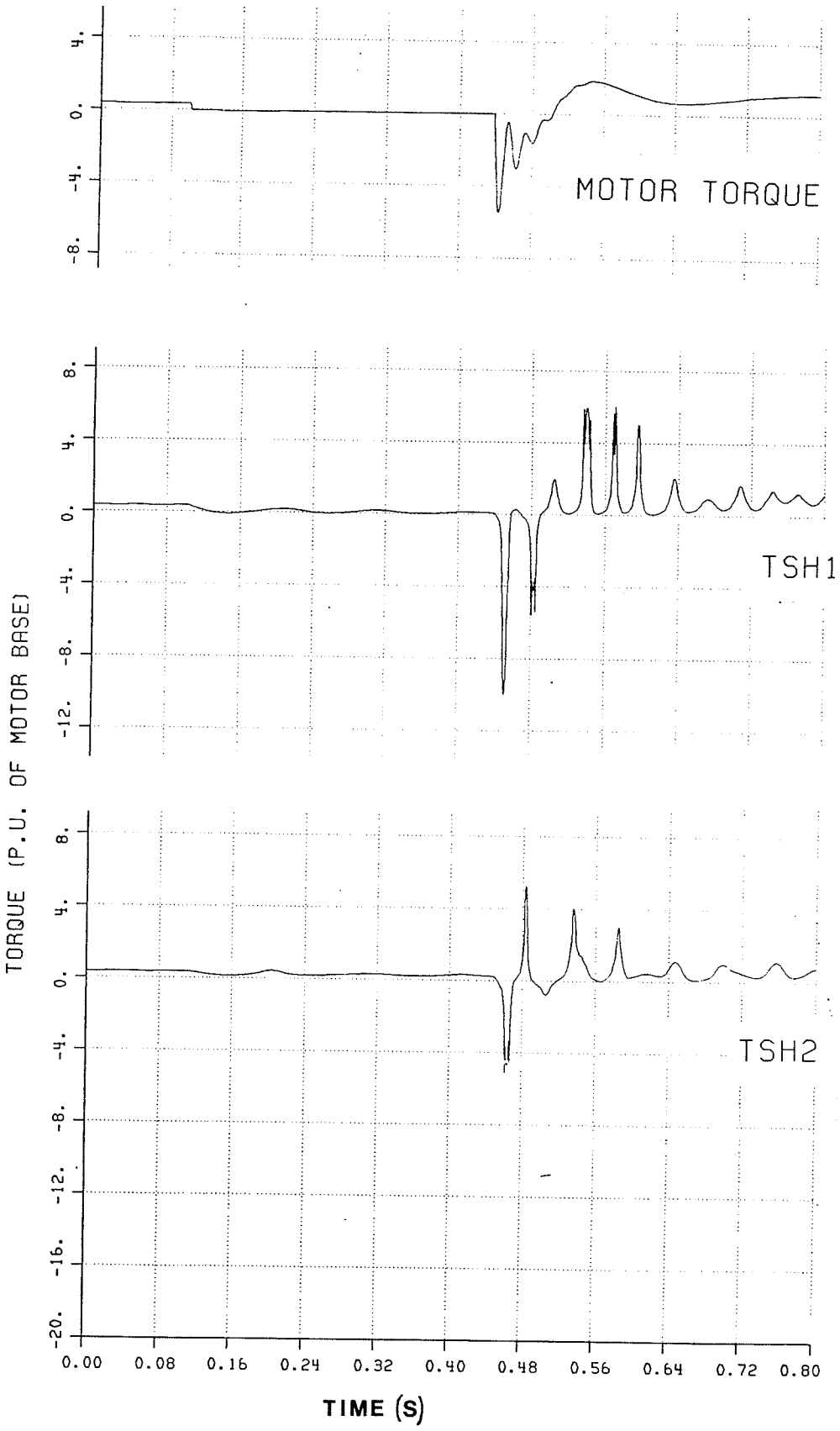

Fig. 25 Power Interruption With New Flywheel and Wedge Blocks Using The Manufacturer's Estimate of Damping

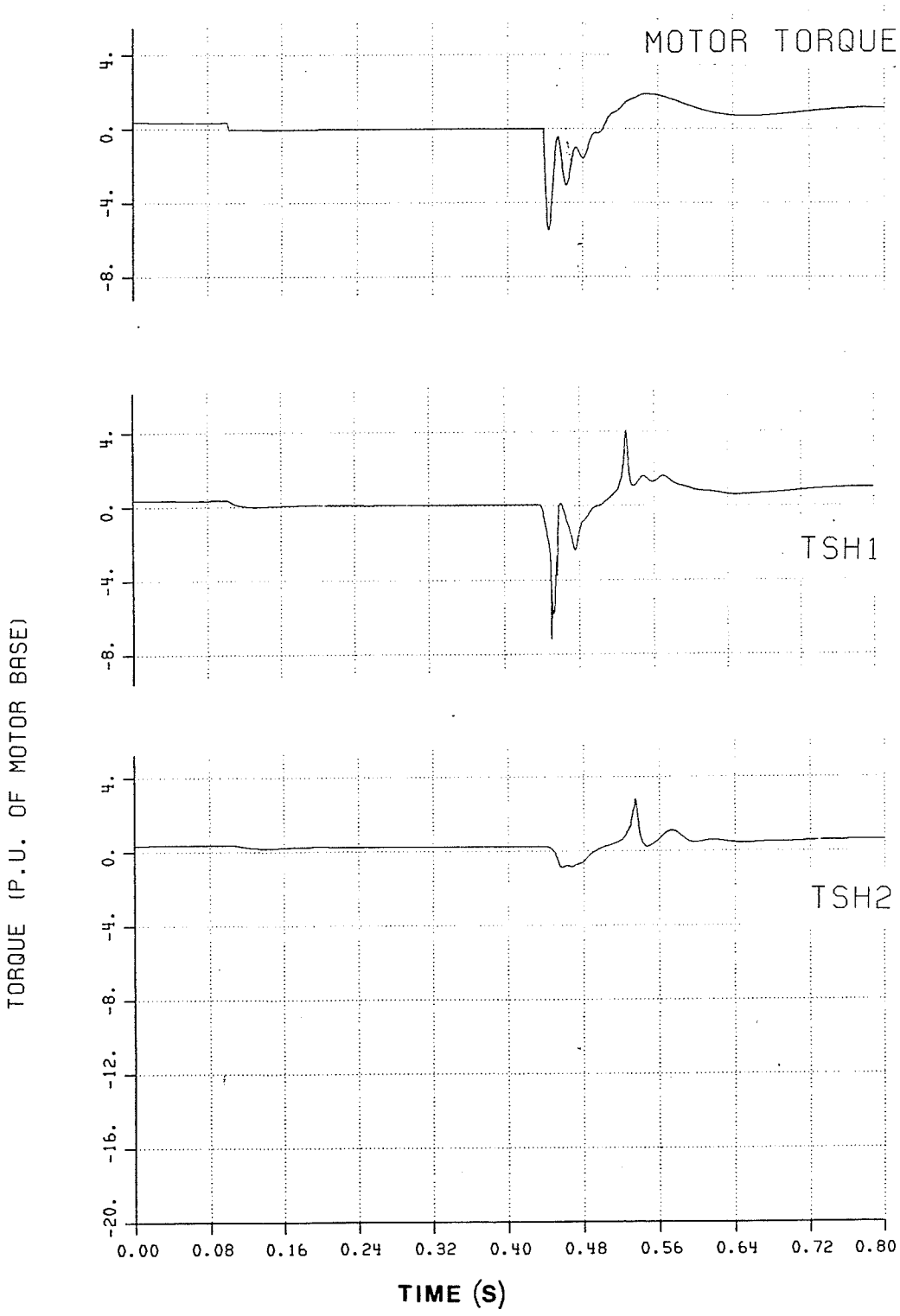

Fig. 26. Power Interruption With New Flywheel and Wedge Blocks Using the Larger Damping Estimate

In all the cases the motor electrical torques are similar but depending on how the damping within the rubber block, the type of rubber block, or the inertia of the flywheel was represented, the torques created at the two couplings will vary. Damping reduces torques after the initial negative torque as well as reducing the translation of torque to the second coupling. In looking for the cause of the problem, the undamped system represents the worst case. Power interruption to the motor creates potentially large negative torques at the coupling between the motor and the flywheel but only with a delay time of around 25 cycles which is not practical. The more logical representation of the system including damping creates only smaller torques with the same delay time of 25 cycles. The type of rubber block and the flywheel inertia represented has the effect of changing the cycle duration of the interruption at which the maximum shaft torques occur along with the type of torques created. The cycle duration of power interruption varied between 20 1/4 cycles and 25 3/4 cycles. Note that even the 20 1/4 cycle delay is much longer than the typical breaker reclosure of 4-9 cycles. The worst system configuration found was one which included the heavier old flywheel and the stiffer wedge blocks while the best configuration included the new lighter flywheel and the more resilient round rubber blocks.

3.5 HV Breaker Opening (Isolation of 4 kV bus on 138 kV filters)

The next area investigated was the type of torques created if the filter banks on the high voltage side were included in the study system and the high voltage breaker was opened (Fig. 27).

These filter banks now included are needed for filtering 5th, 7th and 11th harmonics present in the system. The total filter bank MVAR is approximately 80 MVAR (for more detail see Appendix A, Electrical Paramaters). In normal operation the low side breaker (4.16 kV) would be opened first. That is, if there was a fault on the 4 kV bus, when maintenance is to be done on the filter banks

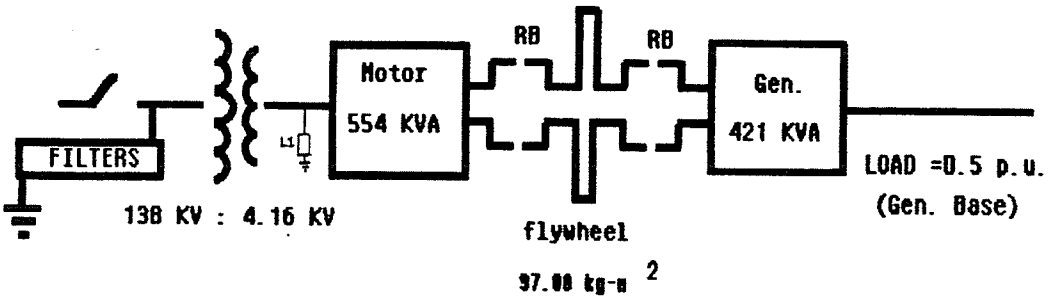

Fig. 27.

System Configuration for HV Breaker Opening with Filter Banks Included

or when a fault occurs on the filter bank (protection) in which a bus transfer to the 4 kV bus will take place initiated by the opening of the 4 kV breaker (4-9 cycles later another bus will supply the 4 kV bus). However, if a fault occurred on the 138 kV bus according to the operators it is possible for the 138 kV breaker to open first. This is the situation of interest.

Simulations were run depicting the case where the high voltage breaker had opened for a few cycles (9 cycles) and then reclosed. The motor electrical torque created is larger than the previous study of power interruption with the filter banks not included. The torque is also predominately negative and is independent of the reclosure time. The type of torque transmitted to the shaft is an initial negative torque to the coupling between the motor and flywheel of 12 p.u. which is quite large. Subsequent torques continue to oscillate as this initial run does not include damping and for this same reason torques at the second coupling between the flywheel and generator are similar (Fig. 29).

The motor voltage and motor current shown in Fig. 30 indicate what is happening to produce the high torque. The motor voltage has dropped and become closer to a D.C. voltage while the motor current has increased from the previous 40 A rms value to 2.3 KA peak which quickly decays and oscillates at a low frequency. Superimposed on the motor current and voltage waveform during the interruption is a frequency close to 60 Hz due to the rotor flux and the fact the motor is still turning.

Analytically these results can be confirmed by reduction of the system to a parallel capacitor-inductance equivalent system (Fig. 28).

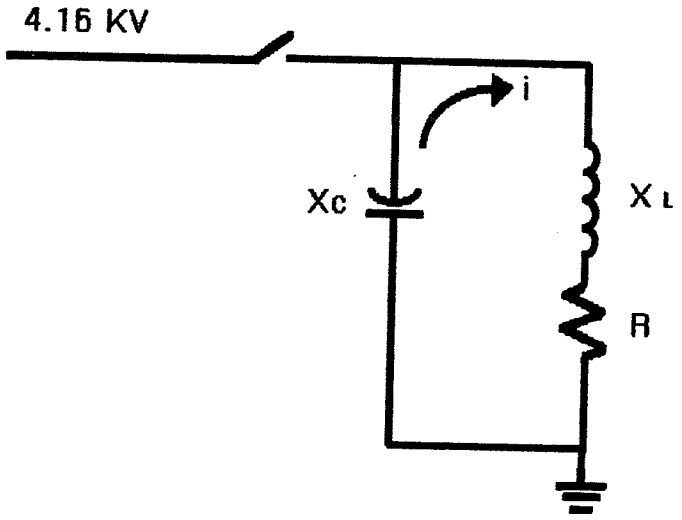

Fig. 28. Equivalent Filter Bank - Motor System

The equivalent capacitance of the filter bank brought to the low side of the transformer can be calculated from the MVAR rating as follows:

$$X_c = \frac{(2.402 \text{ kV/phase})^2}{26.38 \text{ MVAR/phase}} = j\ 0.219\ \Omega$$

giving a capacitor value of 0.012F.

The actual filter banks are tuned to filter out 5th, 7th and 11th harmonics. They include resistance and inductance in series with the capacitance. In order to simplify analysis the filter bank has been reduced to only capacitance.

The inductance of the MG set can be calculated from the equivalent circuit of the MG set.

$$X''_d = X_a + \frac{Xmd\ (Xf + Xkf)}{Xmd + Xf + Xkf} = 0.241 \text{ p.u. } (7.53\Omega)$$

Hence, $$L_m = \frac{7.53}{377} = 0.02 \text{ H}$$

For the transformer inductance we have:

$$Ibase = \frac{2.5MVA/phase}{2.402x10^3V} = 1040A.$$

$$Z_b = \frac{2.402x10^3V}{1040A} = 2.3\,\Omega$$

Assuming the transformer inductance at 10% as we have for the program we set

$$L_t = \frac{.23}{377} = 0.0006H$$

This makes the total inductance equal to:

$$L = L_m + L_t = 0.0206H$$

The resistance R is unknown and is predominately rotor resistance of the motor.

The energy, Wc, in the capacitor before t = 0 is

$$W_c = 1/2CV_O2 = 1/2(0.012)(\sqrt{2}\cdot(2.4 \times 10^3))^2$$
$$= 69.2 \text{ KJ}$$

Note: Before t=0 the small impedance $X_c=0.219\Omega$ is essentially a short circuit when compared to $X_L = 7.77\,\Omega$. This means the current Io = 0 before t=0 and the energy W_L in the inductor is

zero. After t=0 the energy in the capacitor is transferred to the inductor and resistance R. The energy transferred to the resistance is dissipated in damping forces and accounts for the decay in the current and voltage waveforms (Fig. 30). On the assumption that the capacitor is precharged to the peak voltage Vc and no current is flowing in the inductor, the solution of the circuit in Fig. 30 gives:

$$i = \frac{Vc}{wL} \exp[-\alpha t] \sin wt \text{ and}$$

$$Vc = Vc \exp[-\alpha t] \cos wt \text{ for small values of R}$$

$$\text{Where } w_o = 1/\sqrt{LC} \quad , \alpha = \frac{R}{2L} \quad , w = \sqrt{w_o^2 - \alpha^2}$$

Using $Vc = \sqrt{2} \cdot 2400$ V

$w_o = 63.6$ rad/s (= 10 Hz), and $\alpha = 0$

$i = 2592 \sin wt$ A

This is in good agreement with Fig. 30 where the current peak is 2300A after a quarter cycle and the resonant frequency is 9 to 10 Hz. From Fig. 30, it is obvious that there is considerable damping which must have been produced through the electromechanical torque on the motor. At the first peak of the current, the stored energy in the system was $1/2\ i^2L = 54.5$ KJ while at second (negative) peak of the current the stored energy was only 5.9 KJ and the difference of 48.6 KJ was the energy supplied to the shaft system of the induction motor. This energy was reflected in the high torques experienced by the motor. Another approximation to the torques produced may be derived from the steady state torque slip characteristics of the induction motor shown in Fig. 31 for both the prefault case (w = 377 rad/s) and the post fault case (w = 63.6 rad/s). The operating torque (motoring) quickly swings to generating torque which causes a negative torque to be produced at the motor which is translated throughout the shaft system. The generating torque that is shown is assuming steady state operation (i.e., if the electrical

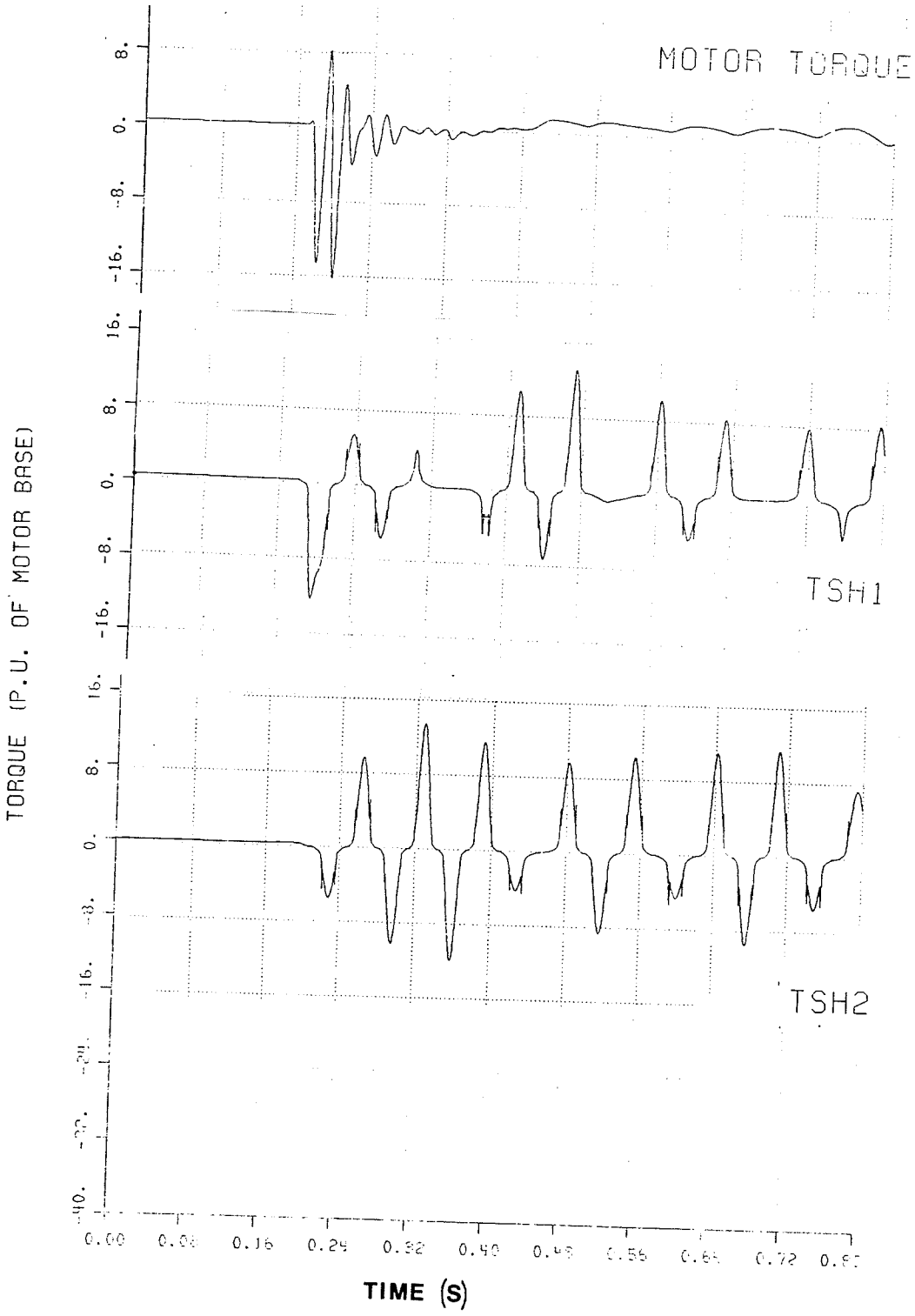

Fig. 29 Torques Created on HV Breaker Opening

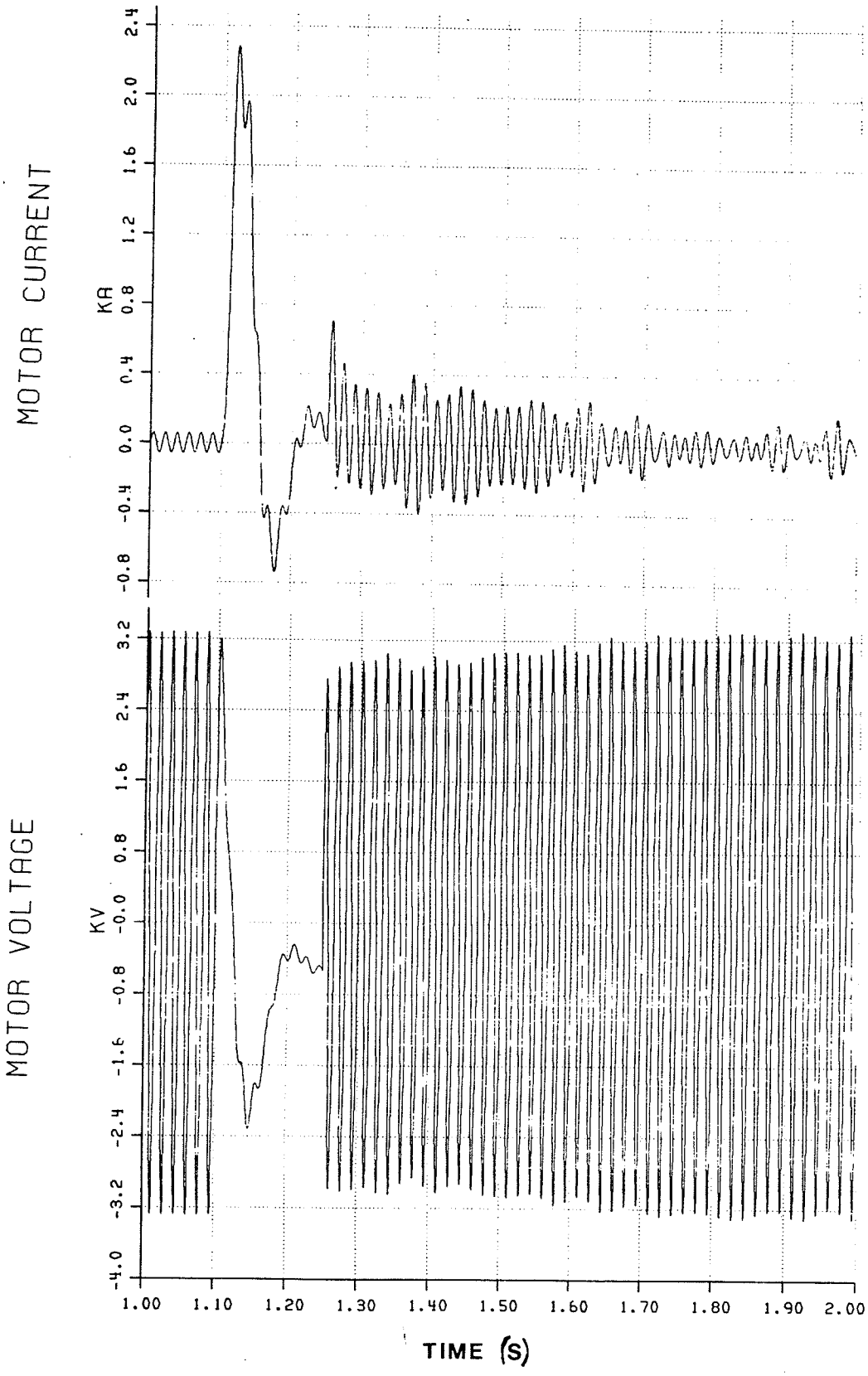

Fig. 30 Voltage and Current Waveforms During HV Breaker Opening

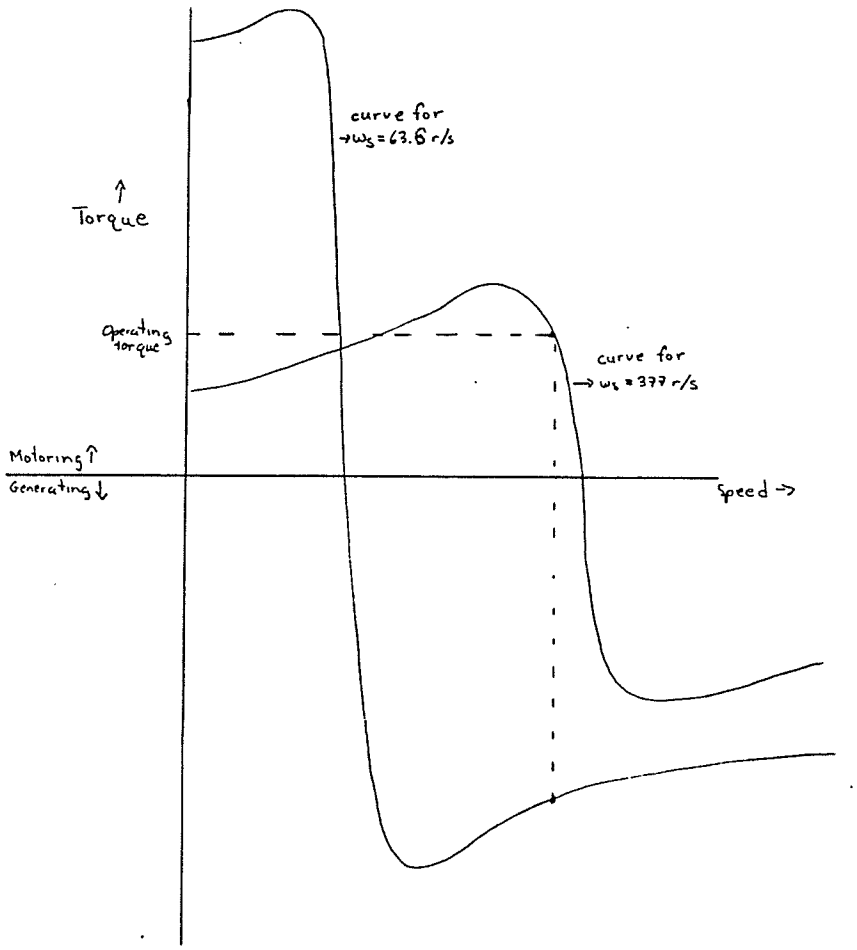

Fig. 31 Steady State Torque Speed Curves

frequency, remained at 63.6 rad/s) while the actual response is under transient conditions and the generating torque is seen as a braking torque (torque in the opposite direction of rotation).

The correct modelling of damping within the system now becomes quite important since the original system is represented here for a case where 12 p.u. torques could appear on the shaft system (capable of causing damage) under practical operating conditions. Again with the original system modelled when damage first occurred, another simulation was run which included the manufacturer's estimate for the damping within the rubber blocks of the couplings. The damping does not affect the electrical motor torque but the torque created at the first and second couplings is affected. The torque created between the motor and flywheel is initiated with a negative torque again, but not quite as large as before (10 p.u.). Subsequent torques at this first coupling are less than 6.0 p.u. and oscillate in both positive and negative directions until decaying to the original load torque value (Fig. 32).

Torques created at the second coupling between the flywheel and the generator are less than 7.0 p.u. and oscillate until decaying to the original load torque value.

The value of 10 p.u. torque created between the motor and flywheel is a critical value. As stated earlier, 11 p.u. torque is needed to initially break the shrink-fit and subsequent torques larger than 8.5 p.u. would contribute to shearing the key. The torques created at the second coupling between the flywheel and generator would be too small to do damage. The torques created after the initial negative torque at the first coupling between the motor and flywheel would also be too small to do damage. This leaves the initial torque created between the motor and flywheel of 10 p.u. that could have damaged the keys and keyways. The damping value used in this case of 151 N•m/rad/sec is only a

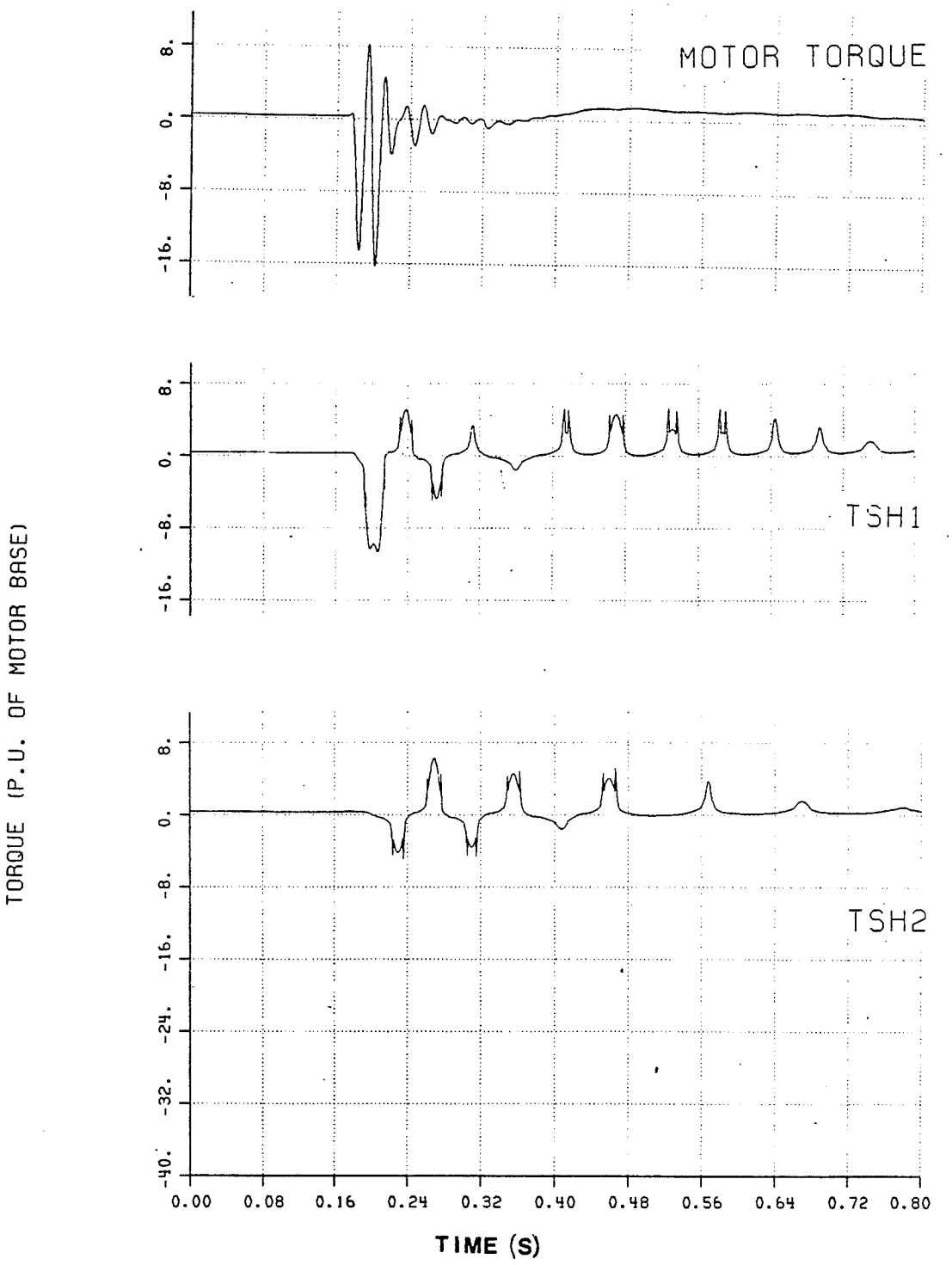

Fig. 32. HV Breaker Opening with Manufacturer's Estimate of Damping Within the Round Blocks

manufacturer's estimate of the rubber block damping under steady-state conditions. Since our case is not under steady-state conditions, a second damping estimate was also simulated (Fig. 33). With this larger estimate of 947 N.m/rad/sec estimated for transient conditions, the motor electrical torque remained the same as expected but the torque created between the motor and the flywheel reached 15 p.u. in the negative direction. Subsequent torques at this first coupling as well as all the torques at the second coupling remained under 4 p.u.

Potentially damaging torques are therefore created with the original system (round block and heavier flywheel) with both the manufacturer's estimate for damping within the rubber under steady-state conditions and with the larger estimate for transient conditions. With the manufacturer's estimate for damping, torques of 10 p.u. are created while with the larger estimate of damping, torques of 15 p.u. are created. In both cases the torques are negative and at the coupling between the motor and flywheel.

The present system was then modelled which represents the stiffer wedge blocks and the new lighter flywheel (Fig. 34). As usual, the motor electrical torque remains the same but the torque created at the first coupling between the motor and flywheel is amplified to 96 p.u. in both positive and negative directions. This mechanical resonance is produced by the type of input electrical motor torque and the system configuration of the lighter flywheel and stiffer wedge blocks. The torques created at the coupling between the flywheel and generator are smaller 20 p.u. but still large enough to do damage.

The same case simulated with the first estimate (manufacturer's steady-state estimate) for damping within the rubber blocks created torques of 65 p.u. in both directions (Fig. 35) at the coupling between the motor and flywheel. The mechancial resonance is somewhat damped now. The torques created at the coupling

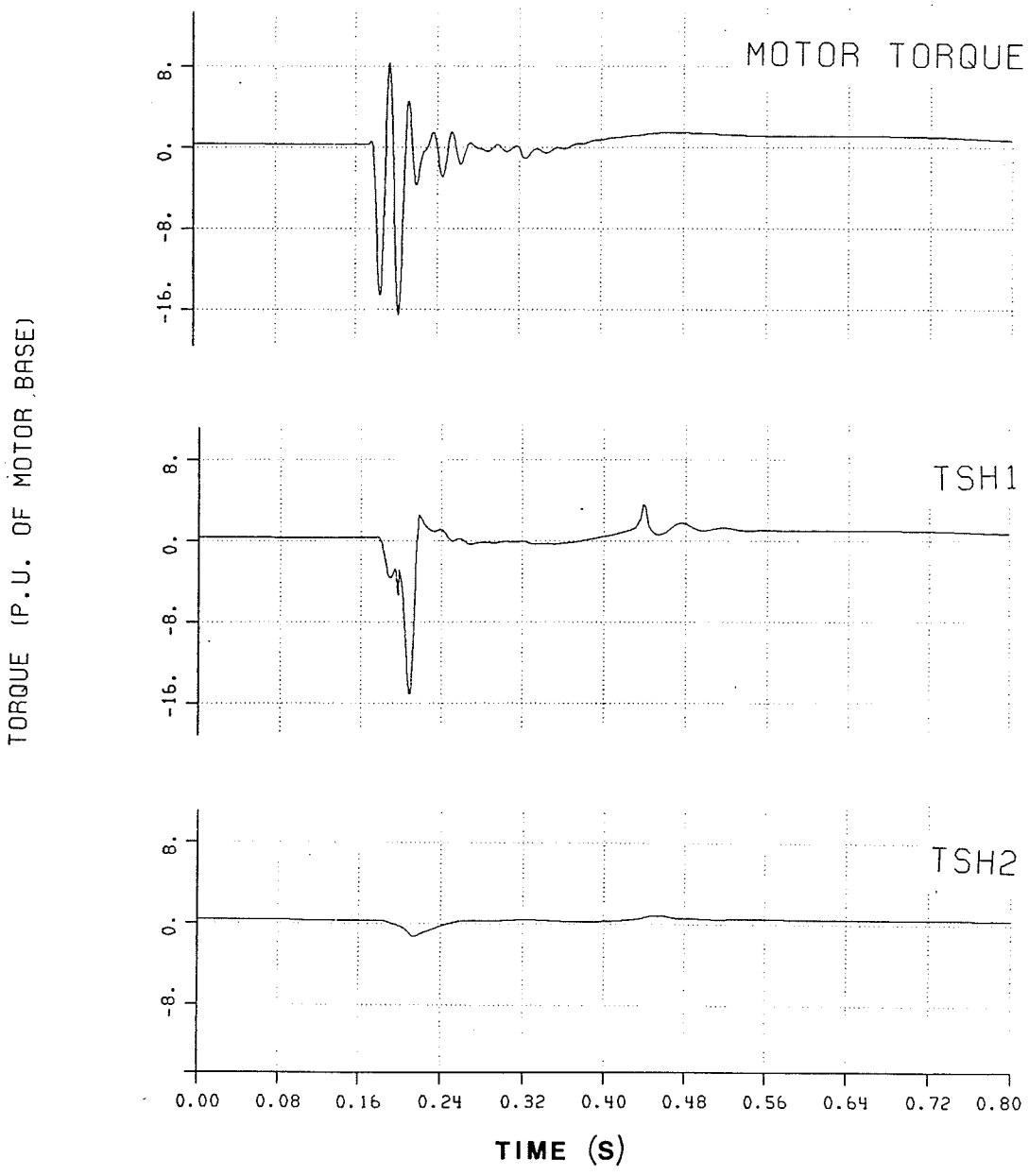

Fig. 33. HV Breaker Opening with The Larger Estimate of Damping Within the Round Blocks

between the flywheel and generator are 15 p.u. in both directons which is still capable of doing damage.

Finally, the same case was simulated with the second estimate (larger estimate for transient conditions) for damping within the rubber blocks (Fig. 36). The torques that are created at the coupling between the motor and flywheel are 20 p.u. and only in the negative direction. Positive torques at this first coupling are less than 8.0 p.u. Torques created at the second coupling between the flywheel and generator are less than 8.0 p.u. in both positive and negative directions.

The high voltage breaker opening across the filter bank exposes a situation where high torques occur throughout the shaft system. The damage that has occurred to the keys and keyways is best explained by the modelling of the original system with the second damping estimate of the rubber blocks. The present system of lighter flywheel and stiffer wedge blocks does not remove the problem and a change in operating procedures is suggested.

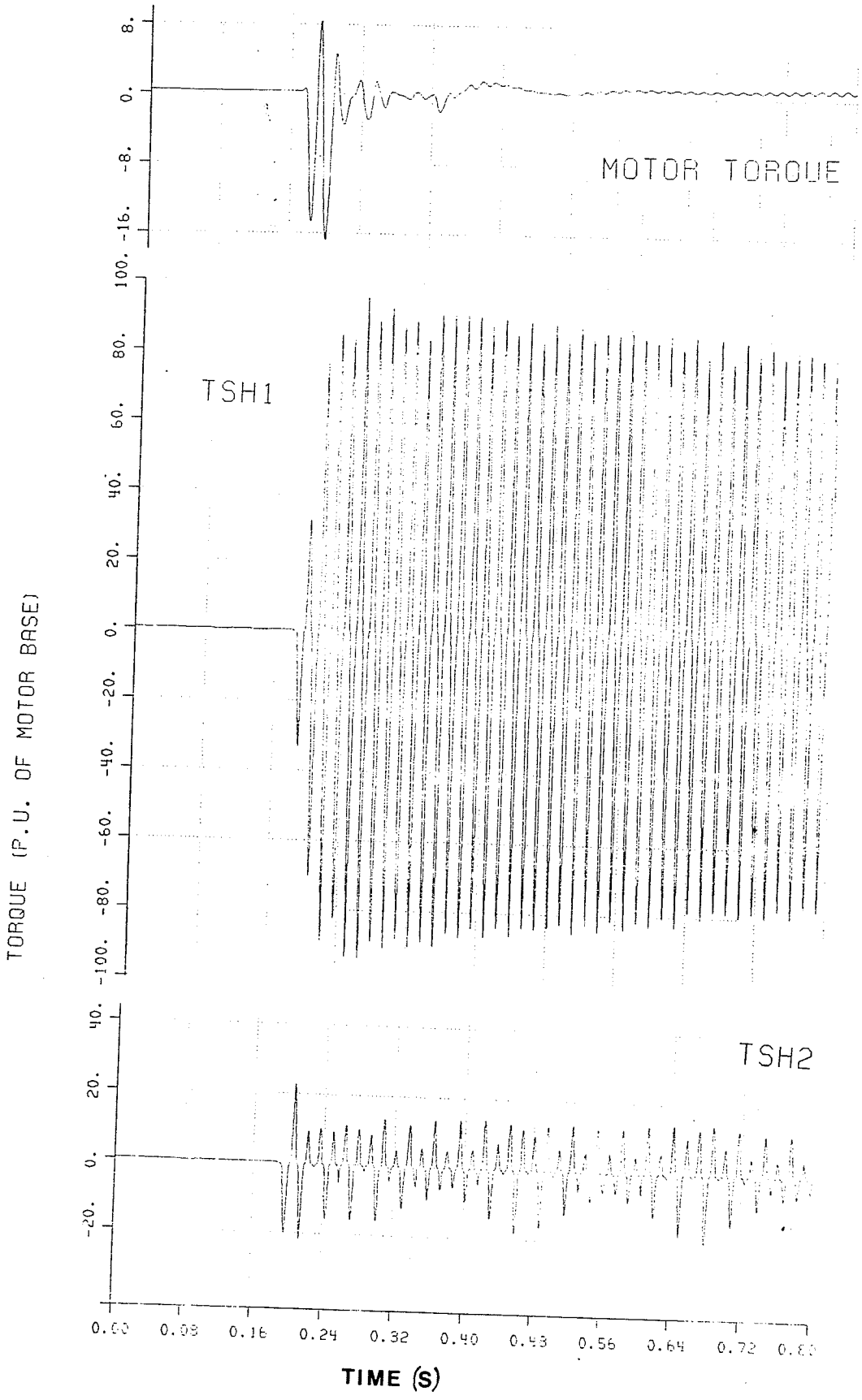

Fig. 34 HV Breaker Opening with New Flywheel and Wedge Blocks

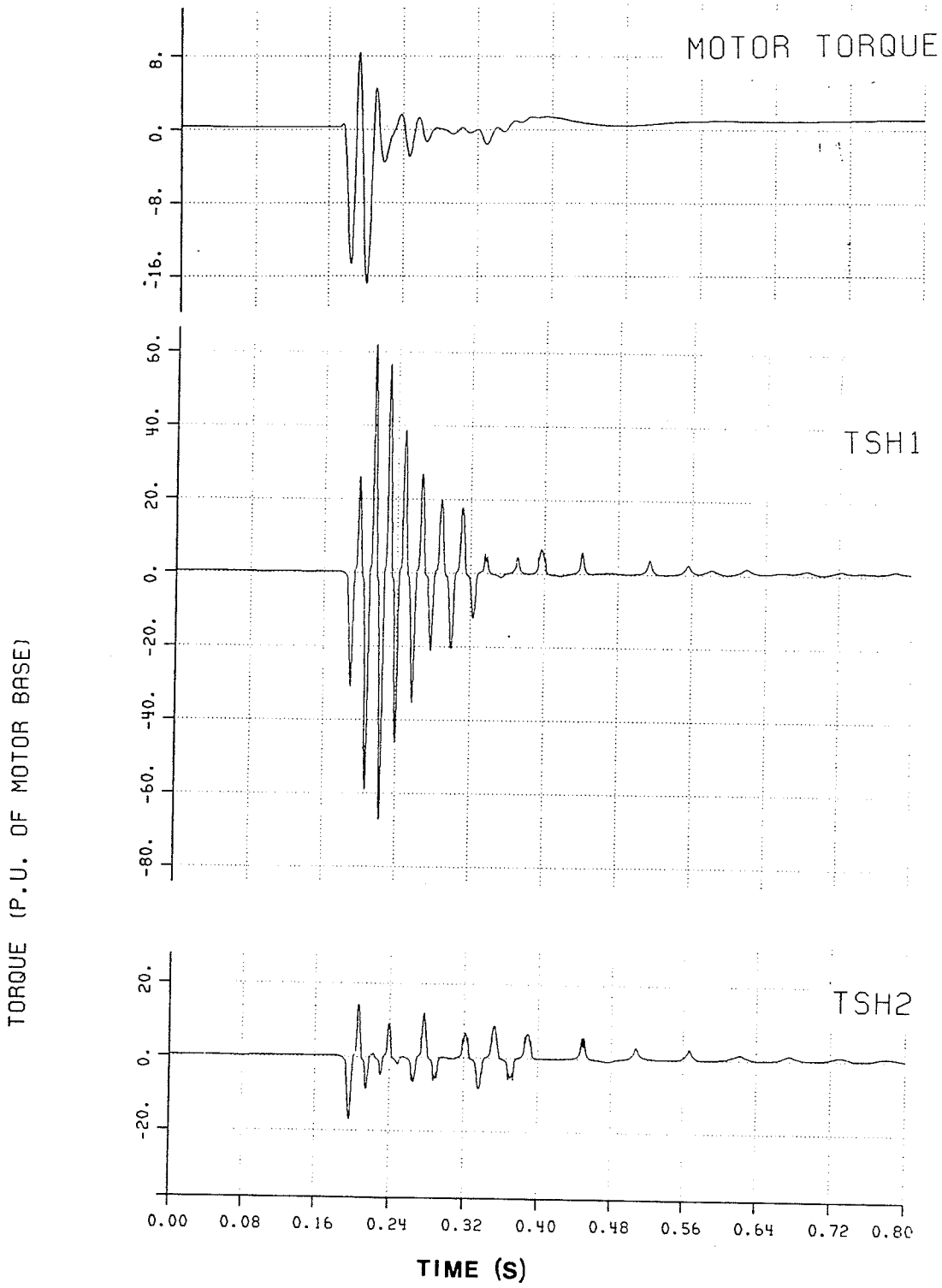

Fig. 35. HV Breaker Opening with New Flywheel and Wedge Blocks Using the Manufacturer's Estimate of Damping

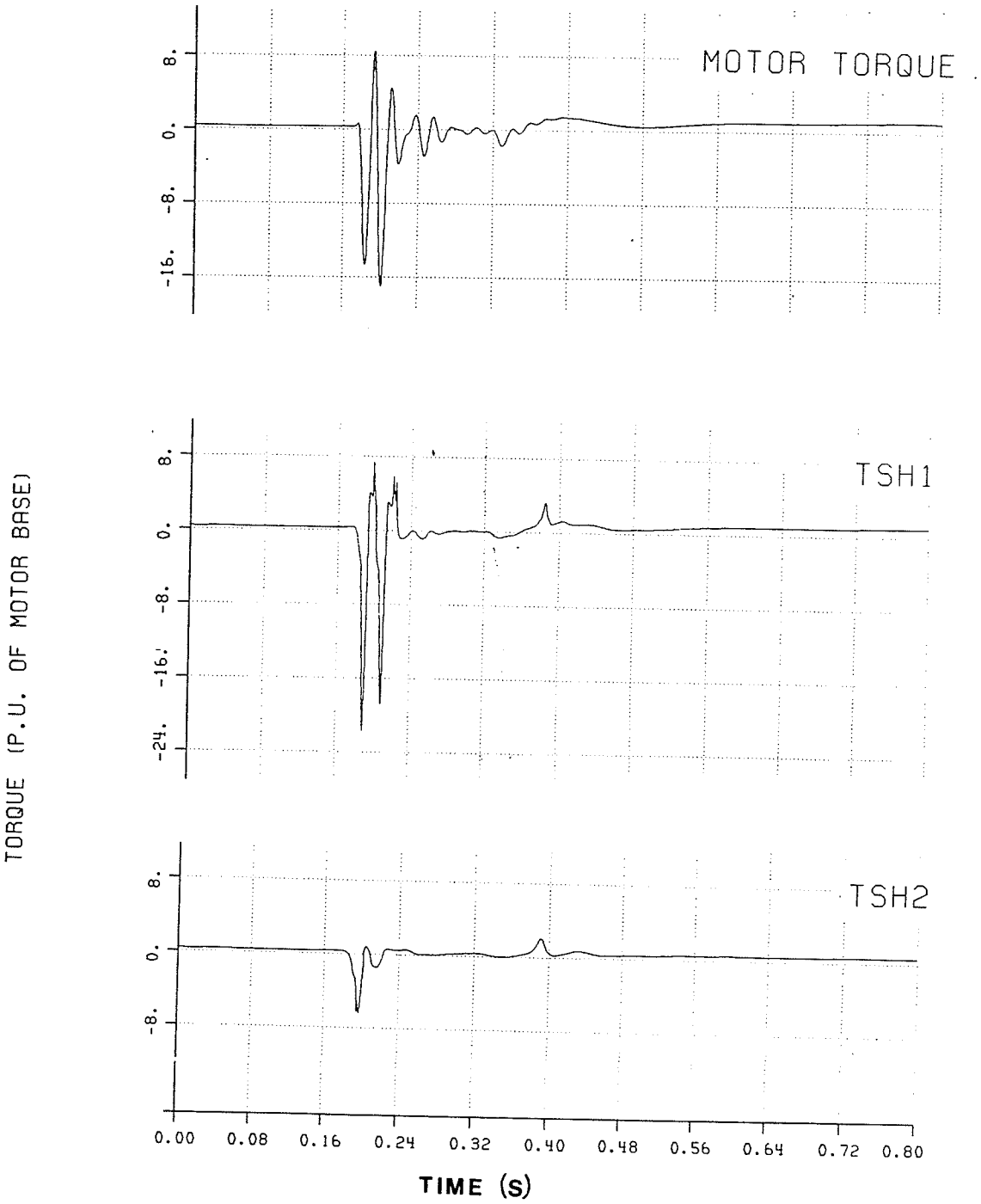

Fig. 36 HV Breaker Opening with New Flywheel and Wedge Blocks Using the Larger Estimate of Damping

CHAPTER 4 CONCLUSIONS

Before stating the conclusions it should be recalled that the critical torque value for shearing the key without shrink-fit interference is around 10 times the rated torque or 8.5 p.u. The critical torque value to initially break the shrink-fit is within the range of 13 to 33 times the rated torque or 11 to 27 p.u. and the damage was predominately due to negative torque. All torques are referred to the motor base with the full load rated torque on the motor being 2 658 lb. ft. and the value of 1 per unit torque equals 1.22 times the full load rated torque on the motor.

Comparisons of each case examined are shown in Figure 37.

1. Starting shaft torques obtained from starting the MG set from standstill are small (less than 1.0 p.u.) and were noted only in the positive direction of rotation. These torques could not have caused the large negative torque between the motor and flywheel that had sheared the keys.

2. Torques obtained from restarting the MG set from half speed are initially small (less than 1.0 p.u. as above) but as the motor approaches slip speed larger torques (less than 6.5 p.u.) are created which again die out once slip speed has been reached. The 6.5 p.u. torques are not large enough to do damage.

3. Sudden step increases in the generator load from 0.05 to 1.0 p.u. produce positive torques that are less than 5.0 p.u. Sudden step decreases in the generator load from 1.0 to 0.05 p.u. produce very small negative torques (-0.4 p.u.). This shows that even with extreme load changes on the generator, shaft torques are small and that this is not the cause of shearing the keys.

4. Synchronization of a second MG set onto the same 600 V bus the first MG set was supplying, creates maximum shaft torques when the phase difference between the bus voltage and the incoming generator voltage is around 180°. Maximum shaft torques of 7.0 p.u. in the positive direction occur at the generator side coupling on the incoming MG set. With the worst case of synchronization (180° out of phase) the torques created on the shaft are not large enough to do damage.

5. Power interruptions on the motor, produced by open-circuiting the motor for several cycles and then reclosing the circuit breaker, creates large negative torques (10.0 p.u. without damping included within the rubber blocks of the couplings) on the coupling between the motor and the flywheel (TSH1), but only when the delay time is around 25 cycles. The 25 cycle delay time is excessively long for typical automatic breaker operation. The 25 cycle delay time is also too quick for the possibility of manual reclosing. With the typical delay time of 4-9 cycles for automatic breaker operation the torques developed were positive and small in nature.

6. Other simulations were run showing the effects of the wedge blocks and the effects of the lighter flywheel. Generally, the lighter flywheel created a more even distribution of torques between the two couplings and the wedge blocks increased the torques created at both couplings. The best combination for torque reduction at the couplings would be round blocks with the lighter flywheel.

7. Damping included within the rubber blocks had the effect of reducing the translation of torque from one coupling to another and reducing subsequent torque oscillations throughout the mechanical system. Damping is an important consideration when potentially damaging torques are found on the undamped system.

8. Open-circuiting the high voltage breaker and isolating the 4 kV bus on the 138 kV filters produces potentially damaging torques (12.0 p.u. without damping included) in the negative direction. The type of torque transmitted to the shaft is an initial negative torque to the coupling between the motor and flywheel that continues to oscillate in both the positive and negative directions and is translated to the second coupling between the flywheel and generator when damping is not included. With damping included in the rubber blocks of the couplings, the initial negative torque remained high while subsequent torques and torques translated to the generator-side coupling were reduced to values that would not cause damage. Torques of 10 p.u. are created with the manufacturer's damping estimate and torques of 15 p.u. are created with the larger damping estimate for transient conditions.

   The damaging torques above are created with the original system of the heavier flywheel and round blocks in the couplings as this was the system when damage was first noticed. The present system, of the lighter flywheel and stiffer wedge blocks, creates even larger torques throughout the shaft system due to mechanical resonance of the input torque and the natural frequency of the shaft system. These torques are of 65 p.u. in both directions at the motor side coupling with the manufacturer's damping estimate and 15 p.u. in both directions at the generator-side coupling. With the larger damping estimate (for transient conditions) the torques are 20 p.u. and only in the negative direction at the motor-side coupling while the generator-side coupling has torques of only 8.0 p.u. (not damaging) in both directions.

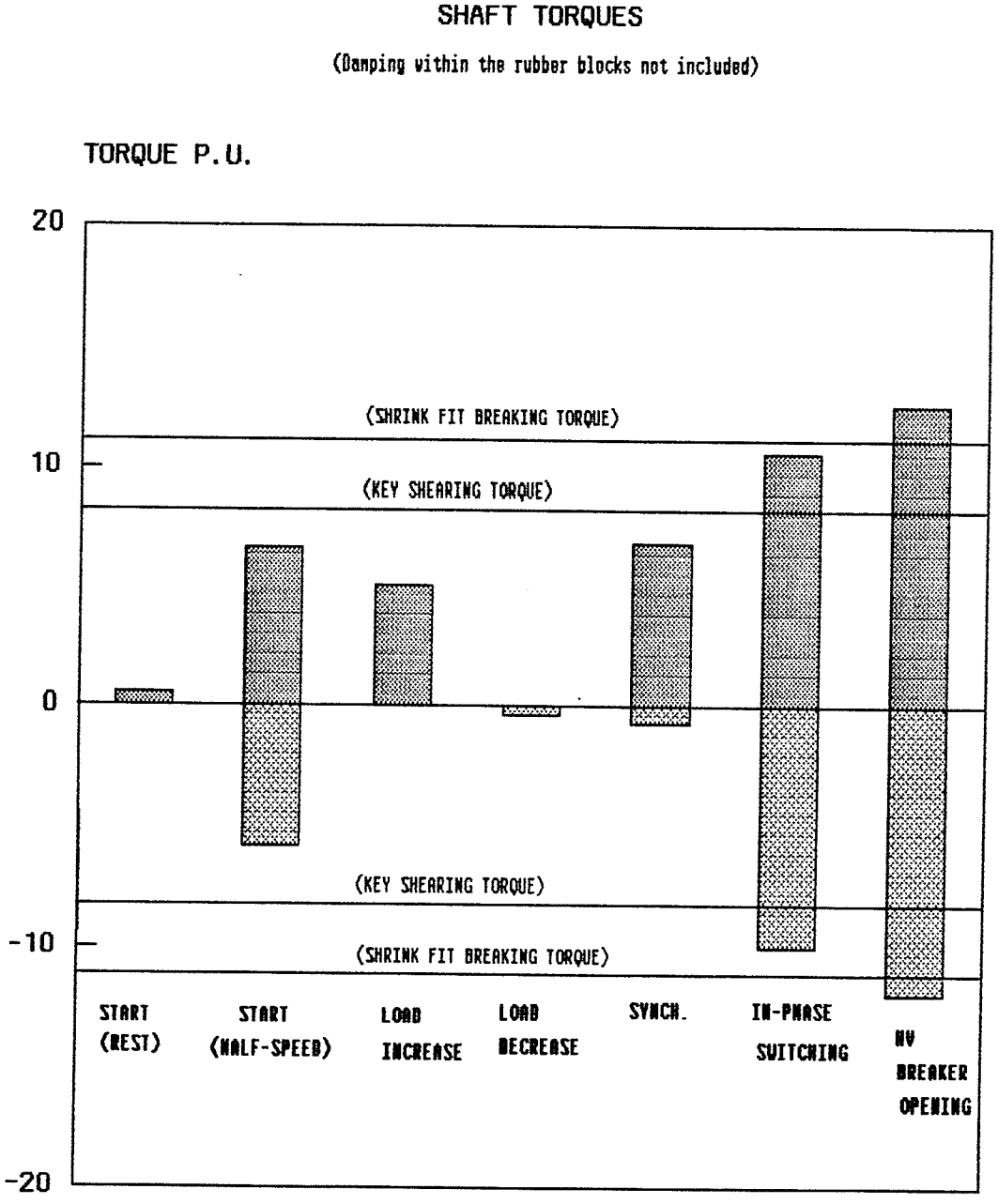

FIG. 37 Comparison of Shaft Torques

CHAPTER 5 RECOMMENDATIONS

The study has shown that the isolation of the 4 kV bus on the 138 kV filter banks will produce damaging torques on the MG sets. Therefore the breaker coordination must be modified to ensure that the low side (4 kV) breaker opens before the high side breaker. Further studies should use the larger damping estimate for the rubber blocks in the couplings as this gives the best agreement with site results. It doesn't appear that further changes to the inertia of flywheel or the type of rubber blocks employed in the coupling will have sufficient influence to prevent further damage.

REFERENCES

[1] R.H. Daugherty, "Analysis of Transient Electrical Torques and Shaft Torques in Induction Motors as a Result of Power Supply Disturbances", IEEE Transactions on Power Apparatus and Systems, Vol. PAS-101, No. 8, August 1982, pp. 2826.

[2] F.P. Flynn et al., "Transient Negative Torques in Induction Motors Due to Rapid Reconnections of the Supply", IEE Proceedings, Vol. 116, No. 12, Dec. 1969, pp. 2009.

[3] F. Maginniss, N.R. Schultz, "Transient Performance of Induction Motors", IEEE Transactions on Power Apparatus and Systems, Vol, 63 pp. 641-645.

[4] H.W. Dommel, "Digital Computer Solution of Electromagnetic Transients in Single and Multiphase Networks", IEEE Transactions on Power Apparatus and Systems, Vol. 88, Apr. 1969, pp. 388-399

[5] D.A. Woodford, A.M. Gole, R.W. Menzies, "Digital Simulation of DC Links and AC Machines", IEEE Transactions on Power Apparatus and Systems, Vol. PAS-102, No. 6, June 1983.

[6] J.E. Shigley, Mechanical Engineering Design, McGraw Hill series in mech. engineering, 1963, pp. 264, pp. 108 and pp. 564.

[7] Manitoba Hydro, Radisson Station 5 kV Switchgear-Metering-Protection One Line Diagram, Drawing #42172-E-10009 Rev. 1.

[8] Manitoba Hydro, Bipole 1 & Bipole 2 Equipment Description Parameters, Drawing #7001-C-75.

[9] Manitoba Hydro, Personal Correspondence with English Electric - AEI Canada Ltd. 1485 Portage Avenue, Winnipeg, Manitoba.

[10] Manitoba Hydro, Flywheel Shaft Drawing #C61581379032.

[11] Holset/Koppers, Engineered Products, Publication No. 157/C, Rexdale, Ontario.

[12] G.E.C. Machines Limited, Installation Operation and Maintenance Instruction Books, Manitoba Hydro Manual J119.1.

[13] G.R. Slemon and A. Straughen, Electric Machines, Addison-Wesley Publshing, Inc., 1980.

[14] Alger P.D., The Nature of Polyphase Induction Machines, John Wiley and Sons, New York, 1951.

[15] B. Adkins and R.G. Harley, The General Theory of Alternating Current Machines, Chapman and Hall Ltd., 1975.

[16] Swarn, S. Kali, "Switching Transients in Large Deep-Bar Squirrel Cage Induction Motors", IEEE P.E.S. Winter Meeting, New York, N.Y., Jan. 28 - Feb 2, 1973, Paper T73006-4.

[17] A.M. Gole, R.W. Menzies, H.M. Turanli, D.A. Woodford, "Improved Interfacing of Electrical Machine Models to Electromagnetic Transients Programs", IEEE Transactions on Power Apparatus and Systems, Vol. PAS-103, No. 9, Sept. 1984.

[18] A. Abolins, D. Lambrecht, J.S. Joyca, LT. Rosenberg, "Effect of Clearing Short Circuits and Automatic Reclosing on Torsional Stress and Life Expenditure of Turbine - Generator Shafts", IEEE Transactions on Power Apparatus and Systems, Vol. PAS-95, No. 1, Jan./Feb. 1976.

[19] P.C. Krause, W.C. Hollopeler, D.M. Triezenberg, P.A. Rusche, "Shaft Torques During Out-of-Phase Synchronization", IEEE Transactions on Power Apparatus and Systems, Vol. PAS-96, No. 4, July/August 1977.

[20] G. Gross, M.C. Hall, "Synchronous Machine and Torsional Dynamics Simulation in the Computation of Electromagnetic Transients", IEEE Transactions on Power Apparatus and Systems, Vol. PAS-97, No. 4, July/Aug. 1978.

[21] Koppers/Holset, Engineering Data Sheets 1989 and 3564, Koppers Company, Power Transmission Division, Baltimore, Maryland.

[22] Holset, Flexible Couplings, Technical Supplement, Koppers Engineering Products, Rexdale, Ontario.

[23] I.M. Canay, "Stresses in Turbo-Generator Sets Due to Electrical Disturbances", Brown Boveri Review, Vol. 62, pp. 435-443, Sept. 1975.

APPENDIX A

KEY SHEARING CALCULATIONS

Key Shearing Calculations

The keys that were sheared are a result of a large torque occurring within the shaft system. In order for the keys to shear they must have been subjected to a large torque several times (cycles of hammering) before damage would occur. The extent of the shearing would depend on the duration of the torque, the magnitude of the torque and the number of cycles of application. Generally if the peak shaft stresses are greater than the yield strength of the material then immediate cracks or breaks of the shaft may occur. In the case observed on site the keys were not broken or cracked but sheared. Shearing occurs when the stresses are below the yield strength and is a product of repeated hammering. The yield strength of a material is the stress magnitude which will pass the material from an elastic condition into a plastic state.

On the site, the shaft is shrink-fitted into the coupling hub. This shrink fit helps prevent rotation of the shaft within the coupling hub and would eliminate any torques from directly hammering on the keys. However, if the torque exceeds the shrink-fit torque then the key will be stressed. Another consideration is that once the shrink-fit has been broken initially the friction coefficient between the coupling hub and the shaft will be less and subsequent smaller torques will overcome the friction torque.

The limiting factor is therefore the initial shrink-fit torque. Another factor is the yield strength of the key material. Further, there is the magnitude of the torque applied at that point, the number of cycles of the application, and the duration of the torque itself.

A few calculations were made to determine the stresses and torques that occur when the shaft (at both couplings) is shrink-fitted into the hub [6].

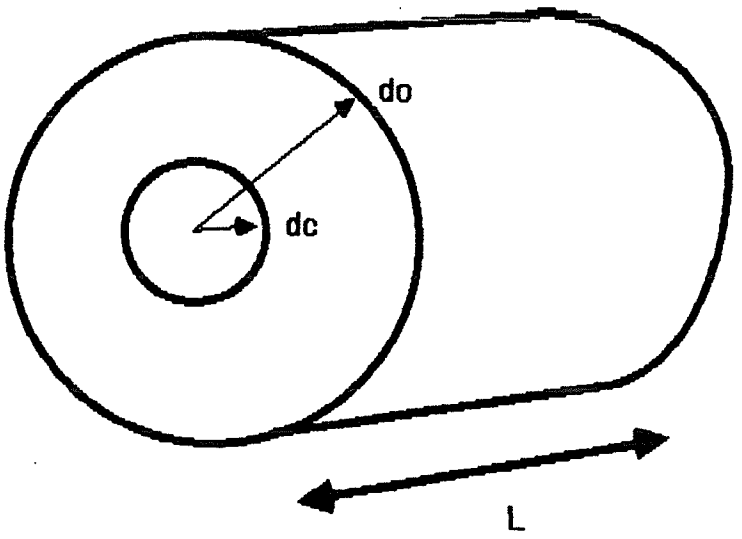

Fig. A1

Shaft Shrink-Fitted Into the Surrounding Coupling Hub.

where:

dc is the nominal diameter of contact surfaces = 90 mm = $\frac{90}{25.4}$ inches

do is the outside diameter of hub = 5.75"

t is the thickness of the hub = $\frac{do-dc}{2}$

di is the inside diameter of inner member = 0.0 (in this case shaft is solid not hollow)

l is the length of the hub = 4.25"

z = safety factor = 1

Pc is the radial pressure between the two members

i is the required intereference to produce maximum allowable stress

s is the stress in the hub (i.e. tangential stress)

f_s is the coefficient of friction between the two surfaces

E is the modulus of elasticity of the hub = 30×10^6 psi for steel

The static coefficient of friction between the two surfaces is difficult to approximate. According to [6] steel on steel carefully cleaned is from 0.4 to 1.0.

$$s = \frac{iE}{d} = \frac{(.003)(30\text{x}10^6)}{\frac{(90)}{(25.4)}} = 25\ 400 \text{ psi}$$

$$Pc = \frac{iE(dc^2-di^2)(do^2-dc^2)}{z(do^2-di^2)dc^3} = 15\ 775 \text{ psi}$$

with $f_s = 0.4$

$$T = \text{fit torque} = \frac{Eitl \cdot \pi \cdot f_s}{1} = 30\text{x}10^6(.003)\frac{(1.75)}{2}(4.25) \cdot \pi \cdot (.4)$$

= 420 581 lb in
= 35 048 lb ft
= 11 p.u. base torque (3 254 lb ft)

with $f_s = 1.0$

T = 87 621 lb ft
= 27 p.u. base torque (3 254 lb ft)

Additional calculations were made for the torque needed to shear the Key [6] without having the shrink-fit.

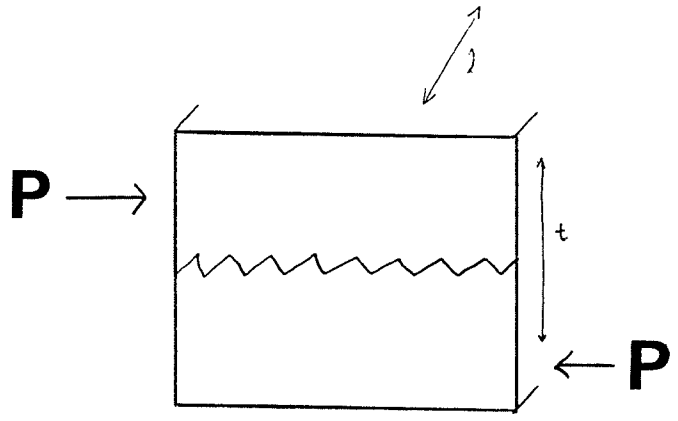

assuming:
Sy = ultimate strength
= 60 000 psi
for steel

$Ssy = (0.75)(Sy)$

$Ssy = (0.75)(60\ 000) = 45\ 000$ psi

$$\frac{Ssy}{n} = \frac{F}{tl}$$

$t = \frac{25}{25.4}$ inches = 0.984 in

$l = 4.25$ inches

$n = 1$ = safety factor

$r = \frac{45}{25.4}$ inches = $\frac{\text{diameter}}{2}$

therefore $F = 188\ 190$ lbs

$$F = \frac{T}{r} = \frac{T}{\frac{(45)}{(25.4)}} = 188\ 190 \text{ lbs}$$

$T = 333\ 407$ lb in = 27,784 lb ft

= 8.5 p.u. base torque (3 254 lb ft)

It was found that the torque needed to break the shrink-fit is anywhere from 11 p.u. to 27 p.u. (or 13 to 33 times the rated torque) depending on the exact value of the coefficient of the friction between the coupling hub and the shaft. It was also found that, without shrink-fitting the shaft, the torque needed to shear the Key with several cycles of application is 8.5 p.u. (or 10.4 times the rated torque).

Once the shrink-fit is initially broken subsequent smaller torques could overcome the friction torque remaining between the coupling hub and shaft. A torque larger than 8.5 p.u. could then contribute to shearing the keys.

APPENDIX B

MACHINE PARAMETERS

I. ELECTRICAL PARAMETERS

The actual values were obtained from the Dorsey Converter Station (Manitoba Hydro).

Actual Values

Motor (New Machines)

452.95 kW
4.16 kV
76.95 A
1 192 rpm
544 kV.A

Locked Rotor Test

V = 937.5 V
I = 76.95 A
P = 17.6 kW

No Load Test

V = 4.16 kV
I = 23.36 A
P = 9 kW

Also resistance

Ra = 0.5285 Ω

The motor parameters were developed from the previous list of actual values. By using the generalized machine theory the equivalent circuit of the motor can be represented as an equivalent circuit consisting of the direct and quadrature axis (see Figure B1). The program then uses the equivalent circuit to work out the voltages and currents in the machine for each single time step.

A simpler circuit of a single cage induction motor was first derived because this was the circuit that could be obtained directly from the locked rotor test and no load test results which were available.

The single cage induction motor equivalent circuit did not include values for X_{kd} and R_{kd} in Figure 1. As a result, the single cage induction motor model had a different torque-time curve than the actual machine on the site. The actual machine on the site was a deep bar motor with a torque time curve that resembled that of a double cage induction motor.

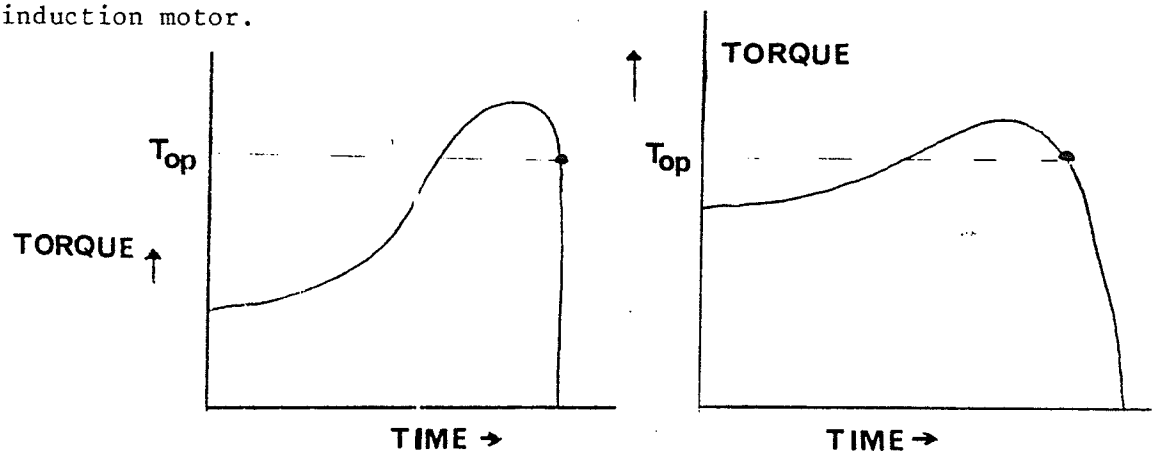

Single Cage

Double Cage

Top = Operating Torque

The single cage model was accurate in the operating range of the motor but not in the starting regions of the motor. A double cage induction motor equivalent circuit was developed. In developing the double cage induction motor it was assumed that the ratio of the change in starting resistance to the change in running reactance was one. This is normally the value used.

An equal reflection of impendances to the quadrature axis as were on the direct axis was also assumed as this is typically the case.

Saturation was not included in the motor model.

MOTOR

Ref. [12] 452.95 kW 4.16 kV 76.95 A 1 192 rpm 554 kV.A

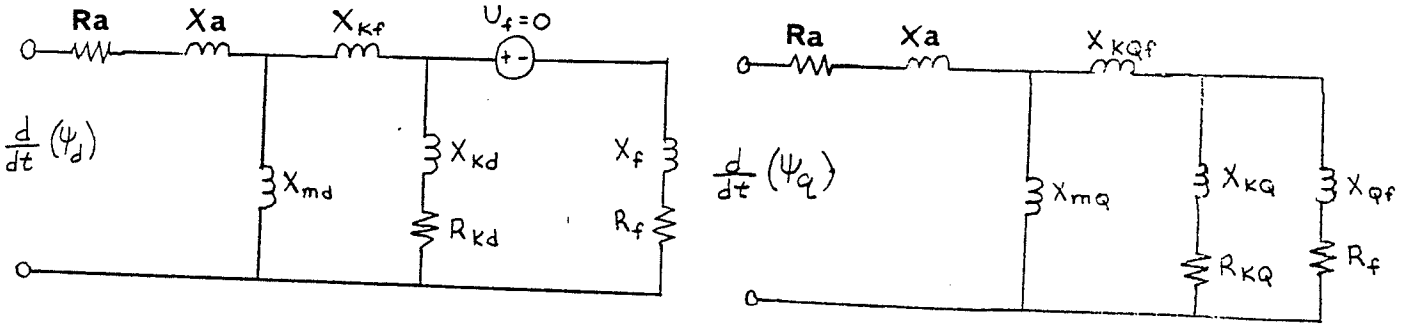

Direct Axis

Quadrature Axis

Figure B1 Equivalent Circuit of Motor for Program

The base power for a three phase machine is that supplied when the base current flows at base voltage and at unity power factor in all three phases [15]. Hence, the base power in an a.c. machine is not the actual rated power, but the power corresponding to the rated kV.A.

$$P_b/\text{phase} = V_b/\text{phase} \cdot I_b/\text{phase}$$

Here, $Vb/\text{phase} = \frac{4.16\ \text{kV}}{\sqrt{3}}$ = (rated voltage/phase) and

$I_b/\text{phase} = 76.95$ (i.e. rated full load current)

Therefore, $P_b/\text{phase} = \frac{4.16\ \text{kV}}{\sqrt{3}} \cdot 76.95 = 184.8168$ kV.A/phase

All calculations in this report for consistency will be rounded off to four decimal places.

Derived Values (for program)

Motor (single cage)

stator resistance,	$R_a = 0.01694$ p.u.
field resistance,	$R_f = 0.0148$ p.u. @ s = 1
field resistance,	$R_f = 0.0081$ p.u. @ s = 0.0067
direct-axis damper reactance,	$X_{kd} = R_{kd} = \infty$
stator reactance,	$X_a = 0.1116$ p.u.
direct-axis leakage reactance,	$X_{kf} = 0.0558$ p.u.
direct-axis magnetizing reactance,	$X_{md} = 3.1866$ p.u.
field reactance,	$X_f = 0.0558$ p.u.
quadrature-axis equivalents,	$X_{kf} = X_{kqf}$, $X_{md} = X_{mq}$, $R_{kq} = R_{kd}$, $X_{kd} = X_{kq}$ $X_f = X_{qf}$

Motor (double cage)

stator resistance,	$R_a = 0.01694$ p.u.
field resistance,	$R_f = 0.0148$ p.u. @ s = 1
field resistance,	$R_f = 0.0088$ p.u. @ s = 0.0067
stator reactance,	$X_a = 0.1116$ p.u.
direct-axis damper reactance,	$X_{kd} = 0.0$ p.u.
direct-axis leakage reactance,	$X_{kf} = 0.1032$ p.u.
direct-axis magnetizing reactance,	$X_{md} = 3.1866$ p.u.
field reactance,	$X_f = 0.0320$ p.u.
direct-axis damper reactance,	$R_{kd} = 0.232$ p.u.
quadrature-axis equivalents,	$X_{kf} = X_{kqf}$, $X_{md} = X_{mq}$, $R_{kd} = R_{kq}$, $X_{kd} = X_{kq}$ $X_f = X_{qf}$

The generator parameters were again developed from the previous list of actual values and again by using the generalized machine theory. The equivalent circuit of the generator can be represented as in Fig. B2.

The generator was to be modelled by actual values only but there was not enough data to model the parameters fully. Since the generator only played a secondary role in the torques created along the shaft (i.e. the generator was just basically acting as an inertia) its modelling did not have to be as accurate as that for the induction motor.

Old generator data was subsequently used to fully model the generator parameters. The old generator data was for a similar machine with approximately the same kV.A rating and it was believed that the p.u. values thus derived would then also be similar.

Actual Values - Continued

Generator (New Machines)
600 V
421 kV.A
1 200 rpm
405A

Resistances:

R_a = 0.0067 Ω /phase
R_f = 0.111 Ω /phase

Generator (Old Machines) (Data obtained from Manitoba Hydro)
600 V
1 782 rpm
421A
250 lb ft^2
437.5 kV.A
X_d = 1.5 p.u.
X'_d = 0.17 p.u.
X''_d = 0.15 p.u.
X_q = 0.66 p.u.
X''_q = 0.30 p.u.

GENERATOR

Ref. [12] (600 V 421 kV.A 1 200 rpm 405A)

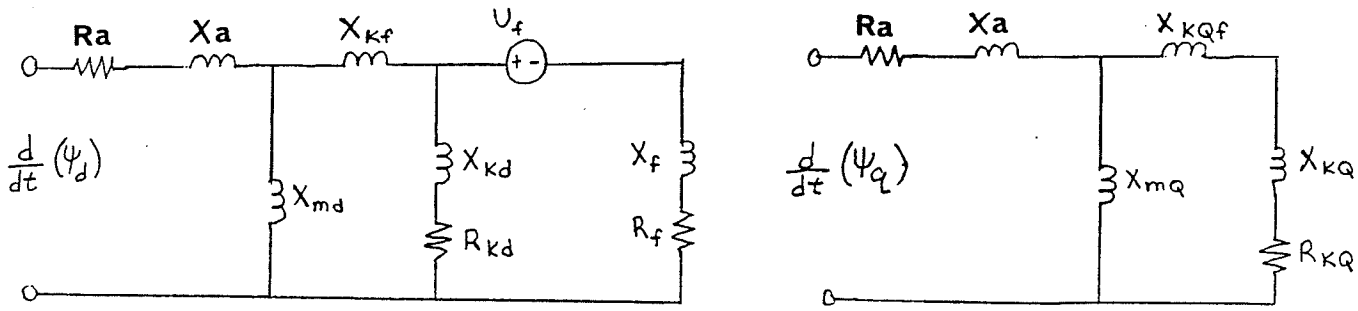

direct axis quadrature axis

Fig. B2 Equiv. Circuit for Program

The base power is defined as the power that is supplied when the base current flows at base voltage and at unity power factor in all three phases.

$$P_b/\text{phase} = V_b/\text{phase} \times I_b/\text{phase}$$

Here $V_b/\text{phase} = \frac{0.600 \text{ kV}}{3}$ (rated voltage per phase)

and I_b phase = 0.405 kA (i.e. full load rated current)

All calculations will again be rounded to four decimal places.

$$P_b/\text{phase} = \frac{0.600 \text{ kV}}{\sqrt{3}} \cdot 0.405 \text{ kA} = 140.2961 \text{ kV.A/phase}$$

$$Z_b/\text{phase} = \frac{V_b/\text{phase}}{I_b/\text{phase}} = \frac{0.600 \text{ kV}}{\sqrt{3} \times 0.405 \text{ kA}} = 0.8553\,\Omega/\text{phase}$$

Derived Values for program (cont'd)

Generator (new data only) (defined as earlier)

R_a = 0.0078 p.u.

R_f = 0.1298 p.u.

X_{md} = 1.2365 p.u.

X_a = 0.2267 p.u.

X_{kf} = 0.0, $X_{kd} = \infty = X_{kq}$, $R_{kd} = \infty = R_{kq}$

X_f = 0.0, R_f = 0.0, $X_{md} = X_{mq}$

Note: These derived values were never actually used since the program would become numerically unstable with the values of 0.0 for so many elements. Instead the old machine data shown below was used to model the generator.

Generator (old machine data)

X_a = 0.1 p.u.

R_a = 0.0078 p.u.

R_f = 0.1298 p.u.

R_{md} = 1.4 p.u.

X_{kf} = 0.03685 p.u.

X_{kd} = 0.1749 p.u.

X_f = 0.03685 p.u.

X_{mq} = 0.56 p.u.

X_{kq} = 0.3111 p.u.

R_{kd} = 0.1 p.u.

R_{kq} = 0.1 p.u.

Actual Values (Cont'd)

Transformers (e.g. SST3) [7]

primary side voltage = 138.0 kV L-L rms
secondary side voltage = 4.16 kV L-L rms
connected in Y-Y
7.5 MV.A

Filters (Ref. [8])
29.79 MVAR 5th 1.0852 Ω 0.0614 H 5.48 μF
17.12 MVAR 7th 1.52 Ω 0.0614 H 2.337 μF
34.23 MVAR 11th 0.75 Ω 0.0152 H 3.84 μF

Derived Values (Cont'd)

Parallel Load (i.e. the adjacent load to the motor shared on the 4 kV bus).

Load = 15.73 + 82.8j at 60 Hz
R = 15.73 Ω
$L = \frac{82.8}{377} = 0.2196$ H

The parallel load was derived from the hathogram results of an on site test.

II. MECHANICAL SYSTEM PARAMETERS

Inertia

Motor inertia [9], (J_1)

	= 189.3 lb-in-sec^2	*
	= 15.775 lb-ft-sec^2	*
	= 508 lb-ft^2	
	= 21.41 kg-m^2	
	= 0.3051 sec	**

Old flywheel inertia [9], (J_2)

	= 858.3 lb-in-sec^2	*
	= 71.525 lb-ft-sec^2	*
	= 2 303 lb-ft^2	
with shaft included	= 2 303.78 lb-ft^2	***
	= 97.08 kg-m^2	

New flywheel inertia [10], (J_2)

	= 411.8 lb-in-sec^2	*
	= 34.3 lb-ft-sec^2	*
	= 1 105 lb-ft^2	
with shaft included	= 1 105.78 lb-ft^2	***
	= 46.60 kg-m^2	

Generator inertia [9], (J_3)

	= 264.6 lb-in-sec^2	*
	= 22.05 lb-ft-sec^2	*
	= 710 lb-ft^2	
	= 29.92 kg-m^2	
	= 0.5611 sec	**

* lb-in-sec^2 and lb-ft-sec^2 are gravitation inertias, i.e. lb-ft^2 $= \frac{g(\text{lb-in-sec}^2)}{(12)} = \frac{(\text{lb-ft-sec}^2)g}{(1)}$

where g is gravitational acceleration constant of 32.2 ft/sec^2

** The inertia can also be expressed in terms of an inertia constant H which is defined as follows:

$$H = \frac{\text{stored energy of synchronous speed in kW-sec}}{\text{Rated kV.A}}$$

$$H = \frac{1/2\ JxW0^2}{\text{Rated kV.A}}$$

*** An additional calculation was made for the inertia of the shaft within the flywheel (assuming an approximate 4" shaft diameter) and this value of 0.78 $lb\text{-}ft^2$ was added to the inertia of the flywheel.

Stiffness

The torsional stiffness of both the round and wedge blocks of the 3.5 Hp/rpm size was provided by the manufacturer for different angle deflections [11] (the following pages show tables for both round and wedge blocks and the stiffness curves). The size of 3.5 was the size of the coupling and rubber blocks that were used on the site. Also, the rubber blocks used on the site were of 50° durometer i.e. SM50 as opposed to SM60 or SM70 [11].

Round Blocks (size 3.5) 50° durometer

peak torque = 43 900 lb in = 4 960 N.m

peak angle deflection = 7.40° = 0.1292 radians

$\frac{4960}{0.1292}$ = 38 290 N.m/rad . $\frac{12}{10}$ = 46 068 N.m/rad*

0 rad	=	0%	46 068 . $\frac{5}{100}$	= 2 303 N.m/rad
0.0087 rad	=	7.5%	46 068 . $\frac{2.8}{15}$	= 8 599 N.m/rad
0.0262 rad	=	22.5%	46 068 . $\frac{6.5-2.8}{15}$	= 11 363 N.m/rad
0.0408 rad	=	35%	46 068 . $\frac{10.3-6.5}{10}$	= 17 506 N.m/rad
0.0525 rad	=	45%	46 068 . $\frac{15.2-10.3}{10}$	= 22 573 N.m/rad
0.0641 rad	=	55%	46 068 . $\frac{20.8-15.2}{10}$	= 25 798 N.m/rad
0.0758 rad	=	65%	46 068 . $\frac{27.4-20.8}{10}$	= 30 405 N.m/rad
0.0874 rad	=	75%	46 068 . $\frac{35.4-27.4}{10}$	= 36 854 N.m/rad
0.0991 rad	=	85%	46 068 . $\frac{52.4-35.4}{10}$	= 78 316 N.m/rad
0.1067 rad	=	91.55%	46 068 . $\frac{100-52.4}{7.8}$	= 281 133 N.m/rad

* The 12/10 ratio factor was included since the wedge block type couplings were used on site and had 12 round blocks inserted in them whereas the round block type couplings (not used) actually had room for only 10 round blocks.

"CB" Holset Coupling — Torque Deflection Curves

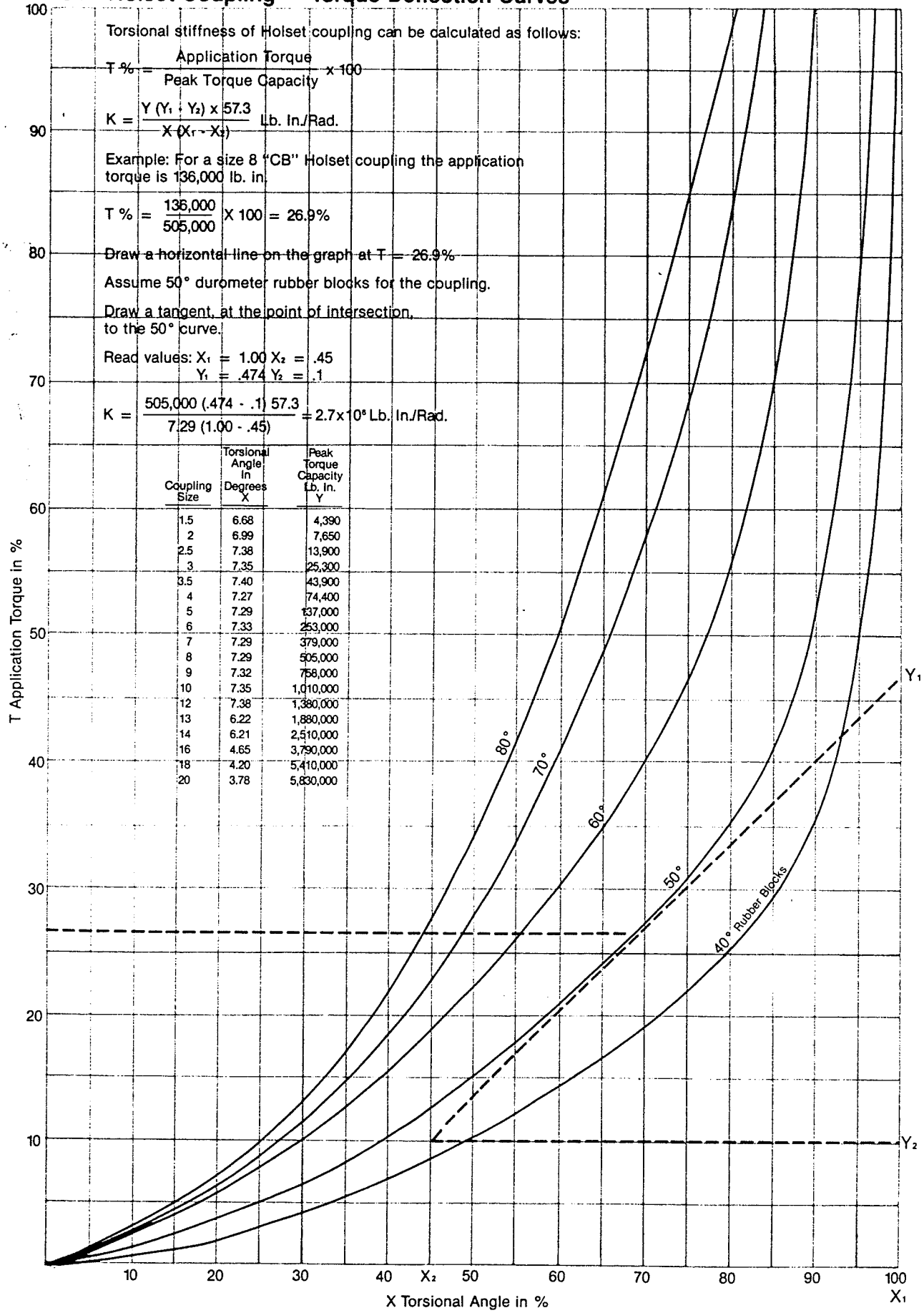

Torsional stiffness of Holset coupling can be calculated as follows:

$$T\% = \frac{\text{Application Torque}}{\text{Peak Torque Capacity}} \times 100$$

$$K = \frac{Y\,(Y_1 - Y_2) \times 57.3}{X\,(X_1 - X_2)} \text{ Lb. In./Rad.}$$

Example: For a size 8 "CB" Holset coupling the application torque is 136,000 lb. in.

$$T\% = \frac{136{,}000}{505{,}000} \times 100 = 26.9\%$$

Draw a horizontal line on the graph at T = 26.9%

Assume 50° durometer rubber blocks for the coupling.

Draw a tangent, at the point of intersection, to the 50° curve.

Read values: $X_1 = 1.00$ $X_2 = .45$
$Y_1 = .474$ $Y_2 = .1$

$$K = \frac{505{,}000\,(.474 - .1)\,57.3}{7.29\,(1.00 - .45)} = 2.7 \times 10^6 \text{ Lb. In./Rad.}$$

Coupling Size	Torsional Angle In Degrees X	Peak Torque Capacity Lb. In. Y
1.5	6.68	4,390
2	6.99	7,650
2.5	7.38	13,900
3	7.35	25,300
3.5	7.40	43,900
4	7.27	74,400
5	7.29	137,000
6	7.33	253,000
7	7.29	379,000
8	7.29	505,000
9	7.32	758,000
10	7.35	1,010,000
12	7.38	1,380,000
13	6.22	1,880,000
14	6.21	2,510,000
16	4.65	3,790,000
18	4.20	5,410,000
20	3.78	5,830,000

Wedge Blocks (size 3.5) 50° durometer

peak torque = 65 700 lb in = 7 432 N•m

peak angle deflection = 2.23 = 0.0389 rad

$\frac{7\ 423}{0.0389}$ = 190 823 N•m/rad

0 rad	=	0%	190 823	. $\frac{15}{100}$	= 28 623	N•m/rad
0.0026 rad	=	7.5%	190 823	. $\frac{4.3}{15}$	= 54 703	N•m/rad
0.0079 rad	=	22.5%	190 823	. $\frac{9.6-4.3}{15}$	= 67 424	N•m/rad
0.0234 rad	=	35%	190 823	. $\frac{13.4-9.6}{10}$	= 72 513	N•m/rad
0.0159 rad	=	45%	190 823	. $\frac{17.6-13.4}{10}$	= 80 146	N•m/rad
0.0194 rad	=	55%	190 823	. $\frac{23.3-17.6}{10}$	= 108 769	N•m/rad
0.0229 rad	=	65%	190 823	. $\frac{31.3-23.3}{10}$	= 152 658	N•m/rad
0.0264 rad	=	75%	190 823	. $\frac{41.3-31.3}{10}$	= 190 823	N•m/rad
0.0300 rad	=	85%	190 823	. $\frac{58 - 41.3}{10}$	= 318 674	N•m/rad
0.0335 rad	=	94.98%	190 823	. $\frac{100-58}{10}$	= 801 457	N•m/rad

"WB" Holset Coupling — Torque Deflection Curves

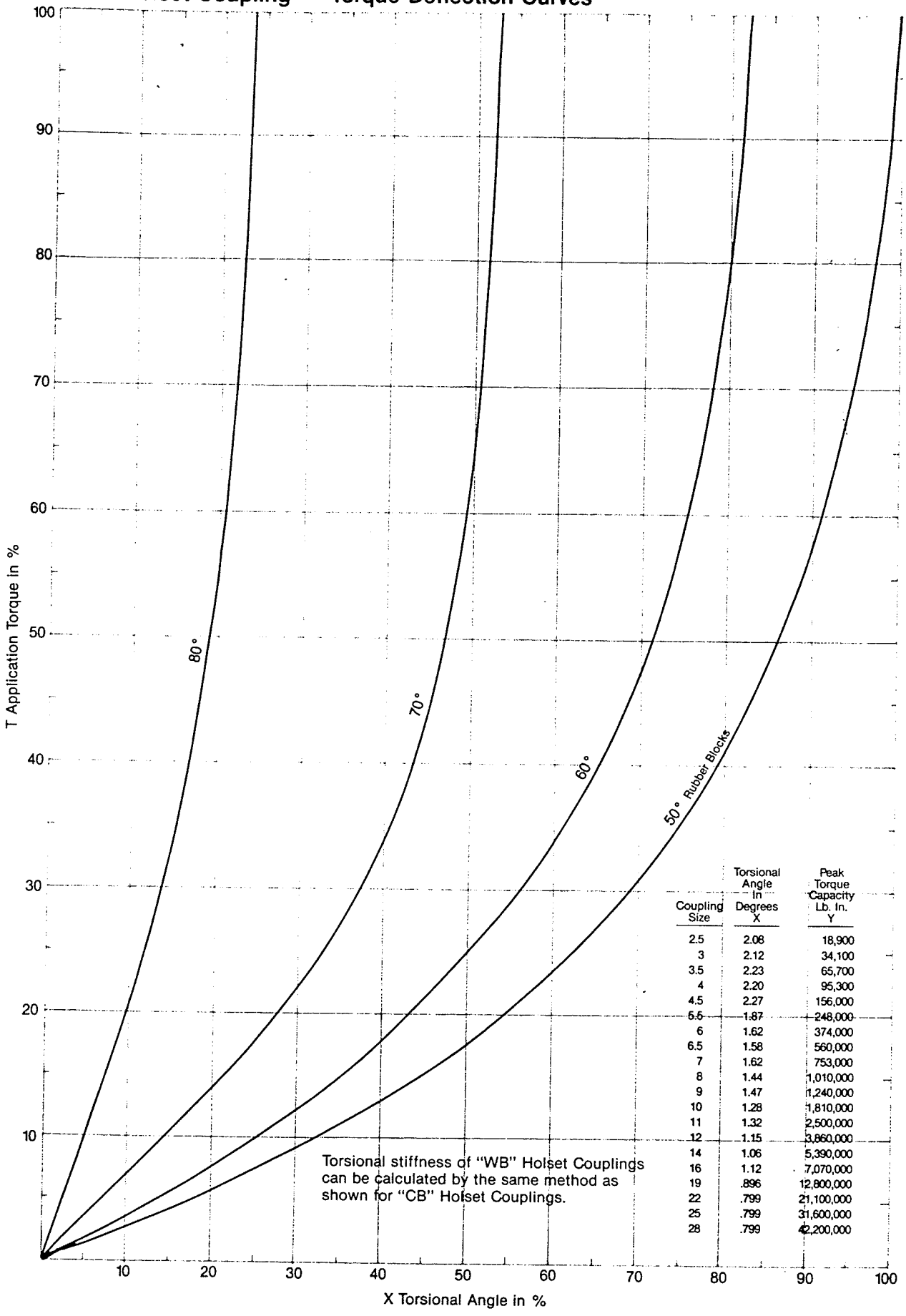

Coupling Size	Torsional Angle In Degrees X	Peak Torque Capacity Lb. In. Y
2.5	2.08	18,900
3	2.12	34,100
3.5	2.23	65,700
4	2.20	95,300
4.5	2.27	156,000
5.5	1.87	248,000
6	1.62	374,000
6.5	1.58	560,000
7	1.62	753,000
8	1.44	1,010,000
9	1.47	1,240,000
10	1.28	1,810,000
11	1.32	2,500,000
12	1.15	3,860,000
14	1.06	5,390,000
16	1.12	7,070,000
19	.896	12,800,000
22	.799	21,100,000
25	.799	31,600,000
28	.799	42,200,000

Torsional stiffness of "WB" Holset Couplings can be calculated by the same method as shown for "CB" Holset Couplings.

Damping Within the Round Blocks

$$D = \frac{K}{12w}$$

- K is the torsional stiffness of the rubber
- W is the vibration frequency in rad/s
- 12 is a constant derived from the manufacturer for 50° durometer rubber
- D is the specific damping coefficient

From Ref. [11] K at full load
torque is 1.27×10^6 Kp cm = 1.1×10^6 lb.in. = 0.1245×10^6 N.m

$$D = \frac{0.1245 \times 10^6}{12(69)}, = 151 \text{ N.m/rad/s}$$

This value represents the value of damping within the rubber estimated for a constant input vibration to the system and a constant stiffness K of the rubber.

Another estimate was also used which would represent larger damping forcing that might occur under transient condition.

$$D = \frac{0.1245 \times 10^6}{12(11.0)} = 947.0 \text{ N.m/rad/s}$$

Damping Within the Wedge Blocks

Again the same points hold as with the round blocks except the stiffness is now 2.16×10^6 kp cm = 1.8×10^6 lb. in. = 0.212×10^6 N.m.

$$D = \frac{K}{12w} = \frac{0.212 \times 10^6}{12(89.8)} = 196 \text{ N.m/rad/s}$$

and the larger damping estimate of:

$$D = \frac{0.212 \times 10^6}{12(14.3)} = 1\ 235.0 \text{ N.m/rad/s}$$

APPENDIX C

DERIVATION OF MACHINE PARAMETERS

SECTION 6

TECHNICAL DATA

MOTORS - RADISSON

Driven equipment	A.C. Generator
Number of motors	Three
Serial Nos.	CLG7457/1 and -/2 and -/3
Type of drive	Directly coupled
Mounting	Horizontal, foot mounting
Manufacturer	GEC Machines Limited
Rated	450 kW
Synchronous speed	1200 r/min
Full load speed	1192 r/min
Enclosure	Enclosed ventilated rip-proof
Manufacturers type	C400-3A
Rated volts: phase: frequency:	4160V, 3 phase 60 Hz
Class of insulation	'B'
Insulation treatment	Varnish impregnated
Time rating	Continuous maximum rating
Service factor	1.0
Ambient temperature	43°C max.
Rated full load current	76A
Locked rotor current	450 amperes
Torque - locked rotor	0.7 x FLT
Torque - pull up	0.7 x FLT
Torque - breakdown	2.0 x Flt
Singular gap	.6 mm
Weight complete	3 035 kg
Efficiency 100% FL	94.5%
75%	94.28%
50%	93.75%
Power factor 100% FL	0.86
75%	0.83
50%	0.74
Bearings	Ransome Hoffman Pollard
Type	4 203 V m Ball (Spring-loaded at NDE)
Rated life	Greater than 100 000 hrs
Expected operating temp.	Less than 90°C

Lubricant	Grease: Shell ALVANIA RA
Rotor bar material	Copper
Motor GD^2	85 kg m^2
Temperature detectors (bearings)	Thermocouple (Copper - Constantan) BICC Type MK DT2-60
Locked rotor PF	0.16
Locked rotor kV.A	3 250
Starting time	6 sec. (at no-load)
Safe stalled time - Maximum	18 secs.

MOTOR

Ref[12] (452.95 kW 4.16 kV 76.95 A 1 192 rpm 554 kV.A)

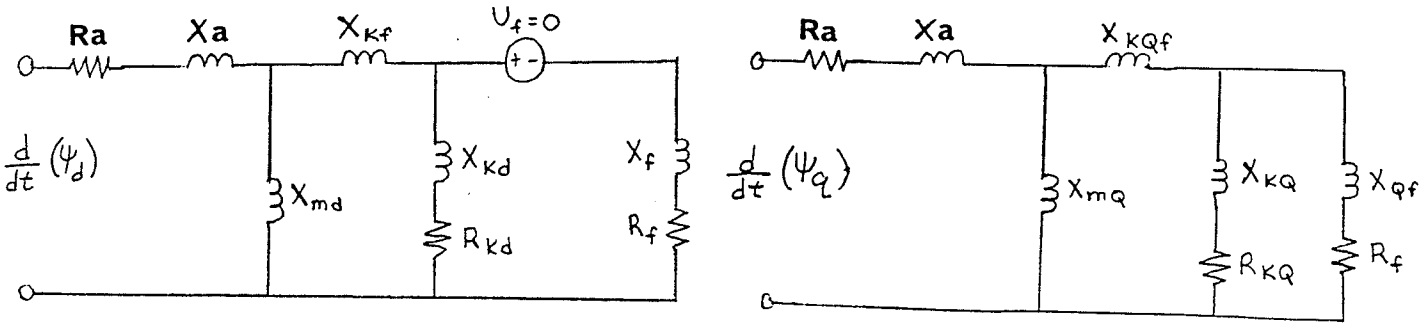

direct axis Quadrature axis

Fig. C1 equivalent circuit of Motor for program

Ref [13] - Locked Rotor Test

$V = 937.5\ V_{L-L}$ rms . I = 76.95 A rms P = 17.6 kW

$$V_{1k} = \frac{937.5\ V_{L-L}}{4.16 \times 10^{3}_{L-L}} = 0.2254 \text{ p.u.}$$

$I_{1k} = 1$ p.u.

$$P_{1k} = \frac{17.6 \text{ kW/3 phases}}{(184.8168 \text{ kV.A/phase}).3} = 0.0317 \text{ p.u.}$$

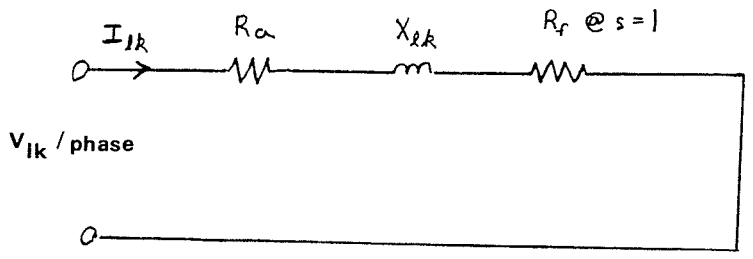

Fig. C2 equivalent circuit for the locked rotor test

$$R_{1k/phase} = \frac{P_{1k}/3 \text{ phases}}{3 \cdot I^2_{1k/phase}} \qquad \text{Ref [13]}$$

Therefore $\frac{P_{1k \text{ p.u.}}}{I^2_{1k \text{ p.u.}}} = R_{1k \text{ p.u.}} = 0.0317 \text{ p.u.}$

$$Z_{1k/phase} = \frac{V_{1k \text{ L-L}}}{\sqrt{3} \cdot I_{1k/phase}}$$

Therefore $Z_{1k} = \text{p.u.} = \frac{V_{1k \text{ p.u.}}}{I_{1k \text{ p.u.}}} = \frac{0.2254 \text{ p.u.}}{1.0 \text{ p.u.}}$

$$\text{p.u.} = 0.2254 \text{ p.u.}$$

$$X_{1k/phase} = \sqrt{Z^2_{1k/phase} - R^2_{1k/phase}}$$

Therefore $X_{1k \text{ p.u.}} = [Z^2_{1k \text{ p.u.}} - R^2_{1k \text{ p.u.}}]^{0.5}$

$$= [(0.2254)^2 - (0.0317)^2]^{0.5}$$

$$= 0.2232 \text{ p.u.}$$

and a close approximation

$$R_{1k} + jX_{1k} = Ra + R_F + jX_L$$

but $Ra = 0.5285\,\Omega$

$$= \frac{0.5285}{31.2122} = \underline{0.0169} \text{ p.u.}$$

Therefore $R_F = R_{1k} - Ra = 0.317 - 0.169$

$= \underline{0.0148}$ p.u. @ s = 1

From Fig. C1

$$X_{1k} = X_a + X_{Kf} + [X_{KD} // X_F] = 0.2232 \text{ p.u.}$$

assume X_{KD} and $R_{KD} = \underline{\infty}$ for single case representation of Fig. C1.

$$X_{1k} = X_a + X_{Kf} + X_F = 0.2232 \text{ p.u.}$$

assume $X_{KF} = X_F$ (for simplicity)

note: $X_l = X_K + X_F$ (i.e. $X_{1k} = X_a + X_l$)

assume $X_a = X_l$

Therefore $X_a = \underline{0.1116}$ p.u. $= X_l$

Therefore $X_{KF} = 0.0558$ p.u. $= X_F$

- <u>No load test</u>

V = 4.16 kV_{L-L}rms I = 23.36 A rms P = 9 kW

Therefore V_{NL} p.u. = 1.0 p.u. I_{NL} p.u. $= \frac{23.36\text{A rms}}{76.95 \text{ A rms}} = 0.3036$ p.u.

$$P_{NL}\text{p.u.} = \frac{9 \text{ kW/3 phases}}{(184.8168 \text{ kV.A/phase})\sqrt{3}} = 0.0162 \text{ p.u.}$$

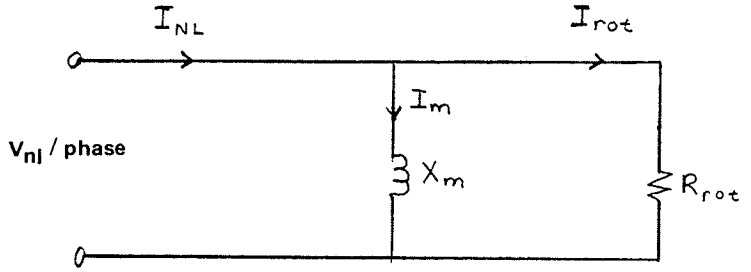

Fig. C3 equivalent circuit for the no-load test

$$\cos \phi = \frac{P_{NL}/3 \text{ phases}}{3\ V_{NL\ L-L} \cdot I_{NL}}$$

Therefore $\cos \phi = \frac{P_{NL\ p.u.}}{V_{NL p.u.} \cdot I_{NL\ p.u.}}$

$$= \frac{0.0162}{1.0 \cdot 0.3036} = 0.0534$$

Therefore $\phi = 86.9389°$

$$I_{roT} = I_{NL} \cos \phi \text{ A.}$$

$$I_m = I_{NL} \sin \phi \text{ A}$$

Therefore $I_{m\ p.u.} = I_{NL\ p.u.} \sin \phi$

$$I_{m\ p.u.} = 0.3036 \text{ p.u.} \cdot \sin 86.9389°$$
$$= 0.3032 \text{ p.u.}$$

$$X_m = \frac{V_{NL\ L-L}}{\sqrt{3} \cdot I_m} = \frac{1.0}{0.3032} = 3.2982 \text{ p.u.}$$

Note from Fig C3 to Fig C1.

$$X_m = X_a + X_{md}$$

Therefore $X_{md\ p.u.} = X_m - X_a = 3.2982 - 0.1116$
$= \underline{3.1866}$ p.u.

Since R_F was only calculated at S = 1 the calculation for R_F at slip speed is below.

Slip speed = 1 192 rpm

$$T = \frac{PmecH}{Wm}$$

PmecH = 452.95 kW

also $$T = \frac{3}{W_s} \cdot \frac{P}{2} \frac{S}{R_F} \cdot Va^2$$

also $$s = 1 - \frac{P}{2} \frac{Wm}{W_s}$$

Therefore $\frac{P}{2} \frac{Wm}{ws} = 1-s$

Therefore $Wm = (1-s)\ \frac{2}{P}\ Ws$

Therefore $\frac{Pmech}{Wm} = \frac{Pmech\ .\ p}{(1-s)\cdot 2\cdot W_s} = 3\ .\ \frac{s}{R_f}\ .\ Va^2\ \frac{(\ P\ )}{2\cdot W_s}$

$$\frac{Pmech}{(1-s)} = \frac{3\ \cdot\ s\ \cdot\ Va^2}{R_F}$$

$$s = 1 - \frac{6}{2}\ \frac{1192}{3600} = 0.0067$$

$$Va = \frac{4.16\ kV}{3} = 2.4018\ kV$$

Therefore R_f/phase @ slip speed =

$$\frac{3\cdot s\cdot Va^2\cdot(1-s)}{PmecH} = \frac{3\cdot(0.0067)\cdot(2.4018kV)^2\cdot(1-.0067)}{452.95\ kW}$$

$$= 0.2543\ \Omega$$

Therefore $R_F p.u._{(SLIPSPEED)} = \frac{0.2543}{31.2122} = \underline{0.0081}$ p.u.

That concludes the data needed to be derived for the single cage model. It must be also noted that the quadrature axis values are simply a reflection to the direct axis values in Fig. C1.

i.e. $X_{Kf} = X_{KQF}$, $X_{md} = X_{mq}$, $R_{Kd} = R_{KQ}$, $X_{KD} = X_{KQ}$

$X_f = X_{QF}$

For the Double Cage there has been a transformation as seen below:

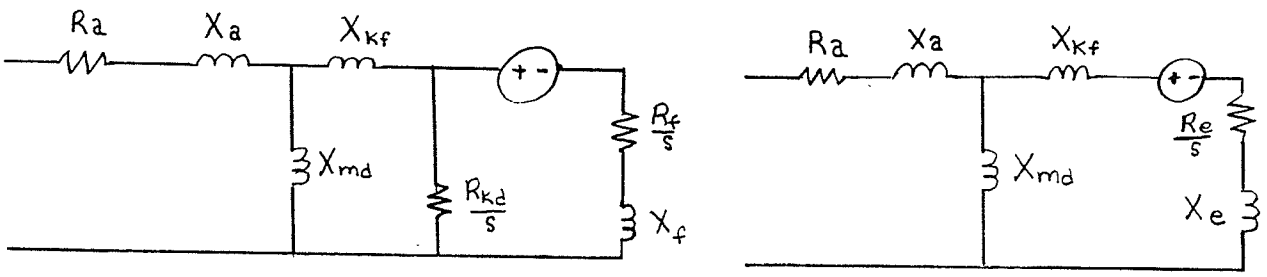

direct axis
double cage

direct-axis
single cage

Fig. C4 Comparison of double and single cage equivalent circuits of the motor

Again Fig. C1 is the equivalent circuit for the motor which is needed for the program. The double cage representation in Fig. C4 is the same except that $R_{Kd} = 0.0$

The following calculations are needed to arrive at the double cage representation in Fig. C4 shown below [14].

The rotor impedance can be written as

$$R_e = \frac{R_{Kd}R_F(R_{Kd}+R_F) + S^2(R_{Kd}X_f^2)}{(R_{Kd}+R_f)^2 + S^2X_f^2}$$

$$X_e = \frac{R_{Kd}^2X_f}{(R_{Kd}+R_f)^2 + S^2X_f^2}$$

At small slips s = 0

$$R_e\Big|_{s=o} = R_0 = \frac{R_K R_f}{R_{Kd} + R_f}$$

$$X_{Kf} + X_e\Big|_{s=o} = X_0 = X_{Kf} + \frac{R_K^2{}_d X_f}{(R_{Kd}+R_f)^2}$$

At stanstill s = 1

$$R_e\Big|_{s=1} = R_{ST} = \frac{R_{Kd}R_F(R_{Kd}+R_F) + R_{Kd}X_f^2}{(R_{Kd}+R_f)^2 + X_f^2}$$

$$X_{Kf}+X_e\Big|_{s=1} = X_{ST} = X_{Kf} + \frac{R_K^2{}_d X_f}{(R_{Kd}+R_f)^2 + X^2{}_f}$$

The increment in starting resistance is:

$$\Delta R = R_{ST}-R_0 = \frac{R_{kd}^2 X^2{}_f}{(R_{Kd}+R_f)[(R_{Kd}+R_f)^2 + X^2{}_f]}$$

The increment in running resistance

$$\Delta X = X_o - X_{st} = \frac{R_{kd}^2 X_f^3}{(R_{kd}+R_f)^2\,[(R_{kd}+R_f)^2 + X^2{}_f]}$$

the ratio of $\frac{\Delta R}{\Delta X} = m = \frac{R_{kd}+R_f}{X_f}$

Depending on the value of m the speed torque curve will vary see below:

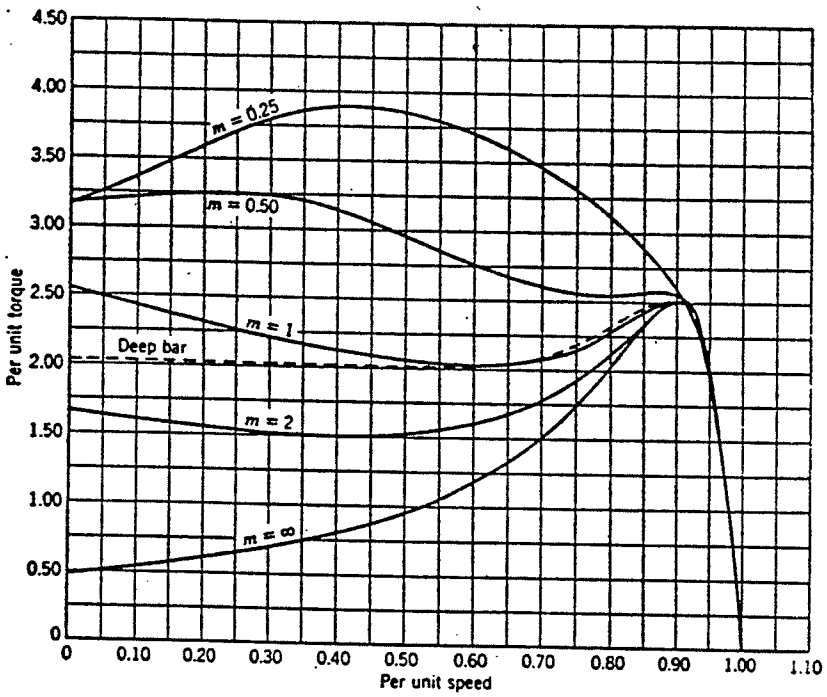

Idealized Torque Curves of Double Squirrel-Cage Motors.

A small value of m gives a much higher torque in the mid-speed range which allows the motor torque to be larger than the mechanical load torque and prevents stalling of the machine. A small value of m, however, gives a much larger starting current. A good criterion according to Ref [14] is to have the highest starting torque per ampere. This occurs at s=1, when m=1 and motors are made with m typically chosen around one.

Subst $R_f = X_{fm} - R_{kd}$

Therefore $\Delta X = \dfrac{R_{kd}^2}{m^2(m^2+1)\,X_f}$ $\qquad m = \dfrac{R_{ST} - R_O}{X_O - X_{ST}}$

Therefore $X_f = \dfrac{R_{kd}^2}{m^2(m^2+1)\cdot\Delta X}$

$$R_o = \frac{R_{kd}R_f}{R_{kd}+R_f} = \frac{R_{kd}R_f}{mX_f}$$

Therefore $R_{kd}R_f = mX_fR_o = \dfrac{mR_oR_x^2{}_d}{m^2(m^2+1)\cdot\Delta X}$

Therefore $R_f = \dfrac{R_oR_{kd}}{m(m^2+1)\cdot\Delta X} = \dfrac{R_oR_{kd}}{(m^2+1)\cdot\Delta R}$

$$R_{st} = \frac{R_{kd}R_fmX_f}{(m^2+1)X_f^2} + R_{kd}X_f^2$$

Therefore $mR_{kd}R_f = (m^2+1)R_{st}X_f - R_{kd}X_f$

Therefore $\dfrac{mR_{kd}^2R_o}{(m^2+1)\cdot\Delta R} = [(m^2+1)R_{st}-R_{kd}]\ \dfrac{R_{kd}^2}{m^2(m^2+1)\cdot\Delta X}$

Therefore $R_{kd} = (m^2+1)R_{st} - \dfrac{m[m^2(m^2+1)\cdot\Delta x]R_o}{(m^2+1)\cdot\Delta R}$

$$R_{kd} = \frac{(m^2+1)^2R_{st}\cdot\Delta R - m^3(m^2+1)\cdot\Delta XR_o}{(m^2+1)\quad R}$$

$$= \frac{(m^2+1)R_{st}\cdot\Delta R - m^3\cdot\Delta XR_o}{R}$$

$$= \frac{(m^2+1)R_{st}\cdot\Delta R - m^2\cdot\Delta R\cdot R_o}{R}$$

$$= (m^2+1)R_{st} - m^2R_o$$

$$= (m^2R_{st} + R_{st} - [m^2R_{st} - m^2\cdot\Delta R]$$

$$R_{kd} = m^2\cdot\Delta R + R_{st}$$

Now the actual values of the double cage parameters can be found by simply knowing R_{st}, X_{st}, PmecH, X_{lk}, and X_{md}, all from the single cage derivation. The procedure is as follows.

The value of R_o can be estimated from the following expression:

$$\left|I^1_A\right| = \left| \frac{jXm}{Ra + \frac{Ro}{s} + j(X_o + X_m)} \right| \cdot \left|I_a\right| \text{ A.}$$

in accordance with the figure below.

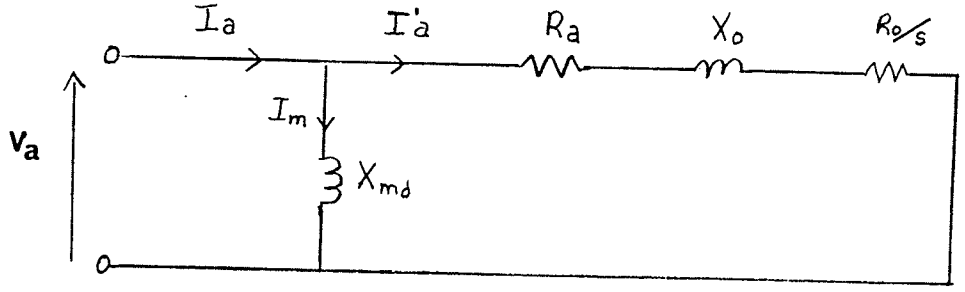

Fig. C5 equivalent circuit employed for analysis (Ref[ ])

assume I_a = 1.0 p.u.

$$\left|I^1_A\right| = \left| \frac{jXmd}{Ra + \frac{Ro}{s} + j(X_o + X_m)} \right| \text{ A}$$

note: R_a = 0.0169 p.u. s = 0.0067 (from earlier)

assume $\frac{Ro}{s} >> R_a$

also $\Delta X_e = \frac{s^2 X_o}{m^2 + s^2}$

$$\left|I^1_A\right| = \left| \frac{jXmd}{\frac{Ro}{s} + j(X_o + Xmd)} \right| \text{ A}$$

$$PamecH = (1-s)\, R_o \left|I^1_A\right|^2$$

$$\frac{PamecH}{1-s} = \frac{R_o}{s} \cdot \frac{X^2_{md}}{\frac{(R_o^2)}{s} + (X_o + X_{md})^2}$$

$$\frac{PamecH}{1-s} = \left[\frac{(R_o)^2}{s} + (X_o + X_{md})^2\right] = X^2_{md}\ \frac{(R_o)}{s}$$

$$\frac{(1-s)}{PamecH} X^2_{md} \frac{(R_o)}{S} = \frac{(R_o)^2}{S} + (X_o + X_{md})^2$$

Therefore $\frac{(R_o)^2}{S} - \frac{(1-s)X^2_{md}}{PamecH} \frac{(R_o)}{S} + (X_o + X_{md})^2 = 0$

Therefore $\frac{R_o}{S} = \frac{\frac{(1-s)X^2_{md}}{PamecH} \pm \sqrt{[\frac{(1-s)X^2_{md}}{Pamech}] - 4(X_o + X_{md})^2}}{2}$

as stated earlier PmecH = 452.95 kW/3 phases

Therefore $PamecH = \frac{452.95 \text{ kW}}{3} = 150.9833$

also P_b/phase = 184.8168 kV.A/phase defined earlier

Therefore $PamecH \text{ p.u.} = \frac{150.9833}{184.8168} = 0.8169 \text{ p.u.}$

X_{md} p.u. = 3.1866 p.u. from single cage

Let $X_a = X_{st} = 1/2\ X_{lk}$ (same assumption as for single cage)

X_{lk} = 0.2232 p.u. from single cage derivation

Therefore X_a p.u. = 0.1116 p.u. = X_{st}

note $X_o = X_{st}$ stated earlier (i.e. at small slips)

Therefore from earlier we have

$$\frac{R_o}{S} = \frac{(1-s)X^2_{md}}{2 \cdot PamecH} \pm 1/2 \sqrt{[\frac{(1-s)X^2_{md}}{PamecH}]^2 - 4(X_{st} + X_{md})^2}$$

$$\frac{R_o}{S} = 0.9549$$

Therefore $R_o = 0.0064$ p.u.

From the single cage derivation

$$R_{st} = R_f\Big|_{S=1} = 0.0148$$

Therefore $\Delta R = R_{st} - R_o = 0.0148-0.0064 = 0.0084$

$= \Delta X$ (i.e. m=1 for reasons mentioned before)

$R_{kd} = m^2 \quad R+R_{st} = 0.0084 + 0.0148$

$= \underline{0.0232}$ p.u.

$$R_f = \frac{R_o R_{kd}}{(m^2+1)\Delta R} = \frac{(0.0064)(0.0232)}{2(0.0084)} = \underline{0.0088} \text{ p.u.}$$

$$X_f = \frac{R_k{}^2{}_d}{m^2(m^2+1)\cdot\Delta X} = \frac{(0.0232)^2}{2(0.0084)} = \underline{0.0320} \text{ p.u.}$$

$$X_o = \Delta X + X_{st} = 0.0084 + 0.1116 = 0.12$$

and $$X_o = X_{kf} + \frac{R_k{}^2{}_d X_f}{(R_{kd} + R_f)^2} = 0.12$$

Therefore $$X_{kf} = 0.12 - \frac{R_k{}^2{}_d X_f}{(R_{kd} + R_f)^2}$$

$$X_{kf} = 0.12 - \frac{(0.0232)^2(0.0320)}{(0.0232 + 0.0088)^2}$$

$X_{kf} = \underline{0.1032}$ p.u.

Note: $R_f = R_{qf}$, $R_{kd} = R_{kq}$, $X_{kd} = X_{kq}$
$X_{kf} = X_{kqf}$, $X_f = X_{qf}$, $X_{md} = X_{mq}$

i.e. identical reflection on the quadrature axis.

also $X_{kd} = \underline{0.0}$ in this transformation (refer to Fig. C1 for the program and Fig. C4 used in analysis)

R_a again = $\underline{0.01694}$ p.u. as in the single cage.

The saturation curve of the magnetizing reactance was a straight line (no saturation) with a slope of one.

0.0,0.0 0.5,0.5 1.2,1.2 1.4,1.4 1.5,1.5 1.6,1.6 17,1.7 2.1,2.1
3.0,3.0 4.0,4.0

- again where the first number entered is X, (magnetizing current) and the second number is Y, (stator voltage) in each pair.

$$H = \frac{\text{stored energy at synchronous speed in KW-sec}}{\text{Rated kV.A}}$$ Ref [15]

J_1 = inertia of motor (including shaft)

motor inertia = 189.3 lb. in sec^2 Ref[9]

= 15.775 lb. ft sec^2

= 508 lb ft^2

$$J_1 = \frac{508 \text{ lb ft}^2}{1} \frac{12\text{x}12 \text{ in}^2}{1 \text{ ft}^2} \frac{2.54 \text{ x } 2.54 \text{ cm}^2}{1\text{m}^2} \frac{1\text{m}^2}{100\text{x}100 \text{ cm}^2} \frac{.45365 \text{ kg}}{1 \text{ lb}}$$

$= 21.4075 \text{ kg -m}^2$

$$H = \frac{1/2 \text{ J.W}_o^2}{\text{rated kV.A}} = \frac{\frac{21.4075}{2} \left[\frac{1200\text{x}\pi}{30}\right]^2}{554 \text{ kV.A}} = 0.3051 \text{ seconds}$$

Note: The value H was only used when running the motor by itself.

The next two pages show the generator specifications [12]. Following them is an equivalent circuit of the generator which is used for the program.

SECTION 10

GENERATOR TECHNICAL DATA - RADISSON

Customer's order no.	
A.C. Generator	Brushless
Serial No.	201 CLG8452/1 to -/3
Frame size	GD 450/355/450
Specification	BS2613/1970
Output	400 kW 421 kV.A
Voltage	600 V
Frequency	60 Hz nominal
Speed	1200 r/min nominal
Insulation	Class 'B'
Enclosure	Drip-proof protected
Full-load stator current	405 amp
Full-load power factor	0.95
Winding resistances	
Stator	0.0067 ohms/phase at 20°C
Rotor	0.111 ohms at 20°C
Air gap	2x4 mm
Bearing(s)	
Make	Ransome Hoffman Pollard
Type - DE	Ball BRM 105
NDE	Ball BRM 105 - spring loaded
Rectifiers (brushless machines only)	
Make	Westinghouse Brake - English Electric Semi-Conductors Ltd.
Type S4SN125	3 off - DRG.E61585169004 Item 11
S4SR125	3 off - DRG.E61585169004 Item 12
Bearing thermocouples (Copper/Constantan)	
Make	B.I.C.C., Prescto, Lancashire
Type	MKDT2-60
	2 per Machine (one in each bearing)
	GEC Drg. No. C615 8517 7025 Part No.17

Lubricant (recommended)	Shell Alvania RA grease
Weight (approximate)	2 745 kg
Arrangement drawing	B615 1726 9830.01
Exciter	202CLG8452/7, -/9 -/11
Frame size	CG 12/16
Specification	BS 2613/1970
Type	Brushless
Excitation for full load	29 V 3.5 A
Excitation for no load	13 V 1.7 A
Speed	1 200 r/min nominal
Insulation	Class 'B'
Enclosure	Drip-proof protected
Rotating armature	
Connected	Star
Resistance	0.0108 ohms/phase at 20°C
Stator resistances	7.29 ohms at 20°C
Air gap	2 x 2 mm

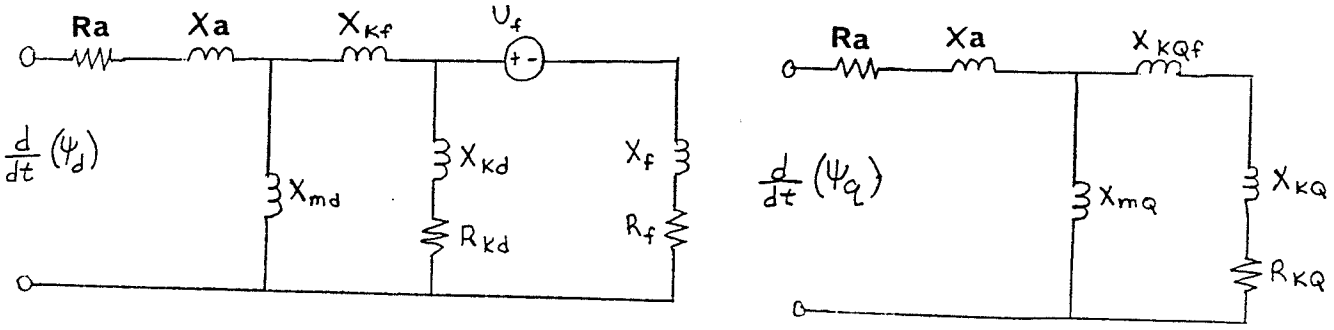

direct axis

quadrature axis

Fig C5 Equivalent Circuit For Program

P_b/phase = V_b/phase . I_b/phase

Therefore V_b/phase = $\frac{0.600 \text{ kV}}{\sqrt{3}}$ (rated voltage per phase)

and I_b/phase = 0.405 kA (i.e. full load rated current)

All calculations will again be rounded to four decimal places.

Therefore P_b/phase = $\frac{0.600 \text{ kV}}{\sqrt{3}}$. 0.405 kA = 140.2961 kV.A/phase

$$Z_b/\text{phase} = \frac{V_b \text{phase}}{I_b/\text{phase}} = \frac{0.600 \text{ kV}}{\sqrt{3} \cdot 0.405 \text{ kA}} = 0.8553 \ \Omega \text{ /phase}$$

R_a = 0.0067

Therefore R_a p.u. = $\frac{0.0067}{0.8553}$ = $\underline{0.0078}$ p.u.

R_f = 0.111 Ω

Therefore R_f p.u. = $\frac{0.111}{0.8553}$ = $\underline{0.1298}$ p.u.

SECTION 11

TYPICAL EXCITATION CURVES

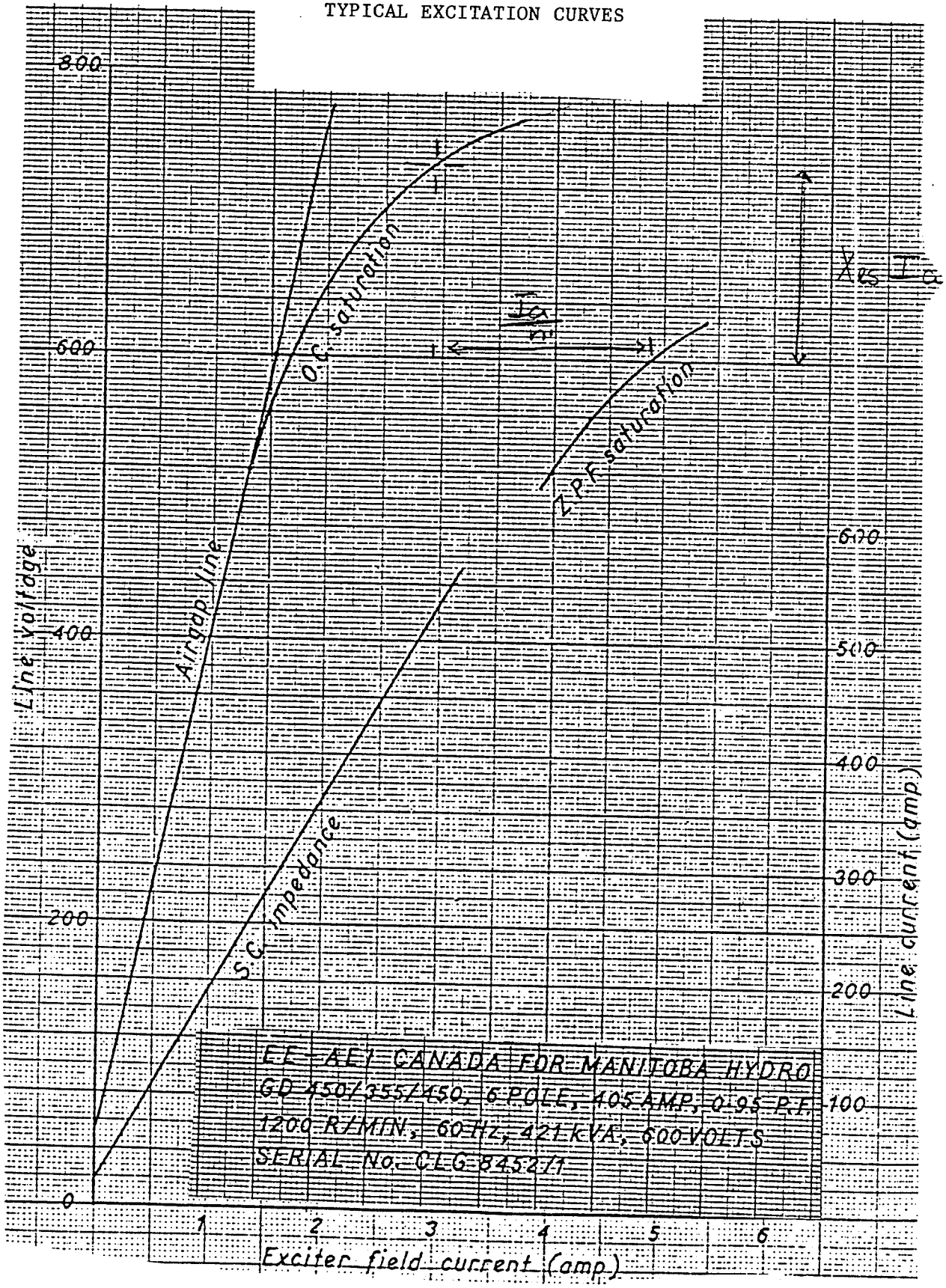

i.e. Using Ref [13], we have the following equivalent circuit of the generator on the zero power factor as used for analysis.

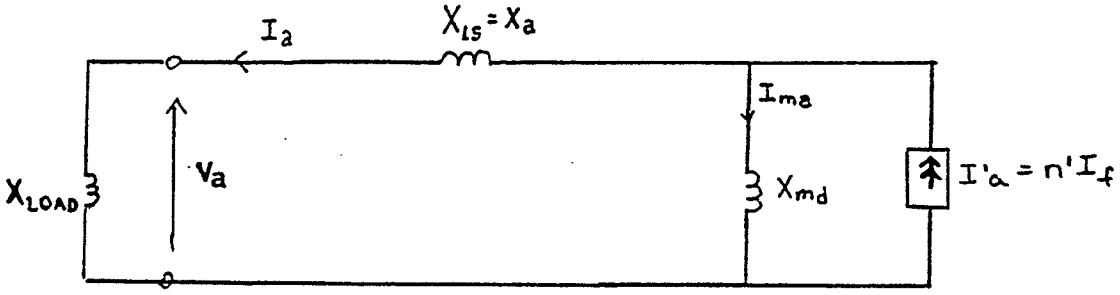

Fig. C6 Equivalent Circuit For Zero Power Factor Test

By using the excitation curves one can approximate $X_{ls}I_a$ and $\frac{I_a}{n^1}$ as described in Ref [13], by matching curves.

here $V_{o.c} = {}_1 jX_{md(n)} n^1 i_f$ at $i_f = 1.55$ A, $V = 600$ L-L

$$n\, X_{md(n)} = \frac{600}{\sqrt{3} \cdot 1.55} = 223.4904$$

Note: I_a = the stator current at which the zero power factor test was carried out. $I_a(n) = 500$ A an arbitrary value at which saturation had not yet started. $X_m a(n)$ is the corresponding magnetizing reactance at which saturation had not yet started.

$$I_{a(n)} = \frac{jX_{md(n)}}{jX_{md(n)} + X_a} n^1 \cdot i_f \qquad \text{from Fig. C5}$$

at a stator current of 500 on the short circuit curve the corresponding field current is 2.8 A.

Therefore 500 A $= \dfrac{223.4904 \cdot 2.8}{X_{md(n)} + X_a}$

Therefore $X_{md(n)} + X_a = 1.2515$

$I_a = 405$ A (stator current for ZPF test)

from curves $I_{Ls}I_a = X_aI_a = \frac{136}{\sqrt{3}} = 78.5196$ V.

Therefore $X_a = 0.1939\ \Omega$

Therefore $X_{md(n)} = 1.2515-0.1939 = 1.0576\ \Omega$

from curves $\frac{I_a}{n^I} = 4.85-2.95 = 1.9$

Therefore $n^I = \frac{405}{1.9} = 213.1579$

Therefore $X_{md(s)} = \frac{Va}{n^I I_f}$ (on O.C. saturation curve)

Note: $X_{md(s)}$= the saturated value of X_{md}.

$$X_{md(s)} = \frac{600}{\sqrt{3} \cdot 213.1579 \cdot 1.65} = 0.9849\ \Omega$$

for the program we need only $X_{md(n)}$, the non-saturated X_{md} and the saturation curve which will be shown later will calculate $X_{md(s)}$.

Therefore $X_{md} = 1.0576\ \Omega$

Therefore X_{md}p.u. $= \frac{1.0576}{0.8553} = \underline{1.2365}$ p.u. $= X_{mQ}$ p.u.

$X_a = 0.1939\ \Omega$

X_a p.u. $= \frac{0.1939}{0.8553} = \underline{0.2267}$ p.u.

And when referring to Fig. C5, the equivalent circuit needed for the program we have no values for X_{kf}, X_{kd}, R_{kd}, X_f, R_f, X_{kq}, and R_{kq}.

These would then be:

$$X_{kf} = 0.0$$
$$X_{kd} = \infty = X_{kq}$$
$$R_{kd} = \infty = R_{kq}$$
$$X_f = 0.0$$
$$R_f = 0.0$$

Using the old machine data we have:

(600 V 1 782 rpm 421 A 250 lb ft^2 437.5 kV.A
$X_d = 1.5$ p.u. $X'_d = 0.17$ p.u. $X''_d = 0.15$ p.u.
$X_q = 0.66$ p.u. $X''_q = 0.30$ p.u.)

The equivalent circuit of Fig. C5 can be derived needing only the knowledge of X_a. X_a was chosen as 0.1 p.u. since in the previous derivation X_a was really the total leakage reactance (i.e. $X_a + X_{kf} + X_{kd}//X_f$) and equalled .2267 p.u.

Note the new p.u. base of impedance is:

$$Z_b/\text{phase} = \frac{V_b/\text{phase}}{I_b/\text{phase}}$$

$$= \frac{600}{\sqrt{3}\cdot 421} = 0.8228\ \Omega\ /\text{phase}$$

which is approximately the same as the previous Z_b/phase = 0.8553 Ω/phase. Also the kV.A ratings of the old machine is 437.5 kV.A which is close to the 421 kV.A rating of the new machines The old machine data was then used to find a better equivalent circuit for the generator.

$$X_a = \underline{0.1}\ \text{p.u.}$$
$$X_d = X_a + X_{md} = 1.5$$
$$X_{md} = \underline{1.4}\ \text{p.u.}$$

$$X_d^1 = X_a + \frac{X_{md}(X_f+X_{kf})}{X_{md} + (X_f + X_{kf})} = 0.17 \text{ p.u.}$$

Therefore $X_f + X_{kf} = 0.0737$

let $X_f = X_{kf} = \underline{0.03685}$ p.u.

$$0.15 \text{ p.u.} = X_d'' = X_a + \frac{(X_f+X_{kf})X_{md}X_{kd}}{X_{md}(X_f + X_{kf})+X_{ma}X_{kd}+(X_f+X_{kf})X_{kd}}$$

Therefore $X_{kd} = \underline{0.1749}$ p.u.

$0.66 \text{ p.u.} = X_q = X_q + X_{mq}$ = Therefore $X_{mq} = \underline{0.56}$ p.u.

$$X_q'' = X_a + \frac{X_{mq}X_{kq}}{X_{mq}+X_{kq}}$$

Therefore $X_{kq} = \underline{0.3111}$ p.u.

R_{kd} was chosen as 0.1 p.u. since it is typically small

$R_{kd} = R_{kq} = \underline{0.1}$ p.u.

The saturation of the magnetizing reactance was obtained from the Open circuit saturation curve.

Here the program assumes 1.0 p.u. field current will give 1.0 p.u. stator voltage (on the air gap line). The exciter field current in amps was 1.55 corresponding to 600 V L-L rms stator voltage. Using 1.55 Amp as 1.0 p.u. field current and 600 V L-L as 1.0 p.u. stator voltage the following saturation curve was obtained:

0.0,0.0 0.645,.667 .806,.833 .968,.933 1.13,1.02
1.29,1.08 1.45,1.13 1.61,1.17 1.94,1.23

- where the first number entered is X_1 (field current) and the second number is Y_1 (stator voltage) in each pair.

H was again calculated.

i.e. H = $\frac{\text{Stored energy at synchronous speed in kW-sec}}{\text{Rated kV.A}}$

J_3 = inertia of generator (including shaft)

= 264.6 lb in sec^2

= 22.05 lb ft sec^2

= 710 lb ft^2

Therefore $J_3 = \frac{710 \text{ lb ft}^2}{1} \frac{12\text{x}12 \text{ in}^2}{1 \text{ ft}^2} \frac{2.54\text{x}2.54 \text{cm}^2}{1 \text{ in}^2} \frac{1\text{m}^2}{100\text{x}100 \text{ cm}^2} \frac{.45359 \text{ kg}}{1 \text{ lb}}$

$= 29.9193 \text{ kg-m}^2$

Therefore $H = \frac{1/2 \text{ J.wo}^2}{\text{rated kV.A}}$

$= \frac{[\frac{1\ 200 \times \pi}{30}]^2}{\frac{1/2(29.9193)}{421 \text{ kV.A}}} = \underline{0.5611} \text{ seconds}$

Note: The inertia value H was only used when running the generator by itself in initial simulations.

Also the generator did not have to be modelled in the same detail as the motor since the generator was only connected to the system through the mechanical torque produced (it also fed generator torque back into the motion equations) and basically served as an inertia.

APPENDIX D

THE PROGRAMS

The flywheel subroutine is first presented. This subroutine is interfaced with the dynamics program (which is part of EMTDC) and the input data file. A typical dynamics file is included after the flywheel program (subroutine DSDYN). The dynamics file represents the 138 kV source as an infinite bus and calls the machine programs, switch programs, and the before mentioned flywheel program. The input data file (MGDBL) represents a typical input file and is included after the subroutine DSDYN. The MGDBL file models all existing bus work including transformers, loads, machine and flywheel parameters.

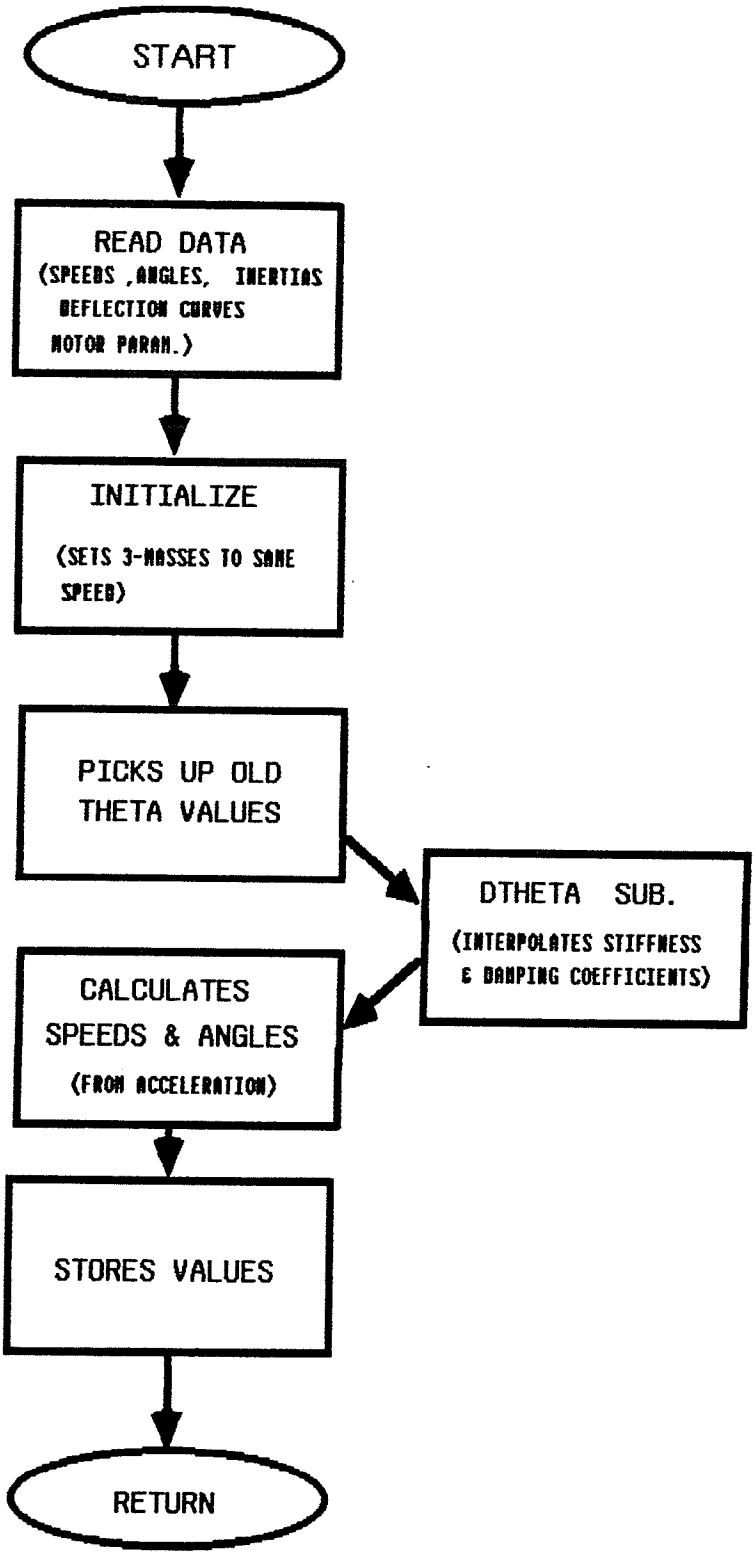

FIG. D1 FLY60 Subroutine Flowchart

```
C
C
      SUBROUTINE FLY60(TM,TG,WM,WF,WG,TSH1,TSH2,THETM
     *,THETF,THETG)
C
C ------------------------------------------------------------------------
C
C THIS SUBROUTINE SIMULATES A 3-MASS  SYSTEM CONSISTING OF A MOTOR A FLY-
C WHEEL AND A GENERATOR. THE ARGUMENT INPUTS ARE THE MOTOR TORQ AND GEN-
C ERATOR TORQ , AND THE ARGUMENT OUTPUTS MOTOR SPEED AND GENERATOR SPEED.
C
C
C
C
$INSERT EMT.E
      COMMON /S1/TIME,DELT /S2/S(5000),N
      COMMON /S4/VAR(100),CON(100),PGB(25)
      REAL TM,TG,WM,WG,DDM,DDG,DM,DG,KM,KG,KKG,KKM
C
C
C
      IF (TIME .GT. 0.0) GO TO 100
C
C 3-MASS SYSTEM PARAMETERS READ ONLY AT BEGINNING OF RUN (T=0) ,
C READING ORDER IN FREE FORMAT.
C CARD1 - INITIAL SPEED OF MOTOR,GEN.,FLYWHEEL,(R/S); BASE ANG. FREQ. (R/S)
C CARD2 - INITIAL ANGLES (MOTOR,FLYWHEEL,GEN)
C CARD3 - DAMPING CURVE; DELTA THETA, D; ENTERED AS X1,Y1,X2,Y2,...X10,Y10
C CARD4 - TORS. STIFFNESS; DELTA THETA,K; ENTERED AS X1,Y1,...X10.Y10
C CARD5 - MOTOR VBASE,IBASE  GEN.; VBASE,IBASE
C CARD6 - INERTIA OF MOTOR, FLYWHEEL, AND GEN. (J1,J2,J3) IN KG-M-M
C
C
      IIN=5
      READ(IIN,*) S(N+1),S(N+12)
      READ(IIN,*) S(N+2),S(N+3),S(N+4)
      READ(IIN,*) (S(N+I),I=41,60)
      READ(IIN,*) (S(N+I),I=21,40)
      READ(IIN,*) S(N+5),S(N+6),S(N+7),S(N+8)
      READ(IIN,*) S(N+9),S(N+10),S(N+11)
C
C SET ALL 3 MASSES TO THE SAME SPEED
C
      S(N+13)=S(N+1)
      S(N+14)=S(N+1)
100   CONTINUE
C
C USES PREVIOUS VALUES OF THETA AND SPEED; ALSO SETS TORQ INPUTS.
```

```
C
      THETM=S(N+2)
      THETF=S(N+3)
      THETG=S(N+4)
      WM=S(N+1)
      WF=S(N+13)
      WG=S(N+14)
      TBMOT=3.0*S(N+5)*S(N+6)/S(N+12)*3.0
      TBGEN=3.0*S(N+7)*S(N+8)/S(N+12)*3.0
      TMOT=TM*TBMOT
      TGEN=TG*TBGEN
C
C ESTIMATES OF THETA AND W ARE MADE (PREDICTOR)
C
      TWOPI=6.2831853
      IF (THETM .LT. TWOPI) GO TO 200
      THETM=THETM-TWOPI
      THETF=THETF-TWOPI
      THETG=THETG-TWOPI
200   CONTINUE
      DTHETM=THETM-THETF
      DTHETG=THETF-THETG
      DWM=WM-WF
      DWG=WF-WG
      CALL DTHETA(ABS(DTHETM),DM,43)
      CALL DTHETA(ABS(DTHETG),DG,43)
      CALL DTHETA(ABS(DTHETM),KM,23)
      CALL DTHETA(ABS(DTHETG),KG,23)
C
      THDOTM=WM
      THDOTF=WF
      THDOTG=WG
C
      AM=(TMOT-DM*DWM-KM*DTHETM)/S(N+9)
      AF=(DM*DWM-DG*DWG+KM*DTHETM-KG*DTHETG)/S(N+10)
      AG=(DG*DWG+KG*DTHETG-TGEN)/S(N+11)
C
      TSH1=DM*DWM+KM*DTHETM
      TSH2=DG*DWG+KG*DTHETG
C
      WMP=WM+DELT*AM
      WFP=WF+DELT*AF
      WGP=WG+DELT*AG
      THM=THETM+DELT*WM
      THF=THETF+DELT*WF
      THG=THETG+DELT*WG
C
```

```
C CALCULATES THE CORRECTED VALUES OF THETA AND W.(CORRECTOR)
C
      IF (THM .LT. TWOPI) GO TO 300
      THM=THM-TWOPI
      THF=THF-TWOPI
      THG=THG-TWOPI
300   CONTINUE
      DDTHM=THM-THF
      DDTHG=THF-THG
      DDWM=WMP-WFP
      DDWG=WFP-WGP
      CALL DTHETA(ABS(DDTHM),DDM,43)
      CALL DTHETA(ABS(DDTHG),DDG,43)




      CALL DTHETA(ABS(DDTHM),KKM,23)
      CALL DTHETA(ABS(DDTHG),KKG,23)
C
      TTDOTM=WMP
      TTDOTF=WFP
      TTDOTG=WGP
C
      ACCLM=(TMOT-DDM*DDWM-KKM*DDTHM)/S(N+9)
      ACCLF=(DDM*DDWM-DDG*DDWG+KKM*DDTHM-KKG*DDTHG)/S(N+10)
      ACCLG=(DDG*DDWG+KKG*DDTHG-TGEN)/S(N+11)
C
      WM=WM+0.5*DELT*(ACCLM+AM)
      WF=WF+0.5*DELT*(ACCLF+AF)
      WG=WG+0.5*DELT*(ACCLG+AG)
      THETM=THETM+0.5*DELT*(TTDOTM+THDOTM)
      THETF=THETF+0.5*DELT*(TTDOTF+THDOTF)
      THETG=THETG+0.5*DELT*(TTDOTG+THDOTG)
C
C STORAGE OF COMPUTED VALUES
C
      S(N+1)=WM
      S(N+13)=WF
      S(N+14)=WG
      S(N+2)=THETM
      S(N+3)=THETF
      S(N+4)=THETG
      WM=3.0*WM/S(N+12)
      WG=3.0*WG/S(N+12)
      WF=3.0*WF/S(N+12)
C
      N=N+60
      RETURN
      END
```

```
C ***************************************************************************
C
      SUBROUTINE DTHETA(C,KD,IS)
      COMMON /S2/S(5000),N
      REAL C,KD
C
      ISF=IS+16
      DO 10 K=IS,ISF,2
      IP=K-1
      IF (S(N+K) .LT. 0.0) GO TO 30
      IF (S(N+K) .GT. C) GO TO 20
10    CONTINUE
C
      GO TO 30
20    DX=S(N+IP+1)-S(N+IP-1)
      DY=S(N+IP+2)-S(N+IP)
      KD=DY/DX*(C-S(N+IP-1))+S(N+IP)
      GO TO 999
C
30    DX=S(N+IP-1)-S(N+IP-3)
      DY=S(N+IP)-S(N+IP-2)
      KD=DY/DX*(C-S(N+IP-3))+S(N+IP-2)
999   RETURN
      END
C ***************************************************************************
```

```
      SUBROUTINE DSDYN
C
C    SUBROUTINE TO ASSEMBLE SOURCE DATA. SPECIAL CONTROLS.
C    VARIOUS SUBROUTINES. AND ANY FORTRAN STATEMENTS.
C
      REAL LIMIT.INTGL3.LDLAG2.IKD.IKQ.IROTOR
$INSERT EMT.E
      DOUBLE PRECISION RDC
      COMMON /S1/TIME.DELT.ICH.PRINT
      COMMON /S2/STOR(5000).NEXC/S3/GVLV(4.4.24).NVLV
      COMMON /S4/VAR(100).CON(100).PGB(25)
      PI=3.1415927
      A1=PI/3+120*PI*TIME
      IF(A1 .GE. (2.0*PI+PI/3.0)) A1=A1-2.0*PI
      A2=A1-2.0*PI/3.0
      A3=A1+2.0*PI/3.0
      B1=COS(A1)
      B2=COS(A2)
      B3=COS(A3)
      ES(1.1)=138.0*B1 /SQRT(3.0)*SQRT(2.0)
      ES(2.1)=138.0*B2 /SQRT(3.0)*SQRT(2.0)
      ES(3.1)=138.0*B3 /SQRT(3.0)*SQRT(2.0)
      ES(19.1)=138.0*B1 /SQRT(3.0)*SQRT(2.0)
      ES(20.1)=138.0*B2 /SQRT(3.0)*SQRT(2.0)
      ES(21.1)=138.0*B3 /SQRT(3.0)*SQRT(2.0)
      ITR=1
      IF(TIME .GT. DELT) GO TO 10
      CON(1)=375.9
      CON(2)=375.9
10    CONTINUE
      VM=VM3PH2(1.7.8.9.0.02)
      VMPU=VM/0.600
      P1=1.0-VMPU
      CON(23)=P1*100
      CALL MIM100(1.4.5.6.1.0.0.0.TMECH.FLD.ITR.CON(25).
     *CON(26).CON(1).OMEGA.IKD.IKQ.IROTOR)
      CON(3)=-(STOR(NEXC+65-100))
      CALL MAC100(1.7.8.9.1.0.CON(23).TMECH.CON(4).CON(24).
     *ITR.CON(21).CON(22).OMEGA.CON(2))
      IF(TIME .LT. 0.8) GO TO 20
      STOR(NEXC+9)=21.41
      STOR(NEXC+10)=97.08
      STOR(NEXC+11)=29.92
      STOR(NEXC+42)=0.0
      STOR(NEXC+44)=0.0
      STOR(NEXC+46)=0.0
```

```
20      CONTINUE
        CALL FLY60(CON(3),CON(4),CON(7),CON(27),CON(8),CON(5)
       *,CON(6),CON(18),CON(19),CON(20))
        CON(1)=CON(7)*376.991
        CON(2)=CON(8)*376.991
        CON(27)=CON(27)*376.991
        CON(9)=VDC(4,1)
        CON(10)=VDC(7,1)
        CON(11)=VDC(5,1)
        CON(12)=VDC(6,1)

        CON(13)=VDC(8,1)
        CON(14)=VDC(9,1)
        CON(15)=CDC(4,13,1)
        CON(16)=CDC(5,14,1)
        CON(17)=CDC(6,15,1)
        CON(4)=CON(4)*3349.2441/4412.0
        CON(28)=CDC(4,25,1)
        CON(29)=CDC(5,26,1)
        CON(30)=CDC(6,27,1)
        CON(31)=VDC(10,1)
        KSW=1
        KSW1=1
        KSW2=1
        KSW3=1
        IF(TIME .GT. 3*DELT) KSW3=0
        IF(TIME .GT. 1.100) KSW=1
        IF(TIME .GT. 1.100) KSW3=0
        IF(TIME .GT. 1.100) KSW1=0
        IF(TIME .GT. 1.167) KSW1=1
C SWITCH BETWEEN 138KV (WITH FILTER) & TRFMR (TO MOTOR)
        CALL SWTCH4(1,1,10,1.0E+08,KSW)
        CALL SWTCH4(1,2,11,1.0E+08,KSW)
        CALL SWTCH4(1,3,12,1.0E+08,KSW)
C SWITCH BETWEEN 4KV (WITH FILTER) & MOTOR
        CALL SWTCH4(1,13,4,1.0E+08,KSW1)
        CALL SWTCH4(1,14,5,1.0E+08,KSW1)
        CALL SWTCH4(1,15,6,1.0E+08,KSW1)
C SWITCH BETWEEN 138KV (WITHOUT FILTER) & TRFMR (TO MOTOR)
        CALL SWTCH4(1,19,22,1.0E+08,KSW2)
        CALL SWTCH4(1,20,23,1.0E+08,KSW2)
        CALL SWTCH4(1,21,24,1.0E+08,KSW2)
C SWITCH BETWEEN 4KV (WITHOUT FILTER) & MOTOR
        CALL SWTCH4(1,25,4,1.0E+08,KSW3)
        CALL SWTCH4(1,26,5,1.0E+08,KSW3)
        CALL SWTCH4(1,27,6,1.0E+08,KSW3)
C LOAD CHANGES
        CALL PRLL2(20.0,1,7,7,0.5,20.0,0)
        CALL PRLL2(20.0,1,8,8,0.5,20.0,0)
        CALL PRLL2(20.0,1,9,9,0.5,20.0,0)
        RETURN
        END
```

```
MGD3L /TITLE
0.0001 2.0 0.0005 /DELT FINTIM PRTDEL
1 /#OF SUBSYSTEMS
27 20 / # OF NODES
0.0 /INIT NODE VOLTS
1 10 1.0  / KSW
2 11 1.0 /  KSW
3 12 1.0 /  KSW
7 0 1.711 / GEN LOAD
8 0 1.711 / GEN LOAD
9 0 1.711 / GEN LOAD
-10 0 1.08 0.0614 4.58 / FILTERS
-11 0 1.08 0.0614 4.58 / FILTERS
-12 0 1.08 0.0614 4.58 / FILTERS
-10 0 1.52 0.0614 2.337 /   "
-11 0 1.52 0.0614 2.337 /   "
-12 0 1.52 0.0614 2.337 /   "
-10 0 0.75 0.0152 3.84 /    "
-11 0 0.75 0.0152.3.84 /    "
-12 0 0.75 0.0152 3.84 /    "
-4 16 15.73  /PARELLEL LOAD
-5 17 15.73  /   "       "
-6 18 15.73  /   "       "
-4 0 1500.0 / STABILIZING RESISTANCE TO GND
-5 0 1500.0 /     "            "      "   "
-6 0 1500.0 /     "            "      "   "
13 4 0.5 / KSW1
14 5 0.5 / KSW1
15 6 0.5 / KSW1
16 0 0.0 .2196 / PARELLEL LOAD
17 0 0.0 .2196 /    "       "
18 0 0.0 .2196 /    "       "
25 4 0.5 /  KSW3
26 5 0.5 /  KSW3
27 6 0.5 /  KSW3
19 22 1.0 / KSW2
20 23 1.0 / KSW2
21 24 1.0 / KSW2
999 /
```

```
1 1.0  /SOURCE THEVENIN
2 1.0 /     "      "
3 1.0 /     "      "
19 1.0 /    "      "
20 1.0 /    "      "
21 1.0 /    "      "
999 /
2 /NO OF CPLD COILS ON 1 CORE
10 0 .00000000 6735.4297 /1 SIDE WNDING
13 0 .00000000 202.99033 .00000000 6.1207228 /2 SIDE WNDING
888 /
11 0 /
14 0 /
888 /
12 0 /
15 0 /
2 /NO OF COILS ON 1 CORE
```

```
22 0 .00000000 6735.429 /1 SIDE WINDING
25 0 .00000000 202.99033 .00000000 6.1207228 /2 SIDE WINDING
888 /
23 0 /
26 0 /
888 /
24 0 /
27 0 /
999 /
999 /NOT LINE DATA
-3.40 3.40 / PRTPLT LMT
20 /#OF CHANNELS
```

```
0 / VAR(I)
0.1116 3.1866 0.1032 0.0 0.032 /XA.XMDO.XKF.XKD.XF
3.1866 0.1032 0.0 0.032 /XMQD.XKQF.XKQ.XQF
0.01694 0.0148 0.0148 0.0232 0.0232 /RA.RF.RQF.RKD.RKQ
0.3051 376.9911 0.0  /H.OMO.DAMPING
0.0 0.0 0.5 0.5 1.2 1.2 1.4 1.4 1.5 1.5 1.6 1.6 1.7
1.7 2.1 2.1 3.0 3.0 4.0 4.0 /
2.4017 0.07695 /BASE KV KA
0.0 0.0 0.0 0.0 /INIT COND
0.1 1.4 0.03685 0.1749 0.03685 /
0.56 0.3111 /
0.0078 0.1298 0.1 0.1 /
0.56 376.991 0.0 /
0.0 0.0 0.645 0.667 0.806 0.833 0.968 0.933 1.13 1.02
1.29 1.08 1.45 1.13 1.61 1.17 1.94 1.23 2.26 1.27 / MAG SATRN
0.346 0.405 /
0.0 0.0 0.0 0.0 /
125.3 376.991 /
6.00 6.00 6.00 /
0.0 700.0 0.0174 700.0 0.0349 700.0 -1.0 -1.0 / D CURVE
0.0 2.303E03 0.0087 8.599E03 0.0262 11.363E03 0.0408
17.506E03 0.0525 22.525E03 0.0641 25.798E03 0.0758
30.405E03 0.0874 36.854E03 0.0991 78.316E03 0.1067
219.284E03 / T S CURVE
2401.7 76.95 346.4 405.0 /
21.51 0.100 0.100 /
999 /
```

APPENDIX E
PER UNIT VALUES

The per unit base for power is that supplied when the base current flows at base voltage and at unity power factor in all three phases, (details in Appendix C), and is not the actual rated power, but the power corresponding to the rated kVA. The base voltage is the rated voltage and the base current is the full load rated current.

The base torque is not the same as the rated torque. The base torque is defined as torque at the base power and the electrical speed 377 rad/sec for a 60 Hz system.

$$T \text{ p.u.} = \frac{\#\text{ of poles}}{2} \quad \frac{P_{base}}{Ws}$$

Therefore, 1.0. p.u. Torque on the motor base is 4412N.m.

The rated torque can be calculated from the rated Hp and the slip speed in rev/min (n).

$$T_{rated} = \frac{33\ 000\ (Hp)}{2 \cdot \pi \cdot n} = 2658 \text{ lb ft}$$

$$= 3604 \text{ N.m}$$

Here, 1.0. p.u. torque on the motor base is 1.22 times the rated torque. Similarly, for the generator the rated torque is 2347 lb ft (3182 N.m), whereas 1.0 p.u. torque on the generator base is 3350 N.m or 1.05 times the rated torque. For simplicity all torques were referred to the motor base in the simulation plots. A 1.0. p.u. torque on the generator referred to the motor base is equivalent to 0.76 p.u.